Integrated fiber microneedles for oral mucosal vaccine delivery

Rachel Creighton

A dissertation

submitted in partial fulfillment of the

requirements for the degree of

Doctor of Philosophy

University of Washington

2021

Reading Committee:

Kim Woodrow, Chair

Deborah Fuller

Karl Böhringer

Program Authorized to Offer Degree:

Bioengineering

University of Washington

Abstract

Integrated fiber microneedles for oral mucosal vaccine delivery

Rachel Creighton

Chair of the Supervisory Committee:
Kim Woodrow, Associate Professor
Bioengineering

The oral mucosa is a promising site for mucosal vaccination because it is easily accessible and contains a rich population of immune cells. However, the current understanding of how vaccine formulation and delivery factors affect the resulting immune response is limited in part by a lack of delivery systems capable of addressing the physical and immunological barriers of the oral mucosa. Several recent studies with immunogen coated solid microneedles have demonstrated that microneedles effectively overcome the physical barriers in the oral mucosa for efficient vaccine delivery. The basic immunogenicity demonstrated in these studies motivates continued exploration of multifunctional microneedle designs capable of incorporating diverse immunogens, controlling release kinetics, and targeting specific immune cell populations

in the oral mucosa. As a step toward this ultimate goal, we developed dissolving microneedles containing polymeric nanofibers. We designed an *in situ* method of nanofiber-microneedle integration that is compatible with a range of relevant microneedle dimensions and preserves the fiber microarchitecture. We demonstrated that nanofibers fabricated from different polymers and encapsulating different pharmaceutical agents are effectively integrated. Finally, we characterized the immunogenicity of integrated fiber microneedles with varying length and release kinetics in the oral mucosa using a model protein antigen. These studies establish integrated fiber microneedles as a highly versatile system which could be used as a tool in future studies to optimize oral mucosal vaccines and to better understand oral mucosal immunity.

TABLE OF CONTENTS

LIST OF FIGURES

LIST OF TABLES

ACKNOWLEDGEMENTS

This work would not have been possible without my advisor Dr. Kim Woodrow. Kim's curiosity and enthusiasm for science are contagious. I am grateful that she was so supportive of new ideas and research directions, while helping me learn how to mitigate risk. I am lucky to have worked with such a passionate and thoughtful mentor that truly cared about helping me develop into an independent scientist. I would also like to thank the members of my supervisory committee, Dr. Deborah Fuller, Dr. Karl Böhringer, Dr. Dan Ratner, Dr. Kelly Stevens, and Dr. David Koelle, for their technical support, thoughtful feedback, enthusiasm, and encouragement. During my doctorate work, I also had the opportunity to work with Dr. Helder Nakaya at the University of Sao Paulo, who graciously welcomed me into his group where I met some wonderful scientists and vastly expanded my scientific breadth by learning some computational biology.

I would like to thank Dr. Sheila Lukehart, Dr. Anna Wald, and the executive committee of the STD and AIDS Research Training Fellowship Program (NIH T32 AI07140) for supporting this work. This program provided me with opportunities to interact and present my work to a diverse audience including clinicians, epidemiologists, and microbiologists. This not only improved my communication skills, but it also provided a unique perspective on my research. I would also like to acknowledge funding support from the National Science Foundation Graduate Research Fellowship Program.

I would like to thank all of my collaborators, specifically Dr. Jaehyung Park who was instrumental in the successful completion of my animal work, and Jolie Phan, Nicole Lim, and Mitchell Ekdahl, the undergraduate researchers I've had the pleasure of mentoring. Thank you to other members of the Woodrow Lab, Dr. Ian Suydam, Dr. Emily Krogstad, Dr. Renuka

Ramanathan, Dr. Anna Blakney, Dr. Shijie Cao, Dr. Hannah Frizzell, who are wonderful examples of the type of scientist I aspire to be. Thank you to Jamie Hernandez, Hannah VanBenschoten, Peter Chien, My-Anh Doan, Kate Faber, Teri Guo, for being great office mates and lab mates, always available to provide feedback, help troubleshoot experiments, or just to chat.

Finally, I would like to thank my friends and family. Earning a Ph.D., particularly finishing during a global pandemic, requires a lot of hard work and persistence. I am fortunate to be surrounded by a community of graduate student and non-graduate student friends to celebrate during successes, commiserate during failures, and to join me in pursuing sources of joy and inspiration outside of the lab. To my sister and brother-in-law, Hannah and Andrew Nandor, thank you for your unconditional friendship and for the sweet video calls with my nieces that always brighten my day. To my parents, Ann and Jeff Philiph, thank you for instilling in me the values of creativity, curiosity, and hard work that set me on this life and career path. This would not have been possible without your encouragement and support. To my husband Wes, thank you for providing a constant positive attitude, for serving as a sounding board when I need to talk through an idea, and for your attempts to learn immunology. I'm looking forward to the next stage of our life together.

Chapter 1. EXECUTIVE SUMMARY AND SPECIFIC AIMS

1.1 BACKGROUND AND MOTIVATION

A majority of human pathogens infect via mucosal surfaces, where local innate and adaptive immune responses can prevent and control infection. While these mucosal immune responses can be generated through parenteral vaccination, evidence suggests that more robust and sustained mucosal immunity is generated by vaccination at mucosal surfaces. Therefore, it is likely that incorporation of mucosal vaccines could improve protection from pathogens that have been difficult to combat with parenteral vaccination alone, such as HIV, *Mycobacterium tuberculosis*, or herpes simplex virus. The oral mucosa is a promising site for mucosal vaccine delivery because it is readily accessible, contains tissues with rich immune cell populations, and has a microenvironment more favorable for biologics compared to other mucosal sites like the gastrointestinal tract. Previous studies have demonstrated that vaccination in the buccal mucosa, sublingual mucosa, or in the lymphoid tissues of Waldeyer's tonsillar ring can elicit systemic immunity at least comparable to intramuscular vaccination[1-3] and mucosal immunity in the oral mucosa and other mucosal tissues such as the vaginal tract and respiratory tract.[2-4] However, the rational design and evaluation of the next generation of oral mucosal vaccines is precluded by an inability of existing oral dosage forms to overcome the physical and immunological barriers of the oral mucosa.

Oral mucosal vaccines are most commonly delivered topically using aqueous suspensions, dissolving tablets, or films. Upon application to the oral mucosa, these vaccines are subject to salivary flow and must be transported through a multilayered stratified squamous epithelium.[5,6] These physical barriers can result in unreliable dosing, an inability to control

vaccine delivery kinetics, and a limited ability to deliver nonpolar molecules.[7-9] Together, these limitations have led to an incomplete understanding of how vaccine dose, delivery location, and delivery kinetics affect systemic and mucosal immunity. As a result of physical barriers, vaccines are primarily delivered to the more permeable sublingual mucosa, where the majority of antigen presenting cells are CD11c- CD11b+ cells that have been shown to mediate tolerance in mice.[10] Other oral mucosal sites, such as the lamina propria of the buccal mucosa, contain larger populations of immunogenic interstitial dendritic cells, some with specialized capabilities to prime CD8+ T cells by cross-presentation.[11] Vaccine delivery systems that target these cells could be used to improve oral mucosal vaccine immunogenicity. Furthermore, antigen presenting cells within the oral mucosa have distinct migration kinetics in response to antigen and adjuvant delivery,[12-14] suggesting an opportunity to modulate vaccine delivery kinetics to optimize immunogenicity.

This project is focused on the development of an integrated fiber microneedle device to address the physical and immunological barriers of oral mucosal vaccination. Electrospun fibers are a highly versatile material for drug and vaccine delivery, capable of high loading and precisely tunable release kinetics. However, electrospun fibers alone are mechanically weak and their direct application to the oral mucosa would offer little advantage over previously developed topical oral dosage forms. To effectively overcome the physical barriers in the oral mucosa, electrospun fibers were integrated with microneedles, which have been established as an effective delivery system for overcoming physical barriers in a variety of tissues including the oral mucosa.[15-18] We anticipate that the attributes of this innovative vaccine delivery device for penetrating the oral mucosa, formulating a diverse range of immunogens, and providing

sustained vaccine release will address gaps in currently available oral mucosal delivery systems to facilitate future development of oral mucosal vaccines.

1.2 SCIENTIFIC PREMISE

Vaccine dosing modalities designed for the oral mucosa must overcome the physical barriers to delivery in the tissue and the immunological barrier of antigen presenting cells that are predisposed for tolerance. The integrated fiber microneedle design is motivated by several key observations:

First, dose dilution and washout are key challenges for oral mucosal vaccine delivery that can be overcome using microneedles. In previous studies, the risk of salivary washout limits the total deliverable vaccine volume and dose.[19] Additionally, unpredictable dose dilution has been a significant challenge in the evaluation of oral tablet formulations designed for sustained release.[9,20] Studies of microneedle-mediated drug and vaccine delivery in the oral mucosa have shown promising results of up to 91% delivery efficiency,[16] motivating continued exploration of microneedles as an oral mucosal dosing modality.

Second, microneedles and electrospun nanofibers can be prepared from virtually any natural or synthetic material to control release kinetics, and they can incorporate active pharmaceutical agents by various material configurations.[21-26] The material versatility of these two delivery methods alone suggests they could enable complex agent release kinetics, mediated by the fibers, the microneedle matrix, or a combination of the two.

Third, electrospun fibers can incorporate a wide variety of active pharmaceutical agents with high loading. Conventional microneedle designs typically require significant changes in the material composition or fabrication process to encapsulate different pharmaceutical agents.[27-29] Additionally, agent loading is often limited to low concentrations to prevent compromised

mechanical properties.[25] Using electrospun fibers to incorporate vaccines into integrated fiber microneedles will enable evaluation of various antigens and adjuvants without modifying the general microneedle fabrication approach.

Based on these observations, the ultimate goal of this work is to develop a microneedle device containing a porous network of electrospun fibers within a polymer matrix with a rapidly dissolving backing layer. We anticipate that upon delivery to the oral mucosa, the fiber-containing microneedles will effectively puncture the tissue and the hydrophilic polymer backing will dissolve, leaving the fiber-containing microneedle tips implanted in the tissue. The fabrication process will be highly tunable to enable integrated fiber microneedles with varying geometry, material composition, and vaccine loading.

1.3 SPECIFIC AIMS

1.3.1 *Develop a method for integration of electrospun fibers with microneedles.*

To preserve the structure and function of electrospun fibers after microneedle integration, fibers were integrated *in situ* using microneedle molds to collect the electrospun fibers. While previous studies have used patterned electrospinning collectors to generate fiber mats with texture or aligned regions, these studies have been limited to low aspect ratio patterns and the patterning effect is often material dependent.[30-32] Here, we develop a versatile method for *in situ* three-dimensional patterning of electrospun fibers using two-layer collectors with an insulating surface layer and grounded recessed patterns. We demonstrate the use of this fiber patterning strategy for integration of electrospun fibers with mechanically robust microneedles.

1.3.2 *Demonstrate compatibility of small molecule, nucleic acid, and protein-loaded fibers with the microneedle integration method.*

To be an effective tool to study oral mucosal vaccination, integrated fiber microneedles must be able to encapsulate physicochemically diverse antigens and adjuvants. Previous studies have demonstrated the ability to encapsulate small molecules, nucleic acids, and proteins into electrospun fibers or microneedles individually. However, the loading of biologics in previously developed electrospun fiber formulations is too low to be relevant for vaccine delivery using integrated fiber microneedles and the loading of pharmaceutical agents in conventional microneedles has been shown to affect the microneedle mechanical properties.[25,33,34] Here we identify candidate formulations of protein and nucleic acids in electrospun fibers with potential for relevant loading in the integrated fiber microneedle device. We also demonstrate that fiber formulations containing small molecules, protein, or nucleic acids are compatible with the fiber microneedle integration process developed in the first aim. Finally, we use two specific formulation examples to compare the release kinetics and mechanical performance of integrated fiber microneedles to conventional matrix microneedles.

1.3.3 *Characterize the immunological function of three distinct integrated fiber microneedle designs in a mouse model.*

Previous studies of microneedle-mediated oral mucosal vaccination have been limited primarily to solid microneedles with a single geometry coated with immunogens, and immunogenicity of these vaccines has been highly variable.[16-18,35,36] Work in the more established field of microneedle mediated dermal vaccination have demonstrated distinct effects of microneedle geometry, release kinetics, and delivery site on immunogenicity.[37-39] Here, we characterize for the first time the humoral and cellular immune response to a model protein

vaccine delivered using integrated fiber microneedles with varying length and release kinetics in the buccal and sublingual mucosa.

1.4 SUMMARY

Together, this work has resulted in the development of an integrated fiber microneedle device designed with capabilities to address gaps in current oral mucosal delivery systems. Importantly, the fiber-microneedle integration method developed in this work could be applied to many applications requiring three-dimensional patterning of electrospun fibers including potential applications in tissue engineering or microfluidics. Additionally, the integrated fiber microneedle device could be used to address challenges with existing conventional microneedle devices such as hydrophobic small molecule drug loading and release or delivery efficiency. Ultimately, we expect that this work will contribute to the field of oral mucosal vaccination as well as the broader fields of drug and vaccine delivery using electrospun fibers or microneedles.

1.5 REFERENCES

1 Shim, B. S. *et al.* Sublingual immunization with recombinant adenovirus encoding SARS-CoV spike protein induces systemic and mucosal immunity without redirection of the virus to the brain. *Virol J* **9**, 215, doi:10.1186/1743-422X-9-215 (2012).

2 Lee, H. J. *et al.* Sublingual Immunization of Trivalent Human Papillomavirus DNA Vaccine in Baculovirus Nanovector for Protection against Vaginal Challenge. *Plos One* **10**, doi:10.1371/journal.pone.0119408 (2015).

3 Cho, H. J. *et al.* Enhanced humoral and cellular immune responses after sublingual immunization against human papillomavirus 16 L1 protein with adjuvants. *Vaccine* **28**, 2598-2606, doi:10.1016/j.vaccine.2010.01.013 (2010).

4 Lundholm, P., Asakura, Y., Hinkula, J., Lucht, E. & Wahren, B. Induction of mucosal IgA by a novel jet delivery technique for HIV-1 DNA. *Vaccine* **17**, 2036-2042 (1999).

5 Humphrey, S. P. & Williamson, R. T. A review of saliva: normal composition, flow, and function. *J Prosthet Dent* **85**, 162-169, doi:10.1067/mpr.2001.113778 (2001).

6 Shojaei, A. H. Buccal mucosa as a route for systemic drug delivery: a review. *J Pharm Pharm Sci* **1**, 15-30 (1998).

7 Law, S., Wertz, P. W., Swartzendruber, D. C. & Squier, C. A. Regional variation in content, composition and organization of porcine epithelial barrier lipids revealed by thin-layer chromatography and transmission electron microscopy. *Arch Oral Biol* **40**, 1085-1091 (1995).

8 White, J. A. *et al.* Serum and mucosal antibody responses to inactivated polio vaccine after sublingual immunization using a thermoresponsive gel delivery system. *Hum Vaccin Immunother* **10**, 3611-3621, doi:10.4161/hv.32253 (2014).

9 Borde, A., Ekman, A., Holmgren, J. & Larsson, A. Effect of protein release rates from tablet formulations on the immune response after sublingual immunization. *Eur J Pharm Sci* **47**, 695-700, doi:10.1016/j.ejps.2012.08.014 (2012).

10 Song, J.-H. *et al.* CCR7-CCL19/CCL21-Regulated Dendritic Cells Are Responsible for Effectiveness of Sublingual Vaccination. *The Journal of Immunology* **182**, 6851, doi:10.4049/jimmunol.0803568 (2009).

11 Nudel, I. *et al.* Dendritic cells in distinct oral mucosal tissues engage different mechanisms to prime CD8+ T cells. *J Immunol* **186**, 891-900, doi:10.4049/jimmunol.1002943 (2011).

12 Dieu, M. C. *et al.* Selective recruitment of immature and mature dendritic cells by distinct chemokines expressed in different anatomic sites. *The Journal of experimental medicine* **188**, 373-386, doi:10.1084/jem.188.2.373 (1998).

13 Aramaki, O., Chalermsarp, N., Otsuki, M., Tagami, J. & Azuma, M. Differential expression of co-signal molecules and migratory properties in four distinct subsets of migratory dendritic cells from the oral mucosa. *Biochem Biophys Res Commun* **413**, 407-413, doi:10.1016/j.bbrc.2011.08.099 (2011).

14 Chalermsarp, N. & Azuma, M. Identification of three distinct subsets of migrating dendritic cells from oral mucosa within the regional lymph nodes. *Immunology* **127**, 558-566, doi:10.1111/j.1365-2567.2008.03031.x (2009).

15 Ma, Y., Boese, S. E., Luo, Z., Nitin, N. & Gill, H. S. Drug coated microneedles for minimally-invasive treatment of oral carcinomas: development and in vitro evaluation. *Biomed Microdevices* **17**, 44, doi:10.1007/s10544-015-9944-y (2015).

16 Ma, Y. *et al.* Vaccine delivery to the oral cavity using coated microneedles induces systemic and mucosal immunity. *Pharm Res* **31**, 2393-2403, doi:10.1007/s11095-014-1335-1 (2014).

17 McNeilly, C. L. *et al.* Microprojection arrays to immunise at mucosal surfaces. *J Control Release* **196**, 252-260, doi:10.1016/j.jconrel.2014.09.028 (2014).

18 Oh, Y. J. *et al.* Ovalbumin and cholera toxin delivery to buccal mucus for immunization using microneedles and comparison of immunological response to transmucosal delivery. *Drug Deliv Transl Res*, doi:10.1007/s13346-021-00964-z (2021).

19 Cuburu, N. *et al.* Sublingual immunization induces broad-based systemic and mucosal immune responses in mice. *Vaccine* **25**, 8598-8610, doi:10.1016/j.vaccine.2007.09.073 (2007).

20 Busignies, V. *et al.* Development and pre-clinical evaluation in the swine model of a mucosal vaccine tablet for human influenza viruses: A proof-of-concept study. *International Journal of Pharmaceutics* **538**, 87-96, doi:10.1016/j.ijpharm.2018.01.021 (2018).

21 Jing, Z. *et al.* Biodegradable electrospun fibers for drug delivery. *Journal of Controlled Release* **92**, 227-231, doi:10.1016/S0168-3659(03)00372-9 (2003).

22 Rujitanaroj, P. O., Wang, Y. C., Wang, J. & Chew, S. Y. Nanofiber-mediated controlled release of siRNA complexes for long term gene-silencing applications. *Biomaterials* **32**, 5915-5923, doi:10.1016/j.biomaterials.2011.04.065 (2011).

23 Sill, T. J. & von Recum, H. A. Electrospinning: applications in drug delivery and tissue engineering. *Biomaterials* **29**, 1989-2006, doi:10.1016/j.biomaterials.2008.01.011 (2008).

24 Park, J.-H., Allen, M. G. & Prausnitz, M. R. Biodegradable polymer microneedles: Fabrication, mechanics and transdermal drug delivery. *Journal of Controlled Release* **104**, 51-66, doi:http://dx.doi.org/10.1016/j.jconrel.2005.02.002 (2005).

25 Park, J. H., Allen, M. G. & Prausnitz, M. R. Polymer microneedles for controlled-release drug delivery. *Pharmaceutical Research* **23**, 1008-1019, doi:10.1007/s11095-006-0028-9 (2006).

26 Lee, J. W., Park, J. H. & Prausnitz, M. R. Dissolving microneedles for transdermal drug delivery. *Biomaterials* **29**, 2113-2124, doi:10.1016/j.biomaterials.2007.12.048 (2008).

27 Mc Crudden, M. T. C. *et al.* Design, Formulation, and Evaluation of Novel Dissolving Microarray Patches Containing Rilpivirine for Intravaginal Delivery. *Advanced Healthcare Materials* **8**, 1801510, doi:10.1002/adhm.201801510 (2019).

28 McCrudden, M. T. *et al.* Laser-engineered dissolving microneedle arrays for protein delivery: potential for enhanced intradermal vaccination. *J Pharm Pharmacol* **67**, 409-425, doi:10.1111/jphp.12248 (2015).

29 Migalska, K. *et al.* Laser-engineered dissolving microneedle arrays for transdermal macromolecular drug delivery. *Pharm Res* **28**, 1919-1930, doi:10.1007/s11095-011-0419-4 (2011).

30 Dempsey, D. K. *et al.* Micropatterning of Electrospun Polyurethane Fibers Through Control of Surface Topography. *Macromolecular Materials and Engineering* **295**, 990-994, doi:10.1002/mame.201000152 (2010).

31 Ding, Z., Salim, A. & Ziaie, B. Selective Nanofiber Deposition through Field-Enhanced Electrospinning. *Langmuir* **25**, 9648-9652, doi:10.1021/la901924z (2009).

32 Cheng, Q., Lee, B. L. P., Komvopoulos, K. & Li, S. Engineering the Microstructure of Electrospun Fibrous Scaffolds by Microtopography. *Biomacromolecules* **14**, 1349-1360, doi:10.1021/bm302000n (2013).

33 Chen, Y., Chen, B. Z., Wang, Q. L., Jin, X. & Guo, X. D. Fabrication of coated polymer microneedles for transdermal drug delivery. *Journal of Controlled Release* **265**, 14-21, doi:10.1016/j.jconrel.2017.03.383 (2017).

34 Loizidou, E. Z. *et al.* Structural characterisation and transdermal delivery studies on sugar microneedles: Experimental and finite element modelling analyses. *European Journal of Pharmaceutics and Biopharmaceutics* **89**, 224-231, doi:10.1016/j.ejpb.2014.11.023 (2015).

35 van Loon, L. A., Krieg, S. R., Davidson, C. L. & Bos, J. D. Quantification and distribution of lymphocyte subsets and Langerhans cells in normal human oral mucosa and skin. *J Oral Pathol Med* **18**, 197-201 (1989).

36 Hasséus, B., Jontell, M., Bergenholtz, G. & Dahlgren, U. I. T-cell costimulatory capacity of oral and skin epithelial cells in vitro: presence of suppressive activity in supernatants from skin epithelial cell cultures. *Eur J Oral Sci* **112**, 48-54 (2004).

37 van der Maaden, K., Sekerdag, E., Jiskoot, W. & Bouwstra, J. Impact-insertion applicator improves reliability of skin penetration by solid microneedle arrays. *AAPS J* **16**, 681-684, doi:10.1208/s12248-014-9606-7 (2014).

38 van der Maaden, K. *et al.* Parameter optimization toward optimal microneedle-based dermal vaccination. *Eur J Pharm Sci* **64**, 18-25, doi:10.1016/j.ejps.2014.08.004 (2014).

39 DeMuth, P. C., Min, Y., Irvine, D. J. & Hammond, P. T. Implantable Silk Composite Microneedles for Programmable Vaccine Release Kinetics and Enhanced Immunogenicity in Transcutaneous Immunization. *Advanced Healthcare Materials* **3**, 47-58, doi:10.1002/adhm.201300139 (2014).

Chapter 2. INTRODUCTION

Adapted from: **Creighton, R.**, Woodrow, K.A: Microneedle-mediated vaccine delivery to the oral mucosa. Adv. Healthc. Mater. 2018. 8. 1801180. Copyright Wiley-VCH GmbH. Reproduced with permission.

2.1 ABSTRACT

The oral mucosa is a minimally invasive and immunologically rich site that has been underutilized for vaccination due to physiological and immunological barriers. To develop effective oral mucosal vaccines, key questions regarding vaccine residence time, uptake, adjuvant formulation, dose, and delivery location must be answered. However, currently available dosage forms are insufficient to address all of these questions. An ideal oral mucosal vaccine delivery system would improve both residence time and epithelial permeation while enabling efficient delivery of physicochemically diverse vaccine formulations. Microneedles have demonstrated these capabilities for dermal vaccine delivery. Additionally, microneedles enable precise control over delivery properties like depth, uniformity, and dosing, making them an ideal tool to study oral mucosal vaccination. Select studies have demonstrated the feasibility of microneedle mediated oral mucosal vaccination, but they have only begun to explore the broad functionality of microneedles. This chapter describes the physiological and immunological challenges related to oral mucosal vaccine delivery and provides specific examples of how microneedles can be used to address these challenges. It summarizes and compares the few existing oral mucosal microneedle vaccine studies and offers a perspective for the future of the field.

2.2 BACKGROUND

A vast majority of pathogens infect humans via mucosal surfaces, where local immune responses serve as the first line of defense to prevent infection. Mucosal responses that are particularly key in providing protection include innate immune factors like γδ T cells, and adaptive immune factors like mucosal IgA antibodies and antigen specific cytotoxic T cells.[1-3] Intraepithelial lymphocytes like γδ T cells perform multiple functions, including maintaining the epithelial barrier and killing infected cells.[4,5] Secretory IgA antibodies bind pathogens to inhibit their entry into the mucosa, induce phagocytosis through CD89 binding, and activate the complement cascade through the lectin pathway and the alternative pathway.[6,7] Upon pathogen entry, cytotoxic T cell responses can restrict infection by selectively killing infected cells.[8,9] Vaccine studies in mice deficient in TLR signaling and IgA antibody secretion have confirmed the importance of both innate and adaptive immunity in protection from infection.[10] Collectively, these local responses can prevent pathogen entry and infection at mucosal sites and are the primary effector mechanisms desired for effective mucosal vaccines.

Evidence strongly suggests that mucosal immune responses are strongest when elicited from mucosal rather than parenteral routes of administration.[1,11] Studies directly comparing mucosal or parenteral vaccination show that mucosal vaccine delivery generates a higher quantity of mucosal IgA antibodies and a higher frequency of mucosal cytotoxic T lymphocytes. Data also suggests that mucosal vaccination generates more sustained mucosal immune responses than those from parenteral vaccination.[12-15] However, parenteral and mucosal administration will likely need to be combined to elicit both robust systemic and mucosal immune responses.[12,16-20] For example, compared to intramuscular prime and boost alone, sublingual prime with a whole inactivated flu virus combined with an intramuscular boost

Table 2.1. Systemic and mucosal immune responses elicited from parenteral or mucosal vaccines

Vaccine type	Routes Tested	Systemic Response		Mucosal Response		Source
Protein (cholera toxin)		IgG	IgA	IgG[a)]	IgA[a)]	[21]
	GI [b)]	+	+	++	++	
	IR [c)]	+	++	-	-	
	I vag [d)]	++	++	+++	+++	
	TD [e)]	+++	+	-	-	
Protein (HPV 16 L1)		IgG		Vaginal IgA	Saliva IgA	[15]
	IN [f)]	+		+++	+	
	SL [g)]	+++		+++	+++	
	I vag	-		-	-	
	TD	++		+	-	
	IM [h)]	+		+	-	
Adenoviral vector ($GagPol_{SIV}$, Env_{SIV})		CD4	CD8	Bronchoalveolar lavage CD4	Bronchoalveolar lavage CD8	[22]
	IN	+	+	++	++	
	Aerosol	++	-	+++	+++	
	IM	+++	+	+	-	
Adenoviral vector (Ag85A)		IFN-γ		Lung CD4	Lung CD8	[12]
	IN	-		++	++	
	IM	+++		-	++	
Adenoviral vector (glycoprotein B of herpes simplex virus)		CTL memory		Mesenteric lymph node CTL memory		[23]
	IN	+		+++		
	IM	+++		-		
Adenoviral vector (spike protein of SARS-CoV)		IgG	CD8	Bronchoalveolar lavage IgA	Lung CD8	[24]
	SL	++	+	++	+++	
	IN	++	+	++	+++	
	IM	+++	+++	n.d.[i)]	+	
Live attenuated (Bacillus Calmette-Guerin)		T cell (CD4, CD8)		T cell (CD4, CD8)		[25]
	IN	++		++		
	TD	++		-		
Baculovirus nanovector (trivalent human papillomavirus-16L1, -18L1, -58L1)		IgG	CD4 CD8	Vaginal IgA		[26]
	SL	++	++ +++	+++		
	IM	+++	+++ +++	++		
Salmonella vector (glycoprotein D of herpes simplex virus 2)		IgG	CD4 CD8	Peyer's Patch CD8	Vaginal CD8	[27]
	GI	+	+ +++	+++	+	
	IM	+++	+ +	-	-	
Plasmid DNA (tat, gp160, gag)		IgG	IgA	Lung IgA Lung IgG	GI IgA GI IgG	[28]
	IN	+++	+++	++ +++	+ +	
	Buccal	++	++	+++ +++	++ -	
	Oral gene gun	+	+	- +	++ +	
	IM	++	++	++ ++	+ -	

a) Location of mucosal antibody responses was not specified; Abbreviations: b) gastrointestinal; c) intrarectal; d) intravaginal; e) transdermal; f) intranasal; g) sublingual; h) intramuscular; i) not determined.

generated significantly higher hemagglutinin inhibition titers and nasal IgA titers.[16] More research is needed to determine the optimal prime-boost schedule, delivery methods, and vaccine formulations depending on the specific pathogen, but a body of data support the continued development of mucosal vaccines for the prevention of pathogens that are otherwise challenging to combat with parenteral vaccination alone.

A promising attribute of mucosal vaccination is that immune responses can be elicited at distal locations from the site of induction. Compartmentalization of mucosal immune mechanisms occur in specific patterns and have been reviewed in detail by others, but a brief overview will be given here for context.[1,11,29] Following mucosal vaccine administration, antigens are taken up by mucosal tissue resident antigen presenting cells, which then migrate to the draining lymph node through chemokine signaling. In the lymph node, these antigen presenting cells induce up-regulation of receptors such as β7 integrins and CCR9 on effector cells. After travelling through the circulation, effector cells home back to the site of antigen encounter through interactions with ligands such as MAdCAM-1 expressed on mucosal high endothelial venule cells or CCL25 expressed by mucosal epithelial cells. Because integrins and cytokines are differentially expressed at mucosal surfaces, vaccination at one mucosal surface can induce effector responses at that site and at additional mucosal sites.[11] Vaccine delivery to several mucosal surfaces can result in distal effector responses, including intranasal (effector responses in respiratory and vaginal mucosa), oral mucosal (OM) (effector responses in the oral, respiratory, vaginal, rectal mucosa), and gastrointestinal (effector responses in the oral, gut mucosa) (Table 2.1).[15,21,24,28]

Compared to parenteral vaccines, development of effective mucosal vaccines has been slow due to unique physical and immunological barriers present in mucosal compartments. For

example, delivery via the gastrointestinal route requires protection of the vaccine components in the harsh gastric environment and effective absorption and activation in the gut. To survive the low pH of the stomach, most oral vaccines are live attenuated formulations, which are known to cause some adverse events.[30,31] The intranasal route carries a risk of severe neurological adverse effects, despite its demonstrated ability to elicit highly effective immune responses.[32] Other mucosal routes like intravaginal and intrarectal vaccination may induce strong immune responses locally in the genital tract, but systemic responses and mucosal immune responses in distal locations are modest. Currently, there are licensed mucosal vaccines for five different pathogens: rotavirus, poliovirus, *Salmonella* Typhi, *Vibrio cholera,* and influenza. Most of these vaccines are delivered orally to the gastrointestinal associated lymphoid tissue with the exception of the influenza mucosal vaccine, which is delivered intranasally.[33] The currently licensed gastrointestinal vaccines such as RotaTeq ®, Rotarix ®, and the oral polio vaccine require up to four doses, show variable efficacy, and there are some safety concerns due to their live attenuated formulation.[30,31] Additionally, while the intranasal flu vaccine is highly effective in children, its efficacy in adults is highly variable for reasons that are not well understood.[34-36] Development of more effective mucosal vaccines will require a better understanding of both the physiological and immunological barriers specific to different mucosal compartments.

One mucosal site that warrants further study is vaccination to the oral cavity, which includes the buccal and sublingual mucosa and the palatine and lingual tonsils in Waldeyer's Tonsillar Ring (WTR). These tissues are rich in immune cells, but access to and activation of these cells requires overcoming barriers like saliva, stratified squamous epithelium, and a predisposition for immunological tolerance. Existing dosing strategies to the oral cavity have a limited ability to address both physiological and immunological barriers. For example, while

aqueous suspensions allow formulation of many vaccine compositions, they have low oral residence time and are primarily limited to sublingual delivery. Oral dosing strategies that can decouple and overcome these barriers will promote our understanding of oral immunity and enable development of optimized vaccines for oral mucosal delivery. Microneedles have been studied extensively for intradermal vaccine delivery and possess characteristics like tunable geometry, dimension, and materials design to address questions about oral mucosal immunity. Very few studies have applied microneedles to the oral cavity, and there is significant room for innovation in this field. Ultimately, this work could lead to innovative oral mucosal microneedle vaccines and also a better understanding of oral mucosal immunity.

2.3 THE ORAL MUCOSA IS A PROMISING AND UNDERUTILIZED ROUTE OF VACCINE DELIVERY

The oral cavity is an attractive route for mucosal vaccination, but it has been underutilized in previous studies compared to intranasal and gastrointestinal routes. The oral cavity is easily accessible, minimally invasive, contains rich lymphoid tissue, and it has a pH that is more favorable for biologics compared to the gastrointestinal tract. Additionally, evidence suggests that oral mucosal vaccine delivery elicits systemic humoral and cellular immune responses comparable to intramuscular vaccination, and enhances levels of mucosal antibody responses locally and at distal sites such as the nasal cavity and female reproductive tract.[15,26,37,38] However, vaccine delivery to the oral cavity has been limited by a lack of appropriate dosage forms to address physical barriers such as salivary flow and barriers to immune activation such as the predisposition for oral mucosal immune cells to be tolerogenic.

2.3.1 *Immunization in the WTR, buccal, and sublingual mucosa of the oral cavity*

The oral mucosa is a particularly promising route for vaccination due to direct access to the rich lymphoid tissue of the Waldeyer's tonsillar ring (WTR), specifically the palatine and lingual tonsils.[39-41] Like Peyer's patches in the gut, tonsils are not fully encapsulated by connective tissue, allowing direct antigen uptake. While the outer surface of the tonsils consists of a non-keratinized stratified squamous epithelium, the tonsils contain large crypts lined by a lymphoepithelium (Figure 2.1a). This non-uniform network of reticulated epithelial cells, antigen presenting cells, and lymphocytes function as transporters for secreted IgG, IgA, and IgM antibodies and provides a direct method of antigen transport.[42-44] The subepithelial lymphoid tissue consists of B-cell rich secondary lymphoid follicles surrounded by T-cell rich interfollicular regions, and it contains a variety of dendritic cell (DC) subsets capable of inducing immunogenic or tolerogenic responses.[45] Lymphocytes infiltrate the follicular and interfollicular

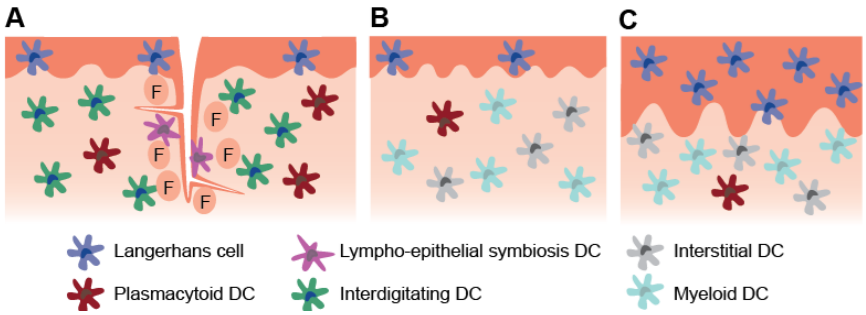

Figure 2.1. Schematic representation of the mucosal structure and select dendritic cell subsets.

a) The lingual and palatine tonsils are covered with ~100 µm thick stratified squamous epithelium and contain crypts lined by a non-uniform lymphoepithelium. The outer epithelium primarily contains Langerhans cells, while the crypt epithelium contains lympho-epithelial symbiosis DCs along with macrophages and lymphocytes (not depicted). Other DC populations including plasmacytoid DCs and interdigitating DCs densely populate the follicular region (F). Germinal center DCs are also present within germinal centers (not depicted). b) In humans, the sublingual epithelium ranges from 100-200 µm thick, while the buccal epithelium ranges from 500-800 µm thick. c) The murine buccal epithelium contains approximately 2.5 times the number of Langerhans cells in the sublingual epithelium. Submucosal DC subsets are not well characterized in humans, but evidence suggests that interstitial and myeloid DCs are present and plasmacytoid DCs may infiltrate during inflammation.

regions via capillaries, high endothelial venules, or through interruptions in the basement membrane.[46]

Because of its specialized lymphoid function, the WTR is an attractive site for immunization that may be accessed through intranasal or oral mucosal routes. Previous studies have accessed the WTR primarily through intranasal aerosol vaccine delivery, which has demonstrated potent immune responses.[47-49] However, adverse neurological effects such as Bell's palsy may occur due to vaccine entry into the olfactory bulb.[32,40,50] While continued studies of intranasal vaccine delivery are identifying new adjuvants and new delivery systems to improve the safety profile of these vaccines,[51-53] alternative strategies to access the WTR are also warranted. A select number of studies have vaccinated animals by applying the vaccine directly to the palatine or lingual tonsils (Table 2.1).[19,54-56] In one study, tonsillar delivery of a vaccinia vector expressing HIV envelope and SIV gag-pol proteins generated neutralizing antibodies and protected primates from SIV challenge when combined with an intramuscular protein boost.[19] Another study delivered an adenoviral vector to the tonsils and observed systemic antigen specific cellular and humoral immune responses that led to a 83-fold reduction in peak viral RNA during challenge compared to intramuscular delivery.[54] Finally, in a study of tonsillar delivery of a live attenuated SIV vaccine, researchers found that a tonsillar SIV challenge was controlled locally in the tonsils, primarily by γδ T cells and mature DCs. Systemically, there were no significant increases of viral RNA in the blood of vaccinated primates or of productively infected cells in lymphoid organs.[56] Therefore, the oral mucosal route has demonstrated success as a relatively simple route for vaccination of the rich WTR lymphoid tissue.

Vaccines have also been delivered to the sublingual and buccal mucosa in the oral cavity, and has been reviewed in full by Kraan et al.[57] Both sites contain a stratified squamous epithelium, but the epithelium of the buccal mucosa is approximately four times thicker than the sublingual mucosa.[58] While both sites lack the organized mucosal lymphoid tissue present in the tonsils, they contain diverse populations of antigen presenting cells (Figure 2.1b, 2.1c).[59-61] Both contain Langerhans cells within the mucosal epithelium, which are the primary antigen sampling cells, although in humans the frequency of Langerhans cells in the buccal mucosa is approximately 2.5-fold greater than the sublingual mucosa.[62] Although not well characterized in humans, there are significant differences between the submucosal DC population of the buccal and sublingual mucosa in mice. For example, the murine buccal submucosa contains a much higher frequency of langerin+CD103+ DCs and langerin-CD103+ DCs compared to the sublingual mucosa. These DCs are capable of priming CD4 and CD8 T cells, making them a potential vaccine target. However, only the sublingual mucosa contains plasmacytoid DCs, another potential vaccine target that are unresponsive to bacterial TLRs, but respond strongly to single stranded RNA through TLR7 and TLR9.[63,64] Plasmacytoid DCs are able to enter the sublingual submucosa from circulation, produce type 1 interferon, and induce T cell activation in the draining lymph nodes.[65] It was also recently determined in rhesus macaques that the buccal mucosa contains a significantly higher population of conventional myeloid dendritic cells and interstitial dendritic cells compared to the sublingual mucosa.[66]

Vaccine delivery to the sublingual and buccal mucosa can generate mucosal immune responses at distal sites including the urogenital tract, the respiratory tract, and the intestinal tract.[26,49,67,68] A wide variety of systemic and mucosal immune responses have been induced by vaccine delivery to these sites (Table 2.1). Despite the differences in immune cell populations

between different regions of the oral mucosa, it is challenging to identify patterns in immune outcomes from existing vaccine studies potentially because immune responses are confounded by differences in vaccine bioavailability at different mucosal locations. For example, topical aqueous vaccination in the sublingual mucosa is generally more common and has more reliably generated humoral and cellular mucosal immune responses compared to aqueous formulations in the buccal mucosa (Table 2.1). Notably, studies that have observed mucosal immune responses after buccal vaccination used specialized delivery systems

Table 2.2. Systemic and mucosal immune responses induced by vaccination at different regions of the oral mucosa

Delivery location	Vaccine type	Systemic Response				Mucosal Response						Source
Buccal	Measles virus nucleoprotein	IgG	CD8			No IgG in lung						69
	Killed whole cell Streptococcus pneumonae	IL-17A responses				n.d. [a]						70
	Synthetic HPV long peptide[b]	CD8				Buccal CD8						71
	Plasmid DNA (HA) [b]	CD8				n.d.						72
	Protein (OVA)[c]	IgG				Buccal IgA	Lymph node IgA	Peyer's Patch IgA				73
	Plasmid DNA (HIV- tat, gp160, gag) [d]	IgG	IgA			Lung IgA	Lung IgG	No GI IgG				28
Sublingual	Adenoviral vector (HIV-gag)	CD8				Submandibular Lymph node CD8						74
	RSV glycoprotein	IgG				BAL IgA	CD4					75
	Adenoviral vector (RSV glycoprotein)	IgG	CD8			BAL IgA	CD8					76
	Protein (HPV 16 L1)	IgG	CD8			Vaginal IgA	Saliva IgA					15
	Adenoviral vector (HIV-1 Env)	IgG	IgA			Vaginal IgG	Vaginal IgA					77
	Adenoviral vector (spike protein of SARS-CoV)	IgG	CD8			BAL IgA	Lung CD8					24
	Tetanus toxoid	IgG				Saliva IgA	Vaginal IgA	Rectal IgA				78
	Inactivated influenza	IgG	IgA	CD4	CD8	BAL IgG	BAL IgA	Nasal IgA	Saliva IgA	Rectal IgA		10
	Live influenza	IgG				BAL IgG	BAL IgA	Nasal IgA	Saliva IgA	Rectal IgA		10
	Protein (OVA)	IgG	CD8			Saliva IgG	Saliva IgA	Nasal IgG	Nasal IgA	BAL IgG	BAL IgA	79
WTR	Single cycle immunodeficiency virus vaccine [e]	IgG	CD8			n.d.						54
	Recombinant modified vaccinia virus Ankara [d]	IgG	CD8			n.d.						55
	Attenuated recombinant vaccinia vector (HIV SF162 Env, SIV gag-pol)	IgG	IgA	CD8		Saliva IgG	Rectal IgG					19

[a] not determined; [b] Vaccine injected in buccal mucosa using hypodermic needle; [c] Vaccine delivered to buccal mucosa using Microjet technology; [d] Vaccine administered using Syrijet Mark II needleless injector; [e] Vaccine administered by oral spray; [f] bronchoalveolar lavage.

such as hypodermic needles or various needleless injection systems.[28,66,73,80] Despite these apparent limitations of buccal delivery, existing studies establish a strong rationale for the ability of various oral mucosal locations to induce broad, potent immune responses.

2.3.2 *Oral mucosal vaccination compared to dermal vaccination*

Dermal vaccine delivery has many of the same advantages of oral mucosal vaccine delivery such as ease of delivery, patient acceptability, and generation of mucosal and systemic immune responses. Although some studies have suggested oral mucosal and dermal delivery are analogous, others suggest that immune cell populations in the oral mucosa have different phenotype and function that make it a potentially more effective route of vaccination.[66,81,82] For example, one study found that the population of oral mucosal Langerhans cells highly expressing MHC and co-stimulatory molecules was larger than dermal Langerhans cells. In the same study, oral mucosal Langerhans cells induced a stronger mixed lymphocyte response compared to skin Langerhans cells due in part to a lack of secreted suppressive soluble factors.[82] A study in rhesus macaques found that HIV antigen-specific serum IgG responses and IgG and IgA responses in the rectal, vaginal, and oral mucosa were significantly greater from mixed sublingual and buccal vaccination compared to intradermal and subcutaneous vaccination.[66] Furthermore, the buccal mucosa contains 37-fold higher levels of T lymphocytes in the epithelium compared to the epithelium of dermal tissue.[81] Immune responses resulting from dermal delivery are sometimes more analogous to parenteral delivery routes like intramuscular delivery, while delivery to the oral mucosa reliably results in immune responses analogous to other mucosal delivery routes (Table 2.1). Dermal vaccination fits into a unique category as a vaccine delivery route as it shares some properties with mucosal delivery and some with parenteral delivery. However,

together this evidence from cellular analysis of oral mucosal and dermal tissue and evidence from route-specific vaccination studies suggest that the oral mucosa possesses immune cells with unique phenotype and function compared to dermal tissue.

2.3.3 *Challenges of oral mucosal vaccine delivery*

The oral mucosa contains many barriers to vaccine delivery, including the physical mucosal barrier and the tolerogenic immune barrier. Oral tissues are subject to daily salivary flow of 1-1.5 L at an unstimulated rate of 0.1 mL/min.[83] This flow can dilute and completely remove vaccines before they can be taken up by antigen presenting cells in the tissue. As a result, most studies using the sublingual route require small volumes (<10 μL) and animal sedation for efficient vaccine uptake.[79] Apart from the physical barrier that saliva presents, it also contains a range of enzymes that may alter the vaccine prior to antigen presenting cell uptake. The salivary flow rate and the composition of saliva can vary with factors like age, gender, diet, and location in the mouth, further complicating oral mucosal delivery.[84,85] Additionally, the mucosal tissue itself is literally a physical barrier to vaccine delivery. To protect underlying tissues from the mechanical forces of chewing, the oral mucosa is structured as a multilayered stratified squamous epithelium. In regions where masticatory forces are especially strong, like the hard palate and the gingiva, a tough keratinized layer also protects the tissue. The thickness of the human oral epithelium varies greatly depending on specific location, ranging from 500-800 μm in the buccal region and 100-200 μm sublingually.[58] Studies have indicated that large molecules move through these epithelial layers primarily by intercellular transport. However, the intercellular space of the oral epithelium contains lipids and molecules like ceramides and glycosylceramides that limit the intercellular transport of nonpolar molecules.[86,87] This barrier mechanism limits the depth that

large molecules may penetrate into the tissue, meaning that uptake of topically applied vaccines is limited to Langerhans cells located superficially within the epithelium.

In addition to these physical barriers of the oral cavity, the tolerogenic environment presents a significant challenge for oral vaccination. A key goal of mucosal immunization is to induce innate immune responses that will overcome tolerance and induce protective adaptive immunity without abrogating natural mucosal barriers. In contrast to the systemic immune system, which responds vigorously to pathogens that enter the sterile circulatory system or internal organs, mucosal administration of immunogens in the absence of inflammatory stimuli is widely recognized to induce a state of active unresponsiveness.[59,88,89] This tolerance is important to maintain the balance of commensal bacteria in the oral cavity and to prevent uncontrolled immune responses to innocuous ingested food particles. In fact, the predisposition for tolerance has been harnessed to treat allergies through sublingual immunotherapy. Oral mucosal tolerance is not fully understood, but it is thought to be mediated through a variety of different mechanisms that includes activation of DCs by TLR2 or TLR4, antigen uptake by CD206 or ICAM-3-grabbing non-integrin binding, and antigen uptake by CD11b+ CD11c- macrophage-like cells.[59,90,91]

Induction of tolerance versus immunogenicity will vary based on the site of delivery in the oral cavity due to differences in antigen presenting cell populations (Figure 2.1). While Langerhans cells are most often the target of oral mucosal vaccines due to their superficial location and high rates of sampling at the surface of the oral epithelium, these cells are also thought to be the key mediators of regulatory T cell responses and may not be the ideal cell population for vaccine uptake.[59] Oral mucosal Langerhans cells constitutively express the FCεR1 receptor, which is important for immune regulation and homeostasis.[92,93] Langerhans cells have

also been found to migrate slowly after activation and to express low levels of co-stimulatory molecules CD86, CD273, and CD274 compared to other oral mucosal DC populations.[94] Submucosal DCs, which are thought to be more immunogenic than Langerhans cells, vary in frequency and phenotype between regions of the oral mucosa, responding to different pathogen-associated molecular patterns and resulting in different immune responses. Furthermore, submucosal DC populations can vary greatly depending on age, presence of oral pathology, and composition of the oral microbiome. A full description of these complexities is outside the scope of this review but has been reviewed elsewhere.[3,89,90,95] These properties of oral mucosal Langerhans cells and distinct DC populations necessitate careful selection of antigen and adjuvant formulations depending on the dosing location to ensure stimulation of the desired immune response.

In addition to vaccine composition and delivery site, delivery kinetics must be considered as a potential factor in the immunogenicity of oral mucosal vaccines. Evidence strongly suggests that sustained delivery of vaccines via transdermal, subcutaneous, or intra-lymph node injection can enhance humoral immune responses up to 19-fold and cellular immune responses up to 10-fold.[96-102] In these studies, vaccine release is sustained for 4 days for intra-lymph node delivery and up to 4 weeks for intradermal delivery.[97,100] Furthermore, sustained vaccine delivery has been shown to improve the persistence of immune responses, demonstrating enhanced serum IgG titers compared to boosted bolus vaccines at an 80 day time point.[101] Due to limitations of currently available dosage forms, the effect of sustained vaccine delivery in the oral mucosa on resulting immune responses is not well understood. While the majority of existing data on oral mucosal vaccination have delivered a bolus of vaccine, one study delivered low doses of antigen at narrow time intervals to achieve tolerance.[103] With repeated dosing, DC morphology changed

to a more rounded structure and had reduced capacity for migration to the draining lymph node. Interestingly, this effect was only observed in the sublingual mucosa, not in the buccal mucosa. Therefore, while sustained vaccine delivery at other anatomical sites has increased vaccine immunogenicity, more experiments are needed to understand how the interplay of vaccine delivery kinetics and delivery location can affect immune outcomes from vaccine delivery to the oral mucosa.

2.3.4 *Strategies to overcome physical and immunological barriers*

Physical barriers may be overcome through the development of dosage forms with high viscosity or mucoadhesion to increase oral mucosal residence time, therefore improving the likelihood of uptake by antigen presenting cells (Figure 2.2). Existing reviews summarize the use of various dosage forms for oral mucosal delivery.[104-106] Technologies such as mucoadhesive gels, films, and tablets have been developed that can reduce the effects of salivary washout and allow more time for antigen uptake without dilution. These semi-solid and solid dosage forms can theoretically overcome select limitations of aqueous topical delivery including the small dosage volume and need for sedation. However, implementation of these dosage forms is still

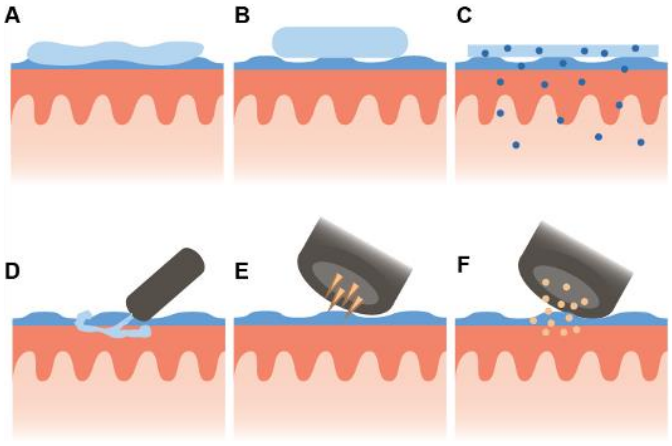

Figure 2.2. Schematics of delivery for selected oral mucosal vaccine dosage forms.

Figure depicts a) a thermo-responsive gel, b) a tablet, c) a film containing nanoparticles, d) MucoJet, e) electroporation, and f) a gene gun.

highly complex. In a study of a thermoresponsive gel for polio vaccination in mice, anesthetization was still necessary to generate any immune responses.[107] Therefore, this gel offers little improvement in comparison with topical aqueous formulations. Tablet formulations have faced similar problems, with one study demonstrating that a fast release tablet offered no advantage over aqueous formulation and an extended release tablet formulation produced very low immune responses.[108] This result is potentially due to an inability to overcome epithelial barriers to transport despite an improvement in residence time. Because these topical dosage forms are unable to breach epithelial barriers, vaccine uptake is likely limited to Langerhans cells. While targeting Langerhans cells has been successful in past studies, this delivery limitation hinders the use of mucoadhesive topical delivery systems to address key questions about oral mucosal immunity and the function of other DC populations residing deeper in the mucosa. An exception to this is films that deliver nanoparticles, which are able to permeate deeper in the mucosa via paracellular transport and eventually enter the lymphatics.[109] However, a lack of control over these trafficking mechanisms still precludes their use as a tool to probe the function of specific oral DC populations.

Alternative technologies for the oral cavity that have also shown promise rely on high velocity or high pressure to increase the permeability of the oral mucosal tissue to enhance uptake (Figure 2.2). These involve products like MucoJet and technologies like electroporation and gene gun.[13,73,110] The MucoJet system is a capsule containing a carbon dioxide-generating propellant. When the capsule is assembled, the propellant contacts water within the capsule, generating carbon dioxide gas and increasing the pressure within the capsule. This increase in pressure creates a high velocity jet of vaccine that can penetrate through the epithelial layer of the mucosa to access antigen presenting cells. The proof-of-concept studies using this device to

deliver the model antigen ovalbumin (OVA) suggest vastly improved systemic IgG and mucosal IgA antibody responses for the MucoJet compared to topical delivery. In contrast to mechanical forces, electroporation has also been used to deliver a 30-volt electric pulse that temporarily creates pores in buccal epithelial cells to permit entry of a DNA vaccine.[13] Electroporation combined with mucosal injection via hypodermic needle resulted in increased mucosal IgA and serum IgG responses compared to mucosal injection alone. While technologies like these can effectively overcome the physical barriers for oral mucosal vaccine delivery, these delivery systems primarily deliver vaccine to the superficial epithelium. Therefore, these technologies still are not able to specifically address questions about the role of different immune cells in oral immunity. Additionally, it is unclear how these systems could be adapted to probe questions about vaccine delivery kinetics.

Because of the plethora of mechanisms to induce oral tolerance, oral mucosal vaccines must be carefully designed to overcome this immunological barrier with the proper adjuvants and delivery vectors to instead activate pro-inflammatory pathways. It is important to note that mucosal adjuvants commonly used in research such as cholera toxin, the heat-labile toxin of *Escherichia coli,* and their mutants are highly toxic when administered orally, limiting their clinical relevance.[111] Furthermore, there is conflicting evidence with regards to the proper adjuvants, adjuvant doses, and delivery vectors. For example, cholera toxin has been used as an adjuvant to induce both oral tolerance and oral immunogenicity.[79,112] In these studies, the conformation of the antigen and adjuvant appear to be significant. The study that induced tolerogenic responses delivered OVA conjugated to the cholera toxin B subunit while the study inducing immunity delivered OVA admixed with cholera toxin. However, this structural comparison was not made in either study, and factors such as the OVA dose differed between the

two studies, making it difficult to discern precisely what aspect of the vaccine formulation caused the induction of immunity versus tolerance. The mechanism of action of different adjuvants must also be taken into account. Evidence suggests that the ADP-ribosylating activity present in cholera toxin and cholera toxin A subunit, but not cholera toxin B subunit, is the primary mechanism of inducing immunity.[113] However, select studies have used the B unit of cholera toxin in the oral mucosa as an immunogenic adjuvant. Clearly the mechanisms for adjuvant activity of cholera toxin and its subunits are not completely understood, particularly in the context of the oral mucosa. For further detail on adjuvant mechanisms of action, readers are referred to a review by Lycke, 2005.[113] Similar conflicting evidence exists for the use of the heat-labile toxin of *Escherichia coli* and its mutants as adjuvants for oral mucosal vaccination.[78,114] Additionally, lipopolysaccharide derivatives have been successfully used in the oral cavity to induce antigen specific immune responses via the TLR4 pathway, despite evidence suggesting the TLR4 pathway stimulates tolerance in oral mucosal Langerhans cells.[92,115] In fact, another study investigating various adjuvants for oral mucosal delivery of HIV gp140 subunit vaccine and tetanus toxoid vaccine found that sublingually delivered monophosporyl lipid A, a TLR4 agonist, suppressed systemic immunogenicity.[116] Reasons for these seemingly conflicting results are unclear, but differences in vaccine application protocols or dosing regimens could be responsible.

Taken together, analysis of previous studies focused on developing new dosage forms and evaluating various adjuvants for oral mucosal delivery reveals key gaps and questions, relating mainly to dosing practicalities, dosing location, function of oral DC populations in immunity, and vaccine delivery kinetics. We propose that innovative microneedle designs could be used as dosage forms for oral mucosal delivery to address these outstanding questions.

2.4 MICRONEEDLES HAVE BROAD CAPABILITIES THAT COULD IMPROVE ORAL MUCOSAL VACCINE DELIVERY

Given the limitations of currently available dosage forms for vaccine delivery to the oral cavity and the large number of questions surrounding oral immunity, there is a strong rationale for developing more effective delivery technologies. An ideal vaccine delivery system for the oral cavity would enable the delivery of physicochemically diverse vaccine compositions (e.g., antigen and adjuvant) while also possessing design attributes that would overcome local physical barriers (e.g., residence time, penetration depth). Decoupling of these properties would allow specific determination of the role that different vaccine compositions delivered to different sites and immune targets cells would have on the resulting immune response. Microneedles have been widely utilized as vaccine delivery systems, primarily intradermally,[97,117-136] and have broad functionality that makes them an ideal strategy to overcome numerous challenges in oral mucosal delivery (Figure 2.3). Microneedles can be fabricated from a variety of materials into different geometries and different sizes to reach specific depths in tissue. They have also been used to deliver a broad range of antigen and adjuvant combinations. Although specific studies of microneedle mediated vaccine delivery to the oral mucosa are limited, several recent studies suggest that microneedles could overcome the limitations of previous dosage forms to improve our understanding of oral mucosal immunity and ultimately improve vaccine delivery to the oral cavity.[137-140]

2.4.1 *Microneedle geometry design*

Microneedles can be fabricated by many different strategies, resulting in a wide range of possible dimensions and geometries (Figure 2.3c, 2.3d). Most studies have used microneedles

with a standard pyramidal geometry and height range from 70 μm to 1.5 mm. However, with the wide range of fabrication techniques available, needles with virtually any dimensions are feasible to fabricate.[121,141] Conical and pyramidal needles may be fabricated using silicon based manufacturing, specialized photopolymerization processing of polymer resist, laser micromachining, and polymer drawing.[142-146] These methods for microneedle fabrication have been reviewed in detail elsewhere.[147] More complex structures with hollow geometry, serrations, and arrowheads are also possible through more complex microfabrication processes.[148-150]

The wide variety of microneedle geometries and dimensions that can be created allow for highly reproducible needle application and optimization of delivery. Multiple studies have already been conducted to study the effect of microneedle shape, height, and tip diameter on

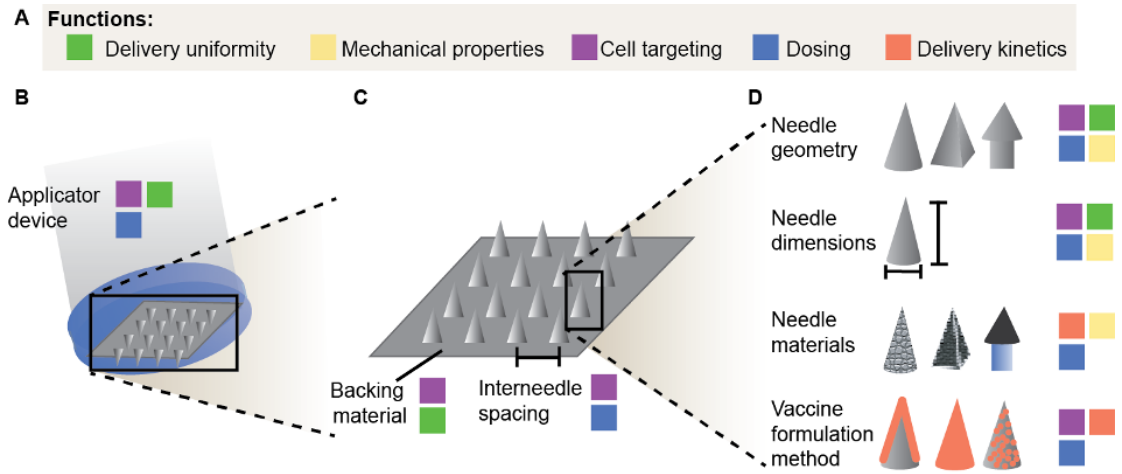

Figure 2.3. Schematic of the microneedle design space and its potential to control various functions related to oral mucosal vaccine delivery.

a) Relevant functions include: delivery uniformity, or equal tissue puncture by all needles in an array and equal delivery of vaccine components from each needle; mechanical properties, including needle strength and sharpness which are critical to easily puncture tissue; cell targeting, either actively or passively by designing the system to access a specific depth in tissue; dosing, specifically dosing efficiency, dose delivered per area of tissue, and dose per needle; and delivery kinetics, whether through design of the needle materials or integration of the vaccine with the needle. b) At the complete device scale, applicator devices may be designed to apply specific, repeatable forces across the microneedle array. c) Within a microneedle array, the backing material selection is an important consideration in ensuring close contact with the entire tissue, and interneedle spacing can affect the microneedle-tissue mechanical interactions. d) At the single needle level, needle geometry, dimensions, and materials all influence mechanical properties of the needles and resulting dose delivered after tissue puncture. Vaccines may be formulated as a coating, within the needle matrix, or encapsulated within a secondary delivery system like nanoparticles to achieve the desired dose and delivery kinetics.

insertion depth and delivery of biologics into dermal tissue.[151-153] The effect of microneedle tip diameter on skin penetration properties has shown that needles with a tip diameter of 5 μm entered the skin with approximately 25 mN of force, while a larger tip diameter of 37 μm required over 150 mN of force.[152] In general, for microneedle tip radii less than 40 μm, the force required for skin penetration is dominated by stretching of the skin around the needle, which is proportional to the circumference of the needle tip, $2\pi r$.[152] With further increases in the tip radius, the force of compressed skin under the needle tip surpasses the force to stretch the skin surface, resulting in an insertion force linearly related to the tip interfacial area.[152,154] The tip diameter also had a significant effect on penetration depth, with a 10 μm increase in tip diameter resulting in approximately a 50 μm decrease in penetration depth.[152] Microneedle geometry is also an important factor that can affect delivery of agents into tissue. A study of the effect of microneedle geometry on penetration of a fluorescent dye found that the needles with the sharpest tip and a pitch angle of 15 degrees resulted in the largest area of fluorescence deposited into the skin. However, needles with a higher aspect ratio resulted in fluorescent signal deeper in the skin.[151] Together, these results provide a rationale to control microneedle geometry and dimensions to ensure microneedles can effectively penetrate skin and efficiently deliver agents.

A particular application for microneedle design is to access specific cell populations that reside at different depths in the tissue. Aqueous formulations are primarily taken up by Langerhans cells in the superficial layers of the mucosal epithelium, while alternative DC populations that may be more immunogenic like interstitial DCs and plasmacytoid DCs reside deeper in the tissue at the mucosa/submucosa interface or in the submucosa (Figure 2.1).[59-61] In studies of dermal vaccination, significantly different serum IgG titers have been generated from microneedle arrays with different needle geometry and interneedle spacing that deliver agents at

different depths in the skin.[155] Given these promising results in dermal tissue, there is a strong rationale to evaluate the effect of microneedle design parameters such as shape, dimension, and interneedle spacing on penetration of different oral mucosal tissues and the resulting immune responses.

2.4.2 *Applicator devices for microneedle array delivery*

Multiple applicator devices have been designed for dermal microneedle insertion to improve the uniformity and the percent of the microneedle height that penetrates into the tissue (Figure 2.3b). Microneedle applicator devices can be used in conjunction with standard microneedle patch designs, or they can act to support individual needles and enable patchless microneedle array delivery.[155-157] Applicator designs include simple buttons, rollers, syringe-inspired devices, and spring loaded devices.[158,159] Details of each of these designs and additional designs have been reviewed elsewhere.[158,159] These devices are particularly important to improve the penetration of short (~300 μm) microneedles that may otherwise incompletely penetrate tissue. Verbaan et al. found that without an electric device to apply needles at high velocity (3 m/s), dermal tissue simply folded around the microneedles without penetration. However, with an applicator, needles were delivered into tissue with efficiency of approximately 83%.[157] Even higher delivery efficiency up to 97% was observed for a patchless microneedle array design in which individual microneedles supported by micropillars were applied to skin using a spring loaded device.[156] Applicators can also improve the reproducibility of microneedle insertion, which is especially significant considering the potential of microneedles to be self-administered. In a study using a simple manual device to apply a static force, van der Maaden et al. found that the applicator improved delivery efficiency and reduced the variance between insertions by non-skilled users.[155]

While existing applicator devices for dermal microneedles are unlikely to be directly translated to oral mucosal microneedle delivery, these studies suggest the promise of designing applicators to improve delivery uniformity, efficiency, and reproducibility. The improvements for oral mucosal delivery will likely be even more dramatic than dermal delivery because of the anatomy of the oral cavity. While dermal tissues are typically supported by muscle or bone, much of the oral mucosa is not. Without a firm backing to provide support, tissue may be more likely to bend around needles rather than puncture.[154,160] Existing oral mucosal microneedle vaccine studies have demonstrated variable needle penetration and dosing efficiency.[137-140] Design of applicators for oral mucosal microneedle vaccination could improve the delivery efficiency and uniformity to previously evaluated tissues such as the buccal region and the tongue. Well-designed applicators could also enable delivery of microneedles to regions that are difficult to access like the lingual or palatine tonsils. Therefore, design of applicators for oral mucosal microneedle delivery is likely to improve the quality of future oral mucosal vaccine studies and also enable delivery of microneedles to previously unexplored oral tissues.

2.4.3 *Microneedle tip implantation*

Several previous studies have been able to implant depots of biodegradable polymers into dermal tissue using microneedles. This tip implantation has been shown to improve delivery efficiency in dermal tissue and could also be particularly advantageous for the moist environment of the oral mucosa.

Silk hydrogels have been loaded into microneedle tips for implantation into skin and serve as a sustained release depot. DeMuth et al. observed that when crosslinked by methanol treatment, silk hydrogel implants maintained the model antigen OVA at detectable levels in the skin up to 16 days after initial microneedle application.[99] Other microneedle designs have

incorporated biodegradable chitosan tips on top of polylactic acid posts.[98,161] Upon application to dermal tissue of rats, the chitosan tips were implanted 600-850 μm below the tissue surface. After 60 minutes, the skin sealed over the implanted chitosan tips, resulting in depots for long term drug release. Compared to non-implantable chitosan microneedle tips fabricated by the same group that released BSA for only 4 days, tip-implantable chitosan microneedles released BSA up to 2 weeks after delivery.

Designing microneedles to achieve implantation of biodegradable tips could be useful in the oral cavity to improve dosing efficiency and to prevent salivary washout effects. With this design, there is greater confidence in the vaccine dose actually delivered into the tissue compared to topical delivery or standard microneedle delivery. Future studies to design these systems would need to consider the kinetics of tissue healing concurrently with vaccine diffusion kinetics to ensure that the tips and the encapsulated biologics are retained in the tissue. If needed, skin resealing kinetics could be optimized by changing features of the needle design such as the length, number of needles, and aspect ratio.[162]

2.4.4 *Vaccine formulations incorporated into microneedles*

Many different vaccine biologics can be formulated into microneedles due to the abundance of materials and designs that are available. Vaccine compositions have included virus-like particles, DNA polyplexes, protein subunit, and viral vectors.[97,123,126,131,134-136,163-166] Vaccine components can be formulated onto solid microneedles as coatings through a variety of dry and wet coating techniques, and these coatings can be further layered to incorporate both antigen and adjuvant.[132] Dissolving microneedles may contain antigen distributed throughout the polymer matrix forming the needle or encapsulated within nano- or microparticles in the needle (Figure 2.3d).[136]

The ability to deliver essentially any formulation of vaccine would be a leap forward for oral mucosal delivery. Previous preclinical studies of oral mucosal vaccine delivery have primarily been limited to inactivated vaccines, protein subunit vaccines, and virus-like particle vaccines. While some promising results have been observed with these vaccines, another key type of vaccine that has not been fully explored for oral mucosal delivery is DNA vaccines. In one study, a DNA-PEI polyplex prime was delivered to the sublingual or intranasal mucosa followed by a protein boost delivered to the same mucosal delivery site.[167] Sublingual delivery resulted in 10-fold lower serum IgG and IgA responses compared to intranasal delivery and insignificant mucosal IgA titers in the vaginal mucosa. In another study, plasmid DNA was incorporated into a non-replicating baculovirus nanovector for sublingual delivery compared to intramuscular delivery.[26] This delivery strategy generated comparable serum IgG titers, CD4+ and CD8+ T cell responses to intramuscular delivery. Mucosal IgA antibody titers were also very comparable to intramuscular delivery, meaning that this delivery system was not able to enhance mucosal immune responses. Other strategies for oral mucosal DNA vaccination such as electroporation have been able to elicit IgA and cellular mucosal immune responses, but the bulky and cumbersome device limits its use to specific regions of the oral mucosa.[13]

Many studies have evaluated microneedles for DNA vaccine delivery to dermal tissue.[132,133,137,168] The majority of these studies have been performed in mice, where microneedle mediated DNA vaccination has induced antigen specific cytotoxic T cell responses comparable to electroporation and antigen specific serum IgG responses superior to subcutaneous and intramuscular delivery.[132,133,168] Microneedles have also been found to enhance gene expression in non-human primates by 140-fold compared to intradermal injection, which suggests that microneedle delivery of DNA will enhance immune responses in non-human primates.[132]

Microneedles have also been used to deliver a DNA vaccine in the oral mucosa of a rabbit, one of very few studies evaluating oral mucosal microneedle vaccination, which will be reviewed further in Section 2.5.[137] Based on the demonstrated success of dermal microneedle mediated DNA delivery and the limitations of DNA delivery to the oral mucosa in previous studies, application of microneedles could overcome a major hurdle in oral mucosal DNA vaccination.

2.4.5 *Microneedle materials design used to control vaccine delivery kinetics*

Dissolving and solid microneedles can be designed to sustain release of antigens and adjuvants over time periods of days to weeks. These sustained release depots have a demonstrated ability to increase the magnitude and persistence of immune responses through dermal administration. Dissolving microneedles can achieve sustained release through incorporation of materials like silk, chitosan, or biodegradable polyesters, while solid microneedles can be coated with materials that will slowly dissociate and degrade *in vivo* (Figure 2.3d). As described above, silk release kinetics can be tuned through methanol treatment, which has been shown to decrease the release rate by approximately two-fold. [99,169] In another study, microneedle tips were fabricated out of chitosan to create depots for sustained release of OVA over 28 days.[97] Microneedles can also be designed to deliver depots of biodegradable polyester microparticles that persist in dermal tissue up to 18 days and in the draining lymph node 10 days after delivery.[170] Sustained release has also been achieved by deposition of polymer multilayer films containing DNA antigen, RNA adjuvant, and polymer cations into dermal tissue through solid microneedles.[132] Depending on the design of the polymers in the film, duration of cell transfection from a reporter plasmid DNA antigen varied from 10 days to 22 days.

Slow release formulations including methanol treated silk, polyester microparticles, and biodegradable films have demonstrated more IFN-γ and TNF-α expressing antigen specific

CD8+ T cells than rapid releasing microneedles or intramuscular bolus vaccination.[99,132,170] Release kinetics also have a significant effect on antibody responses, with the methanol treated silk microneedle formulation eliciting lower serum IgG titers and lower IgG avidity compared to fast release microneedles, but chitosan microneedles eliciting more robust serum IgG levels than bolus intramuscular delivery. [97] These immune responses were consistent even for the different antigens and materials used in each experiment.

Collectively, literature describing sustained vaccine delivery to dermal tissue by microneedles suggests that sustained vaccine release enhances primarily CD8+ effector and central memory T cells. Vaccine release kinetics have not previously been studied in the oral cavity due to limitations of currently available delivery methods. Existing microneedle technology for sustained vaccine delivery in dermal tissue could overcome these limitations to enable a more detailed evaluation of oral mucosal immunity. It is reasonable to infer that similar improvements in the quantity and quality of cellular immune response could be observed in the oral cavity compared to the dermal tissue given some similarities in cell phenotype and function. However, vaccine release kinetics in the oral mucosa needs to be specifically studied because the dermal and oral mucosal tissue are not directly analogous, particularly with regard to immune cell infiltration and migration kinetics.[59] It would also be interesting to evaluate the effects of sustained release on mucosal cellular and humoral immunity, as previous studies in dermal tissue have primarily focused on systemic cellular immunity.

2.5 MICRONEEDLES FOR ORAL VACCINE DELIVERY

Recently, four groups have reported on microneedle mediated delivery of vaccines to the oral mucosa (Table 2.2). Three of these technologies were based on solid coated microneedles, while the fourth used a dissolvable microneedle system. These studies have demonstrated the promise

of microneedles for delivery to the oral mucosa and have also revealed new questions and challenges for future studies.

2.5.1 *Solid coated microneedles for vaccine delivery in a rabbit model*

The first study of microneedle delivery of vaccines to the oral mucosa was published in 2014 by Ma et al.[137] The study focused primarily on a single row of coated stainless steel microneedles applied to either the inner lip or the dorsal tongue of rabbits. Using sulforhodamine as a model, the researchers demonstrated delivery into both the lip and tongue, with efficiency of 63.9% and 91.2% respectively. Needles penetrated approximately 400 μm into the tissue, or 57% of the needle height, while penetrations around 30% of the needle height are more typical in other studies.[171,172] This improvement in penetration depth could be caused by several factors, including the design of the needle array as a 1D rather than 2D array, and the way the tissue was held taut during the needle insertion.

In this study, adaptive immune responses resulting from delivery of 125 μg OVA to the lip were compared to responses from delivery in the dorsal tongue. To achieve this dose, five microneedle arrays were each coated with 25 μg OVA. Similar antigen-specific serum IgG titers were detected after delivery at both sites, and these titers were only significant after two vaccine doses. Meanwhile, all IgA titers were low and variable. Based on these studies, it was concluded that there was no significant difference between delivery to either the lip or the tongue. Immune responses elicited by delivery of a virus like particle and plasmid DNA HIV antigens resulted in similar results as OVA.

This group has also conducted studies with the same microneedle technology to evaluate the effect of salivary washout on microneedle delivery to the oral cavity.[173] Although microneedles deliver biologics directly into the tissue, they do create holes that saliva could enter and still

dilute and wash out the biologic. To evaluate the significance of this effect, a series of in vitro studies were conducted delivering sulforhodamine dye into porcine buccal mucosa mounted in a modified Franz diffusion cell. Unsurprisingly, the dynamic flow conditions resulted in approximately 3-fold increased diffusion out of the tissue compared to static flow conditions. It is unclear how directly these results translate to delivery of vaccine components like proteins and DNA that possess very different diffusion behavior compared to small molecule dyes. Nevertheless, this finding is an important consideration in the dosing of microneedles for oral mucosal delivery and suggests that the use of mucoadhesive films as coverings to prevent this diffusion may help delivery efficiency. It would also be interesting to study how this diffusion varies with microneedle penetration depth, and how it varies in vivo with different delivery locations since salivary flow can vary greatly in different areas of the mouth.[83,84]

Table 2.3. Summary of existing studies of microneedle mediated oral mucosal vaccine delivery

MN Technology	Animal Model	Delivery location	Puncture depth	Delivery efficiency	Vaccine composition	Immune response	Other notes
Solid coated microneedles	Rabbit	Inner lip	~400 μm	63.9%	OVA	IgA, IgG	-Statistical significance of IgA titers in saliva for intramuscular vs. oral mucosal not evaluated
					Virus-like particle, plasmid	IgA, IgG	
		Dorsal tongue	~400 μm	91.2%	OVA	IgA, IgG	-OVA specific IgA and IgG responses induced only after second dose
					Virus-like particle, plasmid	IgA, IgG	
Solid coated microneedles	Mouse	Buccal	250 μm	n.d.	OVA	IgG, IgG1, IgG2a, splenocyte IFN-γ	-Evaluation of immune responses with and without CT adjuvant -Slow coating dissolution requiring microneedles to be clamped to the mucosa for 20 minutes
Microprojection array	Mouse	Buccal	47.8 μm	30%	Fluvax (inactivated split virion)	IgG	-IgG titer similar to intramuscular delivery, lower than dermal
Liposome containing dissolving MNs	Mouse	n.d.[a)]	n.d.	n.d.	Liposomes containing lipid A+ Hepatitis B surface	IgG, IgA, CD8+ T cells	-Specific site of oral mucosal delivery not reported

	antigen or bovine serum albumin	-IgG titer lower than subcutaneous delivery -CD8+ T cell numbers greater than subcutaneous

[a)] Not determined.

2.5.2 *Solid coated microneedles for adjuvanted vaccine delivery in a mouse model*

The most recent published study of oral mucosal microneedle vaccination was reported by Oh et al.[174] This group evaluated humoral and cellular immune responses to OVA with or without cholera toxin delivered using 300 μm long coated polylactic acid microneedles or coated polylactic acid flat discs. Microneedles penetrated 250 μm into the porcine buccal mucosa in an *ex vivo* study. Penetration depth in the mouse model was not evaluated. *In vitro,* a coating containing FITC-labeled OVA dissolved in PBS within 1 minute, however the group noted that microneedles were clamped to the buccal mucosa for 20 minutes for *in vivo* vaccine delivery in mice. At this time point, the group demonstrated with the FITC-labeled OVA that coated microneedles resulted in an approximately four-fold increase in OVA delivery to the porcine buccal mucosa.

In mice, the group reported robust OVA-specific antibody responses following vaccination with coated PLA microneedles and no response from coated flat discs. Inclusion of cholera toxin led to an increase in IgG, IgG1, and IgG2a, although it was unclear if these results were statistically significant. Similar amounts of IFN-γ were secreted from splenocytes of microneedle vaccinated mice when OVA peptides were presented by MHC class I or II. Inclusion of cholera toxin also led to an increase in this cellular response. Overall, this study further strengthens the body of work demonstrating that microneedles can improve delivery of vaccines into the buccal mucosa. Additionally, this is the only current published study that

clearly shows how incorporation of strong mucosal adjuvants can strengthen cellular and humoral immunity elicited by microneedle-mediated oral mucosal vaccination.

2.5.3 *Silicon microprojection array for influenza vaccination in a mouse model*

McNeilly et al. have investigated microprojection arrays for vaccine delivery in the mouse buccal mucosa. The microprojections consisted of 110 μm -long conical structures of silicon sputter-coated with gold and then dry coated with fluorescent nanoparticles or 37 ng of the Fluvax commercial influenza vaccine, an inactivated split virion vaccine. The projections were designed to be long enough for accessing the lamina propria, which is approximately 50 μm below the buccal tissue surface in mice. This study used a clip applicator device to help ensure uniform delivery, but only about two-thirds of the needles penetrated the tissue. The device delivered the Fluvax vaccine to an average depth of 47.8 μm into the murine buccal tissue, but the depth varied from 20 μm to ~100 μm. Meanwhile, the delivery efficiency of the microprojection arrays was around 30%, with about 10% of the vaccine delivered on the tissue surface and the other 60% remaining on the projections.

In the vaccination experiment, immune responses induced by the microprojection array were compared head-to-head with intramuscular injection, oral gavage delivery, and dermal delivery at t= 0 and at t= 4 weeks. The serum IgG titers were highest for dermal delivery, and buccal and intramuscular delivery had similarly lower titers. The only significant IgA titer was detected in the intestine from mice that received the vaccine dermally through the microprojection array. Hemagglutinin inhibition was measured to predict protective efficacy of these different vaccine delivery methods, and protective levels were detected only for dermal and buccal microprojection but not intramuscular delivery. This is a surprising result considering that the Fluvax commercial vaccine is designed for intramuscular injection.[175] The authors attributed the

improved immune responses for dermal compared to buccal delivery to the increased penetration of ~90% in the dermal ear skin. It is not possible to directly compare the immune responses in this study to the 1D stainless steel arrays used by Ma et al. due to differences in animal model, delivery location, vaccine composition, delivery efficiency and method of reporting antibody titers. However, similar trends were observed in both studies, with oral mucosal microneedle vaccine delivery producing similar systemic IgG titers to intramuscular delivery and oral mucosal microneedle delivery resulting in modest and variable mucosal IgA titers.

2.5.4 *Dissolving microneedles containing liposomes for vaccine delivery*

Dissolving microneedle arrays have also been reported for oral mucosal delivery. Poly(vinyl-pyrrolidone) matrix microneedles contained liposomes incorporating lipid-A adjuvant and either Hepatitis B surface antigen (HBs) or bovine serum albumin (BSA) antigen.[139,140] The needles had a base diameter of 250 μm and a height of 660 μm. The microneedles were used to deliver either 4 μg of BSA or 0.5 μg of HBs to the murine oral mucosa, but no data was published regarding the penetration depth in oral mucosal tissue or the delivery efficiency of this system.

Regardless of antigen, microneedle delivery of liposomes to the oral mucosa produced higher levels of serum IgG antibodies than topical oral mucosal delivery but lower levels of serum IgG antibodies compared to subcutaneous and dermal delivery. Oral mucosal microneedle delivery elicited significantly higher levels of CD8+ T cells in the spleen and IgA antibodies in saliva, the intestines, and the vagina compared to any other evaluated delivery method. Out of all three reported technologies, the dissolving microneedles seemingly elicit the most robust mucosal IgA responses. There are several factors that could be responsible for this, including an approximately 100-fold increased dose compared to the microprojection array or the presence of an adjuvant. Additionally, of the three microneedle technologies evaluated for oral mucosal

vaccination, this is the only device for which tissue penetration and delivery efficiency was not reported. This is a particularly important question for this dissolving microneedle system because small amounts of wetting in the moist environment of the mouth could significantly reduce the microneedle tip sharpness and stiffness. While previous studies indicate that dissolving microneedle penetration of moist surfaces such as the cornea and sclera is possible, the microneedle material must be carefully designed to ensure needle penetration before needle dissolution.[176]

2.6 PERSPECTIVES AND OUTLOOK

There is a strong rationale for further evaluation of microneedles for oral mucosal vaccine delivery. These studies may focus on device optimization for generating high quality mucosal immune responses and the use of microneedles as a tool to answer key questions about oral mucosal immunity.

One key gap in oral mucosal microneedle vaccine delivery is the unclear role of dosing location. Microneedles have unique capabilities that enable precise vaccine delivery to locations that may be challenging with other dosage forms. However, existing studies have not fully utilized this function of microneedles for oral mucosal vaccine delivery. Although Ma et al. found that delivery in the lip and sublingually resulted in similar immune responses, this may be due to the specific measurement outputs used in their studies. Ma et al. used IgA and IgG titers to determine the difference between dosing location. However, it is possible that measurements like DC activation markers or cytokine expression could provide more insight into the immune functions of different oral mucosal dosing locations. Therefore, there is still a rationale for vaccine delivery in different oral mucosal locations.

The effect of microneedle mediated vaccine delivery on innate and cellular immunity in the oral mucosa is another key gap in existing studies. In all of the completed studies, the primary immune output was serum IgG or mucosal IgA antibodies, and cellular responses were only evaluated for the dissolving microneedle technology. Meanwhile, none of these studies evaluated innate immune responses. While humoral immune responses are one key goal of vaccination, studies suggest that cellular immune responses are critical for clearing initial infection, particularly at mucosal surfaces where many pathogens enter and establish infection.[8,9] Additionally, previous studies using microneedles for dermal vaccination have demonstrated robust cellular immune responses.[124,136,163] The increased CD8+ T cell responses for the dissolving microneedles suggests that analogous responses in the oral mucosa can be induced by microneedle-mediated vaccine delivery. In future studies, cellular immune responses should be included as a measure of the vaccine immunogenicity and ultimately should be optimized. Future studies should also evaluate innate immune responses to better understand the type, magnitude, and quality of innate response that correlates with lasting adaptive immunity and protection from infection.

There is also clear room for improvement and innovation in the incorporation of adjuvants into oral mucosal microneedle systems. Only two microneedle formulations used for oral mucosal vaccination incorporated an adjuvant, specifically lipid A, a TLR4 agonist, or cholera toxin.[139,140,174] It is unclear what effect the lipid A had on the resulting immune responses since an unadjuvanted control was not included. Inclusion of cholera toxin was shown to increase cellular and humoral immune responses, although it is unclear if the results were statistically significant.[174] Given that responses comparable to intramuscular delivery have been induced without any adjuvant,[137,138] it is plausible that incorporation of adjuvants in oral mucosal

microneedle systems could greatly improve the quality and quantity of mucosal and systemic immune responses, as has been observed for topical dosage forms. The delivery capabilities of microneedles could also improve our understanding of adjuvant behavior in the oral mucosa. Because immune cell populations vary greatly with mucosal depth and with specific mucosal region, the unique ability of microneedles to target adjuvants to specific tissue regions containing target cells could lead to a better understanding of oral mucosal immunity.

Clinical translation of the microneedle fabrication process and applicator design must be considered in the design of microneedles for oral mucosal vaccination. As described in detail within other reviews, key considerations for translation of microneedle products include sterile and scalable manufacture, procedures for quality control, design of applicators and instructions for appropriate use, and careful market analysis.[177,178] Despite investments in microneedle technology by large companies, commercially available products are currently limited to cosmetic microneedle rollers that do not contain any active ingredients, and Fluzone,™ a trivalent inactivated influenza vaccine injected intradermally using a microneedle system called Soluvia™ manufactured by Becton Dickinson.[179-182] Microneedle translation is an active area of research, with recent papers reporting scalable microneedle manufacturing processes, new methods for assessing microneedle performance, and applicators for easy, reproducible application by non-skilled users.[155,158,159,183-185] Additionally, completed clinical trials have demonstrated the promise of microneedle technology for improving vaccination. Fluzone™ exhibited dose sparing in clinical trials, with 9 μg Fluzone™ generating comparable antibody responses to 15 μg of the same trivalent vaccine delivered intramuscularly, and more recently, another clinical trial demonstrated the safety and immunogenicity of a dissolving microneedle patch for influenza vaccination.[182,186] Another primary concern for application of microneedles in

the oral mucosa is acceptability. A recent study evaluated the human perception of buccal microneedle administration in 100 participants.[187] Perceived pain upon application to the palate, buccal mucosa, or tongue were similar to application in dermal tissue. Participants reported that the preferred site of application was the palate. Studies like this are critical when designing oral mucosal microneedle vaccines to develop a system that is both highly immunogenic and acceptable to patients.

2.7 CONCLUSION

Although the oral cavity is a promising site for mucosal vaccination, the current limited understanding of oral mucosal immunity precludes rational development and optimization of the next generation of oral mucosal vaccines. Currently available vaccine delivery systems for the oral mucosa are insufficient to specifically study the role of factors like vaccine composition, dose, and release kinetics on antigen presenting cell uptake and innate and adaptive immune responses. Microneedles possess broad capabilities that have been thoroughly demonstrated for dermal delivery, but demonstrations of these capabilities in the oral mucosa are extremely limited. There are many opportunities for advancement in this field, including the incorporation of adjuvants, the study of innate immune responses, and direct comparison of oral mucosal delivery sites. Future studies should not only optimize microneedle mediated oral mucosal vaccination but also use microneedles as a tool to address gaps in the current understanding of oral mucosal immunity.

2.8 REFERENCES

1 Neutra, M. R. & Kozlowski, P. A. Mucosal vaccines: the promise and the challenge. *Nat Rev Immunol* **6**, 148-158, doi:10.1038/nri1777 (2006).

2 Mazzoli, S. *et al.* HIV-specific mucosal and cellular immunity in HIV-seronegative partners of HIV-seropositive individuals. *Nat Med* **3**, 1250-1257 (1997).

3 Moutsopoulos, N. M. & Konkel, J. E. Tissue-Specific Immunity at the Oral Mucosal Barrier. *Trends Immunol* **39**, 276-287, doi:10.1016/j.it.2017.08.005 (2018).

4 Chen, Y., Chou, K., Fuchs, E., Havran, W. L. & Boismenu, R. Protection of the intestinal mucosa by intraepithelial gamma delta T cells. *Proc Natl Acad Sci U S A* **99**, 14338-14343, doi:10.1073/pnas.212290499 (2002).

5 Spada, F. M. *et al.* Self-recognition of CD1 by gamma/delta T cells: implications for innate immunity. *J Exp Med* **191**, 937-948 (2000).

6 Lamm, M. E. Interaction of antigens and antibodies at mucosal surfaces. *Annu Rev Microbiol* **51**, 311-340, doi:10.1146/annurev.micro.51.1.311 (1997).

7 Roos, A. *et al.* Human IgA activates the complement system via the mannan-binding lectin pathway. *J Immunol* **167**, 2861-2868 (2001).

8 Kaul, R. *et al.* HIV-1-specific mucosal CD8+ lymphocyte responses in the cervix of HIV-1-resistant prostitutes in Nairobi. *J Immunol* **164**, 1602-1611 (2000).

9 Hansen, S. G. *et al.* Effector memory T cell responses are associated with protection of rhesus monkeys from mucosal simian immunodeficiency virus challenge. *Nat Med* **15**, 293-299, doi:10.1038/nm.1935 (2009).

10 Song, J. H. *et al.* Sublingual vaccination with influenza virus protects mice against lethal viral infection. *Proc Natl Acad Sci U S A* **105**, 1644-1649, doi:10.1073/pnas.0708684105 (2008).

11 Holmgren, J. & Czerkinsky, C. Mucosal immunity and vaccines. *Nat Med* **11**, S45-53, doi:10.1038/nm1213 (2005).

12 Wang, J. *et al.* Single mucosal, but not parenteral, immunization with recombinant adenoviral-based vaccine provides potent protection from pulmonary tuberculosis. *J Immunol* **173**, 6357-6365 (2004).

13 Kichaev, G. *et al.* Electroporation mediated DNA vaccination directly to a mucosal surface results in improved immune responses. *Human Vaccines & Immunotherapeutics* **9**, 2041-2048, doi:10.4161/hv.25272 (2013).

14 Hayden, C. A. *et al.* Oral delivery of wafers made from HBsAg-expressing maize germ induces long-term immunological systemic and mucosal responses. *Vaccine* **33**, 2881-2886, doi:10.1016/j.vaccine.2015.04.080 (2015).

15 Cho, H. J. *et al.* Enhanced humoral and cellular immune responses after sublingual immunization against human papillomavirus 16 L1 protein with adjuvants. *Vaccine* **28**, 2598-2606, doi:10.1016/j.vaccine.2010.01.013 (2010).

16 Murugappan, S., Patil, H. P., Frijlink, H. W., Huckriede, A. & Hinrichs, W. L. Simplifying influenza vaccination during pandemics: sublingual priming and intramuscular boosting of immune responses with heterologous whole inactivated influenza vaccine. *AAPS J* **16**, 342-349, doi:10.1208/s12248-014-9565-z (2014).

17 Barnetta, S. W. *et al.* Protection of macaques against vaginal SHIV challenge by systemic or mucosal and systemic vaccinations with HIV-envelope. *Aids* **22**, 339-348, doi:10.1097/QAD.0b013e3282f3ca57 (2008).

18 Pakkanen, S. H., Kantele, J. M., Savolainen, L. E., Rombo, L. & Kantele, A. Specific and cross-reactive immune response to oral Salmonella Typhi Ty21a and parenteral Vi capsular polysaccharide typhoid vaccines administered concomitantly. *Vaccine* **33**, 451-458, doi:10.1016/j.vaccine.2014.11.030 (2015).

19 Thippeshappa, R. *et al.* Oral Immunization with Recombinant Vaccinia Virus Prime and Intramuscular Protein Boost Provides Protection against Intrarectal Simian-Human Immunodeficiency Virus Challenge in Macaques. *Clin Vaccine Immunol* **23**, 204-212, doi:10.1128/CVI.00597-15 (2015).

20 Saeed, M. I., Omar, A. R., Hussein, M. Z., Elkhidir, I. M. & Sekawi, Z. Development of enhanced antibody response toward dual delivery of nano-adjuvant adsorbed human Enterovirus-71 vaccine encapsulated carrier. *Hum Vaccin Immunother* **11**, 2414-2424, doi:10.1080/21645515.2015.1052918 (2015).

21 Eriksson, K. *et al.* Specific-antibody-secreting cells in the rectums and genital tracts of nonhuman primates following vaccination. *Infect Immun* **66**, 5889-5896 (1998).

22 Bolton, D. L., Song, K., Tomaras, G. D., Rao, S. & Roederer, M. Unique cellular and humoral immunogenicity profiles generated by aerosol, intranasal, or parenteral vaccination in rhesus macaques. *Vaccine* **35**, 639-646, doi:10.1016/j.vaccine.2016.12.008 (2017).

23 Gallichan, W. S. & Rosenthal, K. L. Long-lived cytotoxic T lymphocyte memory in mucosal tissues after mucosal but not systemic immunization. *J Exp Med* **184**, 1879-1890 (1996).

24 Shim, B. S. *et al.* Sublingual immunization with recombinant adenovirus encoding SARS-CoV spike protein induces systemic and mucosal immunity without redirection of the virus to the brain. *Virol J* **9**, 215, doi:10.1186/1743-422X-9-215 (2012).

25 Goonetilleke, N. P. *et al.* Enhanced immunogenicity and protective efficacy against Mycobacterium tuberculosis of bacille Calmette-Guérin vaccine using mucosal administration and boosting with a recombinant modified vaccinia virus Ankara. *J Immunol* **171**, 1602-1609 (2003).

26 Lee, H. J. *et al.* Sublingual Immunization of Trivalent Human Papillomavirus DNA Vaccine in Baculovirus Nanovector for Protection against Vaginal Challenge. *Plos One* **10**, doi:10.1371/journal.pone.0119408 (2015).

27 Fló, J., Tisminetzky, S. & Baralle, F. Oral transgene vaccination mediated by attenuated Salmonellae is an effective method to prevent Herpes simplex virus-2 induced disease in mice. *Vaccine* **19**, 1772-1782 (2001).

28 Lundholm, P., Asakura, Y., Hinkula, J., Lucht, E. & Wahren, B. Induction of mucosal IgA by a novel jet delivery technique for HIV-1 DNA. *Vaccine* **17**, 2036-2042 (1999).

29 Lycke, N. Recent progress in mucosal vaccine development: potential and limitations. *Nat Rev Immunol* **12**, 592-605, doi:10.1038/nri3251 (2012).

30 WHO. Polio vaccines: WHO position paper, January 2014--recommendations. *Vaccine* **32**, 4117-4118, doi:10.1016/j.vaccine.2014.04.023 (2014).

31 Rotavirus vaccines. WHO position paper – January 2013. *Wkly Epidemiol Rec* **88**, 49-64 (2013).

32 Mutsch, M. *et al.* Use of the inactivated intranasal influenza vaccine and the risk of Bell's palsy in Switzerland. *N Engl J Med* **350**, 896-903, doi:10.1056/NEJMoa030595 (2004).

33 Shakya, A. K., Chowdhury, M. Y. E., Tao, W. & Gill, H. S. Mucosal vaccine delivery: Current state and a pediatric perspective. *J Control Release* **240**, 394-413, doi:10.1016/j.jconrel.2016.02.014 (2016).

34 Nichol, K. L. *et al.* Effectiveness of live, attenuated intranasal influenza virus vaccine in healthy, working adults: a randomized controlled trial. *JAMA* **282**, 137-144 (1999).

35 Osterholm, M. T., Kelley, N. S., Sommer, A. & Belongia, E. A. Efficacy and effectiveness of influenza vaccines: a systematic review and meta-analysis. *Lancet Infect Dis* **12**, 36-44, doi:10.1016/S1473-3099(11)70295-X (2012).

36 Belshe, R. B. *et al.* The efficacy of live attenuated, cold-adapted, trivalent, intranasal influenzavirus vaccine in children. *N Engl J Med* **338**, 1405-1412, doi:10.1056/NEJM199805143382002 (1998).

37 Gallorini, S. *et al.* Sublingual immunization with a subunit influenza vaccine elicits comparable systemic immune response as intramuscular immunization, but also induces local IgA and TH17 responses. *Vaccine* **32**, 2382-2388, doi:10.1016/j.vaccine.2013.12.043 (2014).

38 Pedersen, G. K. *et al.* Evaluation of the sublingual route for administration of influenza H5N1 virosomes in combination with the bacterial second messenger c-di-GMP. *PLoS One* **6**, e26973, doi:10.1371/journal.pone.0026973 (2011).

39 Brandtzaeg, P. Immune functions of nasopharyngeal lymphoid tissue. *Adv Otorhinolaryngol* **72**, 20-24, doi:10.1159/000324588 (2011).

40 Illum, L. Nasal drug delivery--possibilities, problems and solutions. *J Control Release* **87**, 187-198 (2003).

41 Perry, M. & Whyte, A. Immunology of the tonsils. *Immunol Today* **19**, 414-421 (1998).

42 Brandtzaeg, P. & Korsrud, F. R. Significance of different J chain profiles in human tissues: generation of IgA and IgM with binding site for secretory component is related to the J chain expressing capacity of the total local immunocyte population, including IgG and IgD producing cells, and depends on the clinical state of the tissue. *Clin Exp Immunol* **58**, 709-718 (1984).

43 Perry, M. E. The specialised structure of crypt epithelium in the human palatine tonsil and its functional significance. *J Anat* **185 (Pt 1)**, 111-127 (1994).

44 Takahashi, K. *et al.* Dendritic cells interacting mainly with B cells in the lymphoepithelial symbiosis of the human palatine tonsil. *Virchows Arch* **448**, 623-629, doi:10.1007/s00428-005-0085-1 (2006).

45 Summers, K. L., Hock, B. D., McKenzie, J. L. & Hart, D. N. Phenotypic characterization of five dendritic cell subsets in human tonsils. *Am J Pathol* **159**, 285-295, doi:10.1016/S0002-9440(10)61694-X (2001).

46 Fujihara, K., Kuki, K., Kimura, T. & Tabata, T. An architecture of capillary vessels of the palatine tonsils studied by scanning electron microscope--with special references to comparison with the tonsillar cryptscopic images. *Auris Nasus Larynx* **15**, 191-197 (1988).

47 Jiang, H. L. *et al.* The potential of mannosylated chitosan microspheres to target macrophage mannose receptors in an adjuvant-delivery system for intranasal immunization. *Biomaterials* **29**, 1931-1939, doi:10.1016/j.biomaterials.2007.12.025 (2008).

48 Khatri, K., Goyal, A. K., Gupta, P. N., Mishra, N. & Vyas, S. P. Plasmid DNA loaded chitosan nanoparticles for nasal mucosal immunization against hepatitis B. *Int J Pharm* **354**, 235-241, doi:10.1016/j.ijpharm.2007.11.027 (2008).

49 Kraan, H., Soema, P., Amorij, J. P. & Kersten, G. Intranasal and sublingual delivery of inactivated polio vaccine. *Vaccine* **35**, 2647-2653, doi:10.1016/j.vaccine.2017.03.090 (2017).

50 van Ginkel, F. W., Jackson, R. J., Yuki, Y. & McGhee, J. R. Cutting edge: the mucosal adjuvant cholera toxin redirects vaccine proteins into olfactory tissues. *J Immunol* **165**, 4778-4782 (2000).

51 Smith, A., Perelman, M. & Hinchcliffe, M. Chitosan: a promising safe and immune-enhancing adjuvant for intranasal vaccines. *Hum Vaccin Immunother* **10**, 797-807 (2014).

52 Ren, S. T. *et al.* Intranasal Immunization Using Mannatide as a Novel Adjuvant for an Inactivated Influenza Vaccine and Its Adjuvant Effect Compared with MF59. *PLoS One* **12**, e0169501, doi:10.1371/journal.pone.0169501 (2017).

53 Yoshino, N. *et al.* Polymyxins as novel and safe mucosal adjuvants to induce humoral immune responses in mice. *PLoS One* **8**, e61643, doi:10.1371/journal.pone.0061643 (2013).

54 Stahl-Hennig, C. *et al.* Atraumatic oral spray immunization with replication-deficient viral vector vaccines. *J Virol* **81**, 13180-13190, doi:10.1128/JVI.01400-07 (2007).

55 Earl, P. L. *et al.* Recombinant modified vaccinia virus Ankara provides durable protection against disease caused by an immunodeficiency virus as well as long-term immunity to an orthopoxvirus in a non-human primate. *Virology* **366**, 84-97, doi:10.1016/j.virol.2007.02.041 (2007).

56 Tenner-Racz, K. *et al.* Early protection against pathogenic virus infection at a mucosal challenge site after vaccination with attenuated simian immunodeficiency virus. *Proc Natl Acad Sci U S A* **101**, 3017-3022, doi:10.1073/pnas.0308677101 (2004).

57 Kraan, H. *et al.* Buccal and sublingual vaccine delivery. *Journal of Controlled Release* **190**, 580-592, doi:http://dx.doi.org/10.1016/j.jconrel.2014.05.060 (2014).

58 Shojaei, A. H. Buccal mucosa as a route for systemic drug delivery: a review. *J Pharm Pharm Sci* **1**, 15-30 (1998).

59 Hovav, A. H. Dendritic cells of the oral mucosa. *Mucosal Immunol* **7**, 27-37, doi:10.1038/mi.2013.42 (2014).

60 Lukić, A. *et al.* Characterization of antigen-presenting cells in human apical periodontitis lesions by flow cytometry and immunocytochemistry. *Int Endod J* **39**, 626-636, doi:10.1111/j.1365-2591.2006.01125.x (2006).

61 Jotwani, R. & Cutler, C. W. Multiple dendritic cell (DC) subpopulations in human gingiva and association of mature DCs with CD4+ T-cells in situ. *J Dent Res* **82**, 736-741, doi:10.1177/154405910308200915 (2003).

62 Allam, J. P. *et al.* Distribution of Langerhans cells and mast cells within the human oral mucosa: new application sites of allergens in sublingual immunotherapy? *Allergy* **63**, 720-727, doi:10.1111/j.1398-9995.2007.01611.x (2008).

63 Mascarell, L. *et al.* Oral dendritic cells mediate antigen-specific tolerance by stimulating TH1 and regulatory CD4+ T cells. *J Allergy Clin Immunol* **122**, 603-609.e605, doi:10.1016/j.jaci.2008.06.034 (2008).

64 Ito, T., Wang, Y. H. & Liu, Y. J. Plasmacytoid dendritic cell precursors/type I interferon-producing cells sense viral infection by Toll-like receptor (TLR) 7 and TLR9. *Springer Semin Immunopathol* **26**, 221-229, doi:10.1007/s00281-004-0180-4 (2005).

65 Villadangos, J. A. & Young, L. Antigen-presentation properties of plasmacytoid dendritic cells. *Immunity* **29**, 352-361, doi:10.1016/j.immuni.2008.09.002 (2008).

66 Jones, A. T. *et al.* HIV-1 vaccination by needle-free oral injection induces strong mucosal immunity and protects against SHIV challenge. *Nature communications* **10**, 798-798, doi:10.1038/s41467-019-08739-4 (2019).

67 Benito-Villalvilla, C. *et al.* MV140, a sublingual polyvalent bacterial preparation to treat recurrent urinary tract infections, licenses human dendritic cells for generating Th1, Th17, and IL-10 responses via Syk and MyD88. *Mucosal Immunology* **10**, 924-935, doi:10.1038/mi.2016.112 (2017).

68 Khan, A., Singh, S., Galvan, G., Jagannath, C. & Sastry, K. J. Prophylactic Sublingual Immunization with Mycobacterium tuberculosis Subunit Vaccine Incorporating the Natural Killer T Cell Agonist Alpha-Galactosylceramide Enhances Protective Immunity to Limit Pulmonary and Extra-Pulmonary Bacterial Burden in Mice. *Vaccines* **5**, doi:10.3390/vaccines5040047 (2017).

69 Etchart, N. *et al.* Dendritic cells recruitment and in vivo priming of CD8+ CTL induced by a single topical or transepithelial immunization via the buccal mucosa with measles virus nucleoprotein. *J Immunol* **167**, 384-391 (2001).

70 Lu, Y. J. *et al.* Options for inactivation, adjuvant, and route of topical administration of a killed, unencapsulated pneumococcal whole-cell vaccine. *Clin Vaccine Immunol* **17**, 1005-1012, doi:10.1128/CVI.00036-10 (2010).

71 Yang, M. C. *et al.* Buccal injection of synthetic HPV long peptide vaccine induces local and systemic antigen-specific CD8+T-cell immune responses and antitumor effects without adjuvant. *Cell and Bioscience* **6**, doi:10.1186/s13578-016-0083-9 (2016).

72 Etchart, N., Buckland, R., Liu, M. A., Wild, T. F. & Kaiserlian, D. Class I-restricted CTL induction by mucosal immunization with naked DNA encoding measles virus haemagglutinin. *J Gen Virol* **78 (Pt 7)**, 1577-1580, doi:10.1099/0022-1317-78-7-1577 (1997).

73 Aran, K. *et al.* An oral microjet vaccination system elicits antibody production in rabbits. *Science Translational Medicine* **9**, doi:10.1126/scitranslmed.aaf6413 (2017).

74 Appledorn, D. M., Aldhamen, Y. A., Godbehere, S., Seregin, S. S. & Amalfitano, A. Sublingual administration of an adenovirus serotype 5 (Ad5)-based vaccine confirms Toll-like receptor agonist activity in the oral cavity and elicits improved mucosal and systemic cell-mediated responses against HIV antigens despite preexisting Ad5 immunity. *Clin Vaccine Immunol* **18**, 150-160, doi:10.1128/CVI.00341-10 (2011).

75 Kim, S. *et al.* Dual role of respiratory syncytial virus glycoprotein fragment as a mucosal immunogen and chemotactic adjuvant. *PLoS One* **7**, e32226, doi:10.1371/journal.pone.0032226 (2012).

76 Fu, Y. H. *et al.* Sublingual administration of a helper-dependent adenoviral vector expressing the codon-optimized soluble fusion glycoprotein of human respiratory syncytial virus elicits protective immunity in mice. *Antiviral Res* **105**, 72-79, doi:10.1016/j.antiviral.2014.02.003 (2014).

77 Domm, W. *et al.* Robust antigen-specific humoral immune responses to sublingually delivered adenoviral vectors encoding HIV-1 Env: association with mucoadhesion and efficient penetration of the sublingual barrier. *Vaccine* **29**, 7080-7089, doi:10.1016/j.vaccine.2011.07.008 (2011).

78 Amuguni, J. H. *et al.* Sublingually administered Bacillus subtilis cells expressing tetanus toxin C fragment induce protective systemic and mucosal antibodies against tetanus toxin in mice. *Vaccine* **29**, 4778-4784, doi:10.1016/j.vaccine.2011.04.083 (2011).

79 Cuburu, N. *et al.* Sublingual immunization induces broad-based systemic and mucosal immune responses in mice. *Vaccine* **25**, 8598-8610, doi:10.1016/j.vaccine.2007.09.073 (2007).

80 Yang, M. C. *et al.* Buccal injection of synthetic HPV long peptide vaccine induces local and systemic antigen-specific CD8+ T-cell immune responses and antitumor effects without adjuvant. *Cell Biosci* **6**, 17, doi:10.1186/s13578-016-0083-9 (2016).

81 van Loon, L. A., Krieg, S. R., Davidson, C. L. & Bos, J. D. Quantification and distribution of lymphocyte subsets and Langerhans cells in normal human oral mucosa and skin. *J Oral Pathol Med* **18**, 197-201 (1989).

82 Hasséus, B., Jontell, M., Bergenholtz, G. & Dahlgren, U. I. T-cell costimulatory capacity of oral and skin epithelial cells in vitro: presence of suppressive activity in supernatants from skin epithelial cell cultures. *Eur J Oral Sci* **112**, 48-54 (2004).

83 Humphrey, S. P. & Williamson, R. T. A review of saliva: normal composition, flow, and function. *J Prosthet Dent* **85**, 162-169, doi:10.1067/mpr.2001.113778 (2001).

84 Percival, R. S., Challacombe, S. J. & Marsh, P. D. Flow rates of resting whole and stimulated parotid saliva in relation to age and gender. *J Dent Res* **73**, 1416-1420, doi:10.1177/00220345940730080401 (1994).

85 Veerman, E. C., van den Keybus, P. A., Vissink, A. & Nieuw Amerongen, A. V. Human glandular salivas: their separate collection and analysis. *Eur J Oral Sci* **104**, 346-352 (1996).

86 Law, S., Wertz, P. W., Swartzendruber, D. C. & Squier, C. A. Regional variation in content, composition and organization of porcine epithelial barrier lipids revealed by thin-layer chromatography and transmission electron microscopy. *Arch Oral Biol* **40**, 1085-1091 (1995).

87 Squier, C. A., Cox, P. & Wertz, P. W. Lipid content and water permeability of skin and oral mucosa. *J Invest Dermatol* **96**, 123-126 (1991).

88 Iwasaki, A. Mucosal dendritic cells. *Annu Rev Immunol* **25**, 381-418, doi:10.1146/annurev.immunol.25.022106.141634 (2007).

89 Novak, N., Haberstok, J., Bieber, T. & Allam, J. P. The immune privilege of the oral mucosa. *Trends Mol Med* **14**, 191-198, doi:10.1016/j.molmed.2008.03.001 (2008).

90 Cutler, C. W. & Jotwani, R. Dendritic cells at the oral mucosal interface. *J Dent Res* **85**, 678-689, doi:10.1177/154405910608500801 (2006).

91 Soria, I. *et al.* Oral myeloid cells uptake allergoids coupled to mannan driving Th1/Treg responses upon sublingual delivery in mice. *Allergy* **73**, 875-884, doi:10.1111/all.13396 (2018).

92 Allam, J. P. *et al.* Toll-like receptor 4 ligation enforces tolerogenic properties of oral mucosal Langerhans cells. *J Allergy Clin Immunol* **121**, 368-374.e361, doi:10.1016/j.jaci.2007.09.045 (2008).

93 Shin, J. S. & Greer, A. M. The role of FcεRI expressed in dendritic cells and monocytes. *Cell Mol Life Sci* **72**, 2349-2360, doi:10.1007/s00018-015-1870-x (2015).

94 Aramaki, O., Chalermsarp, N., Otsuki, M., Tagami, J. & Azuma, M. Differential expression of co-signal molecules and migratory properties in four distinct subsets of migratory dendritic cells from the oral mucosa. *Biochem Biophys Res Commun* **413**, 407-413, doi:10.1016/j.bbrc.2011.08.099 (2011).

95 Hajishengallis, G. Too old to fight? Aging and its toll on innate immunity. *Mol Oral Microbiol* **25**, 25-37, doi:10.1111/j.2041-1014.2009.00562.x (2010).

96 Adams, J. R., Haughney, S. L. & Mallapragada, S. K. Effective polymer adjuvants for sustained delivery of protein subunit vaccines. *Acta Biomater* **14**, 104-114, doi:10.1016/j.actbio.2014.11.050 (2015).

97 Chen, M. C., Lai, K. Y., Ling, M. H. & Lin, C. W. Enhancing immunogenicity of antigens through sustained intradermal delivery using chitosan microneedles with a patch-dissolvable design. *Acta Biomaterialia* **65**, 66-75, doi:10.1016/j.actbio.2017.11.004 (2018).

98 Chen, M. C., Huang, S. F., Lai, K. Y. & Ling, M. H. Fully embeddable chitosan microneedles as a sustained release depot for intradermal vaccination. *Biomaterials* **34**, 3077-3086, doi:10.1016/j.biomaterials.2012.12.041 (2013).

99 DeMuth, P. C., Min, Y., Irvine, D. J. & Hammond, P. T. Implantable Silk Composite Microneedles for Programmable Vaccine Release Kinetics and Enhanced Immunogenicity in Transcutaneous Immunization. *Advanced Healthcare Materials* **3**, 47-58, doi:10.1002/adhm.201300139 (2014).

100 Jewell, C. M., López, S. C. & Irvine, D. J. In situ engineering of the lymph node microenvironment via intranodal injection of adjuvant-releasing polymer particles. *Proc Natl Acad Sci U S A* **108**, 15745-15750, doi:10.1073/pnas.1105200108 (2011).

101 Kim, J. *et al.* Injectable, spontaneously assembling, inorganic scaffolds modulate immune cells in vivo and increase vaccine efficacy. *Nature Biotechnology* **33**, 64-U241, doi:10.1038/nbt.3071 (2015).

102 Tam, H. H. *et al.* Sustained antigen availability during germinal center initiation enhances antibody responses to vaccination. *Proceedings of the National Academy of Sciences*, doi:10.1073/pnas.1606050113 (2016).

103 Zhang, C., Ohno, T., Kang, S., Takai, T. & Azuma, M. Repeated antigen painting and sublingual immunotherapy in mice convert sublingual dendritic cell subsets. *Vaccine* **32**, 5669-5676, doi:10.1016/j.vaccine.2014.08.013 (2014).

104 Chinna Reddy, P., Chaitanya, K. S. & Madhusudan Rao, Y. A review on bioadhesive buccal drug delivery systems: current status of formulation and evaluation methods. *Daru* **19**, 385-403 (2011).

105 Silva, B. M. A., Borges, A. F., Silva, C., Coelho, J. F. J. & Simoes, S. Mucoadhesive oral films: The potential for unmet needs. *International Journal of Pharmaceutics* **494**, 537-551, doi:10.1016/j.ijpharm.2015.08.038 (2015).

106 Borges, A. F., Silva, C., Coelho, J. F. J. & Simoes, S. Oral films: Current status and future perspectives II - Intellectual property, technologies and market needs. *Journal of Controlled Release* **206**, 108-121, doi:10.1016/j.jconrel.2015.03.012 (2015).

107 White, J. A. *et al.* Serum and mucosal antibody responses to inactivated polio vaccine after sublingual immunization using a thermoresponsive gel delivery system. *Hum Vaccin Immunother* **10**, 3611-3621, doi:10.4161/hv.32253 (2014).

108 Borde, A., Ekman, A., Holmgren, J. & Larsson, A. Effect of protein release rates from tablet formulations on the immune response after sublingual immunization. *Eur J Pharm Sci* **47**, 695-700, doi:10.1016/j.ejps.2012.08.014 (2012).

109 Mašek, J. *et al.* Multi-layered nanofibrous mucoadhesive films for buccal and sublingual administration of drug-delivery and vaccination nanoparticles - important step towards effective mucosal vaccines. *J Control Release* **249**, 183-195, doi:10.1016/j.jconrel.2016.07.036 (2017).

110 Mitchell, T. J., Kendall, M. A. F. & Bellhouse, B. J. A ballistic study of micro-particle penetration to the oral mucosa. *International Journal of Impact Engineering* **28**, 581-599, doi:10.1016/s0734-743x(02)00150-1 (2003).

111 Fujihashi, K., Koga, T., van Ginkel, F. W., Hagiwara, Y. & McGhee, J. R. A dilemma for mucosal vaccination: efficacy versus toxicity using enterotoxin-based adjuvants. *Vaccine* **20**, 2431-2438, doi:10.1016/s0264-410x(02)00155-x (2002).

112 Sun, J. B., Czerkinsky, C. & Holmgren, J. Sublingual 'oral tolerance' induction with antigen conjugated to cholera toxin B subunit generates regulatory T cells that induce apoptosis and depletion of effector T cells. *Scand J Immunol* **66**, 278-286, doi:10.1111/j.1365-3083.2007.01975.x (2007).

113 Lycke, N. From toxin to adjuvant: basic mechanisms for the control of mucosal IgA immunity and tolerance. *Immunol Lett* **97**, 193-198, doi:10.1016/j.imlet.2004.12.008 (2005).

114 Negri, D. R. *et al.* Persistence of mucosal and systemic immune responses following sublingual immunization. *Vaccine* **28**, 4175-4180, doi:10.1016/j.vaccine.2010.04.013 (2010).

115 Fukasaka, M. *et al.* A Lipopolysaccharide from Pantoea Agglomerans Is a Promising Adjuvant for Sublingual Vaccines to Induce Systemic and Mucosal Immune Responses in Mice via TLR4 Pathway. *Plos One* **10**, doi:10.1371/journal.pone.0126849 (2015).

116 Buffa, V., Klein, K., Fischetti, L. & Shattock, R. J. Evaluation of TLR agonists as potential mucosal adjuvants for HIV gp140 and tetanus toxoid in mice. *PLoS One* **7**, e50529, doi:10.1371/journal.pone.0050529 (2012).

117 Vrdoljak, A. *et al.* Coated microneedle arrays for transcutaneous delivery of live virus vaccines. *J Control Release* **159**, 34-42, doi:10.1016/j.jconrel.2011.12.026 (2012).

118 Kim, Y. C., Yoo, D. G., Compans, R. W., Kang, S. M. & Prausnitz, M. R. Cross-protection by co-immunization with influenza hemagglutinin DNA and inactivated virus vaccine using coated microneedles. *J Control Release* **172**, 579-588, doi:10.1016/j.jconrel.2013.04.016 (2013).

119 Weldon, W. C. *et al.* Effect of adjuvants on responses to skin immunization by microneedles coated with influenza subunit vaccine. *PLoS One* **7**, e41501, doi:10.1371/journal.pone.0041501 (2012).

120 Kim, Y. C. *et al.* Enhanced memory responses to seasonal H1N1 influenza vaccination of the skin with the use of vaccine-coated microneedles. *J Infect Dis* **201**, 190-198, doi:10.1086/649228 (2010).

121 Laurent, P. *et al.* Evaluation of the clinical performance of a new intradermal vaccine administration technique and associated delivery system. *Vaccine* **25**, 8833-8842, doi:10.1016/j.vaccine.2007.10.020|10.1016/j.vaceine.2007.10.020 (2007).

122 Pearton, M., Pirri, D., Kang, S. M., Compans, R. W. & Birchall, J. C. Host responses in human skin after conventional intradermal injection or microneedle administration of virus-like-particle influenza vaccine. *Adv Healthc Mater* **2**, 1401-1410, doi:10.1002/adhm.201300006 (2013).

123 Edens, C., Dybdahl-Sissoko, N. C., Weldon, W. C., Oberste, M. S. & Prausnitz, M. R. Inactivated polio vaccination using a microneedle patch is immunogenic in the rhesus macaque. *Vaccine* **33**, 4683-4690, doi:10.1016/j.vaccine.2015.01.089 (2015).

124 Pearson, F. E., O'Mahony, C., Moore, A. C. & Hill, A. V. Induction of CD8(+) T cell responses and protective efficacy following microneedle-mediated delivery of a live adenovirus-vectored malaria vaccine. *Vaccine* **33**, 3248-3255, doi:10.1016/j.vaccine.2015.03.039 (2015).

125 Kommareddy, S. *et al.* Influenza subunit vaccine coated microneedle patches elicit comparable immune responses to intramuscular injection in guinea pigs. *Vaccine* **31**, 3435-3441, doi:10.1016/j.vaccine.2013.01.050 (2013).
126 Du, G. *et al.* Intradermal vaccination with hollow microneedles: A comparative study of various protein antigen and adjuvant encapsulated nanoparticles. *J Control Release* **266**, 109-118, doi:10.1016/j.jconrel.2017.09.021 (2017).
127 Prausnitz, M. R., Mikszta, J. A., Cormier, M. & Andrianov, A. K. Micro needle-based vaccines. *Current topics in microbiology and immunology* **333**, 369-393 (2009).
128 Kim, Y. C. *et al.* Microneedle delivery of trivalent influenza vaccine to the skin induces long-term cross-protection. *J Drug Target* **24**, 943-951, doi:10.3109/1061186X.2016.1159213 (2016).
129 Pattani, A. *et al.* Microneedle mediated intradermal delivery of adjuvanted recombinant HIV-1 CN54gp140 effectively primes mucosal boost inoculations. *J Control Release* **162**, 529-537, doi:10.1016/j.jconrel.2012.07.039 (2012).
130 Arya, J. & Prausnitz, M. Microneedle patches for vaccination in developing countries. *Journal of Controlled Release* **240**, 135-141, doi:10.1016/j.jconrel.2015.11.019 (2016).
131 Carey, J. B. *et al.* Microneedle-mediated immunization of an adenovirus-based malaria vaccine enhances antigen-specific antibody immunity and reduces anti-vector responses compared to the intradermal route. *Sci Rep* **4**, 6154, doi:10.1038/srep06154 (2014).
132 DeMuth, P. C. *et al.* Polymer multilayer tattooing for enhanced DNA vaccination. *Nat Mater* **12**, 367-376, doi:10.1038/nmat3550 (2013).
133 Kim, N. W. *et al.* Polyplex-releasing microneedles for enhanced cutaneous delivery of DNA vaccine. *J Control Release* **179**, 11-17, doi:10.1016/j.jconrel.2014.01.016 (2014).
134 Alarcon, J. B., Hartley, A. W., Harvey, N. G. & Mikszta, J. A. Preclinical evaluation of microneedle technology for intradermal delivery of influenza vaccines. *Clin Vaccine Immunol* **14**, 375-381, doi:10.1128/CVI.00387-06 (2007).
135 DeMuth, P. C., Moon, J. J., Suh, H., Hammond, P. T. & Irvine, D. J. Releasable layer-by-layer assembly of stabilized lipid nanocapsules on microneedles for enhanced transcutaneous vaccine delivery. *ACS Nano* **6**, 8041-8051, doi:10.1021/nn302639r (2012).
136 Becker, P. D., Hervouet, C., Mason, G. M., Kwon, S. Y. & Klavinskis, L. S. Skin vaccination with live virus vectored microneedle arrays induce long lived CD8(+) T cell memory. *Vaccine* **33**, 4691-4698, doi:10.1016/j.vaccine.2015.04.046 (2015).
137 Ma, Y. *et al.* Vaccine delivery to the oral cavity using coated microneedles induces systemic and mucosal immunity. *Pharm Res* **31**, 2393-2403, doi:10.1007/s11095-014-1335-1 (2014).
138 McNeilly, C. L. *et al.* Microprojection arrays to immunise at mucosal surfaces. *J Control Release* **196**, 252-260, doi:10.1016/j.jconrel.2014.09.028 (2014).
139 Wang, T. *et al.* Mannosylated and lipid A-incorporating cationic liposomes constituting microneedle arrays as an effective oral mucosal HBV vaccine applicable in the controlled temperature chain. *Colloids Surf B Biointerfaces* **126**, 520-530, doi:10.1016/j.colsurfb.2015.01.005 (2015).
140 Zhen, Y. Y. *et al.* Multifunctional liposomes constituting microneedles induced robust systemic and mucosal immunoresponses against the loaded antigens via oral mucosal vaccination. *Vaccine* **33**, 4330-4340, doi:10.1016/j.vaccine.2015.03.081 (2015).

141 Wei-Ze, L. *et al.* Super-short solid silicon microneedles for transdermal drug delivery applications. *International Journal of Pharmaceutics* **389**, 122-129, doi:10.1016/j.ijpharm.2010.01.024 (2010).
142 Donnelly, R. F. *et al.* Design, Optimization and Characterisation of Polymeric Microneedle Arrays Prepared by a Novel Laser-Based Micromoulding Technique. *Pharmaceutical Research* **28**, 41-57, doi:10.1007/s11095-010-0169-8 (2011).
143 Martin, C. J., Allender, C. J., Brain, K. R., Morrissey, A. & Birchall, J. C. Low temperature fabrication of biodegradable sugar glass microneedles for transdermal drug delivery applications. *Journal of Controlled Release* **158**, 93-101, doi:10.1016/j.jconrel.2011.10.024 (2012).
144 Moon, S., Lee, S., Lee, H. & Kwon, T. Fabrication of microneedle array using LIGA and hot embossing process. *Microsystem Technologies-Micro-and Nanosystems-Information Storage and Processing Systems* **11**, 311-318, doi:10.1007/s00542-004-0446-8 (2005).
145 Park, J. H., Yoon, Y. K., Choi, S. O., Prausnitz, M. R. & Allen, M. G. Tapered conical polymer microneedles fabricated using an integrated lens technique for transdermal drug delivery. *IEEE Trans Biomed Eng* **54**, 903-913, doi:10.1109/TBME.2006.889173 (2007).
146 Park, J. H., Allen, M. G. & Prausnitz, M. R. Biodegradable polymer microneedles: Fabrication, mechanics and transdermal drug delivery. *Journal of Controlled Release* **104**, 51-66, doi:10.1016/j.jconrel.2005.02.002 (2005).
147 Kim, Y. C., Park, J. H. & Prausnitz, M. R. Microneedles for drug and vaccine delivery. *Adv Drug Deliv Rev* **64**, 1547-1568, doi:10.1016/j.addr.2012.04.005 (2012).
148 van der Maaden, K. *et al.* Novel hollow microneedle technology for depth-controlled microinjection-mediated dermal vaccination: a study with polio vaccine in rats. *Pharm Res* **31**, 1846-1854, doi:10.1007/s11095-013-1288-9 (2014).
149 Han, M. *et al.* Improvement in antigen-delivery using fabrication of a grooves-embedded microneedle array. *Sensors and Actuators B-Chemical* **137**, 274-280, doi:10.1016/j.snb.2008.11.017 (2009).
150 Gill, H. S. & Prausnitz, M. R. Coated microneedles for transdermal delivery. *J Control Release* **117**, 227-237, doi:10.1016/j.jconrel.2006.10.017 (2007).
151 Bal, S. M. *et al.* Influence of microneedle shape on the transport of a fluorescent dye into human skin in vivo. *J Control Release* **147**, 218-224, doi:10.1016/j.jconrel.2010.07.104 (2010).
152 Römgens, A. M., Bader, D. L., Bouwstra, J. A., Baaijens, F. P. T. & Oomens, C. W. J. Monitoring the penetration process of single microneedles with varying tip diameters. *J Mech Behav Biomed Mater* **40**, 397-405, doi:10.1016/j.jmbbm.2014.09.015 (2014).
153 Donnelly, R. F. *et al.* Optical coherence tomography is a valuable tool in the study of the effects of microneedle geometry on skin penetration characteristics and in-skin dissolution. *J Control Release* **147**, 333-341, doi:10.1016/j.jconrel.2010.08.008 (2010).
154 Davis, S. P., Landis, B. J., Adams, Z. H., Allen, M. G. & Prausnitz, M. R. Insertion of microneedles into skin: measurement and prediction of insertion force and needle fracture force. *Journal of Biomechanics* **37**, 1155-1163, doi:10.1016/j.jbiomech.2003.12.010 (2004).
155 van der Maaden, K., Sekerdag, E., Jiskoot, W. & Bouwstra, J. Impact-insertion applicator improves reliability of skin penetration by solid microneedle arrays. *AAPS J* **16**, 681-684, doi:10.1208/s12248-014-9606-7 (2014).

156 Lahiji, S. F., Dangol, M. & Jung, H. A patchless dissolving microneedle delivery system enabling rapid and efficient transdermal drug delivery. *Sci Rep* **5**, 7914, doi:10.1038/srep07914 (2015).
157 Verbaan, F. J. *et al.* Improved piercing of microneedle arrays in dermatomed human skin by an impact insertion method. *J Control Release* **128**, 80-88, doi:10.1016/j.jconrel.2008.02.009 (2008).
158 Donnelly, R. F., Singh, T. R. R., Morrow, D. I. J. & Woolfson, A. D. in *Microneedle-mediated Transdermal and Intradermal Drug Delivery* 57-78 (John Wiley & Sons, Ltd., 2012).
159 Singh, T. R., Dunne, N. J., Cunningham, E. & Donnelly, R. F. Review of patents on microneedle applicators. *Recent Pat Drug Deliv Formul* **5**, 11-23 (2011).
160 Moronkeji, K., Todd, S., Dawidowska, I., Barrett, S. D. & Akhtar, R. The role of subcutaneous tissue stiffness on microneedle performance in a representative in vitro model of skin. *J Control Release* **265**, 102-112, doi:10.1016/j.jconrel.2016.11.004 (2017).
161 Chen, M. C., Ling, M. H., Lai, K. Y. & Pramudityo, E. Chitosan Microneedle Patches for Sustained Transdermal Delivery of Macromolecules. *Biomacromolecules* **13**, 4022-4031, doi:10.1021/bm301293d (2012).
162 Gupta, J., Gill, H. S., Andrews, S. N. & Prausnitz, M. R. Kinetics of skin resealing after insertion of microneedles in human subjects. *Journal of Controlled Release* **154**, 148-155, doi:http://dx.doi.org/10.1016/j.jconrel.2011.05.021 (2011).
163 Bachy, V. *et al.* Langerin negative dendritic cells promote potent CD8+ T-cell priming by skin delivery of live adenovirus vaccine microneedle arrays. *Proc Natl Acad Sci U S A* **110**, 3041-3046, doi:10.1073/pnas.1214449110 (2013).
164 Cole, G. *et al.* Dissolving microneedles for DNA vaccination: Improving functionality via polymer characterization and RALA complexation. *Hum Vaccin Immunother* **13**, 50-62, doi:10.1080/21645515.2016.1248008 (2017).
165 Moon, S. *et al.* Dose sparing and enhanced immunogenicity of inactivated rotavirus vaccine administered by skin vaccination using a microneedle patch. *Vaccine* **31**, 3396-3402, doi:10.1016/j.vaccine.2012.11.027 (2013).
166 Edens, C., Collins, M. L., Ayers, J., Rota, P. A. & Prausnitz, M. R. Measles vaccination using a microneedle patch. *Vaccine* **31**, 3403-3409, doi:10.1016/j.vaccine.2012.09.062 (2013).
167 Mann, J. F. S. *et al.* Mucosal Application of gp140 Encoding DNA Polyplexes to Different Tissues Results in Altered Immunological Outcomes in Mice. *Plos One* **8**, doi:10.1371/journal.pone.0067412 (2013).
168 Kim, Y. C. *et al.* Increased immunogenicity of avian influenza DNA vaccine delivered to the skin using a microneedle patch. *Eur J Pharm Biopharm* **81**, 239-247, doi:10.1016/j.ejpb.2012.03.010 (2012).
169 Tsioris, K. *et al.* Fabrication of Silk Microneedles for Controlled-Release Drug Delivery. *Advanced Functional Materials* **22**, 330-335, doi:10.1002/adfm.201102012 (2012).
170 DeMuth, P. C., Garcia-Beltran, W. F., Ai-Ling, M. L., Hammond, P. T. & Irvine, D. J. Composite Dissolving Microneedles for Coordinated Control of Antigen and Adjuvant Delivery Kinetics in Transcutaneous Vaccination. *Advanced Functional Materials* **23**, 161-172, doi:10.1002/adfm.201201512 (2013).

171 Lee, J. W., Park, J. H. & Prausnitz, M. R. Dissolving microneedles for transdermal drug delivery. *Biomaterials* **29**, 2113-2124, doi:10.1016/j.biomaterials.2007.12.048 (2008).
172 Sullivan, S. P. *et al.* Dissolving polymer microneedle patches for influenza vaccination. *Nat Med* **16**, 915-920, doi:10.1038/nm.2182 (2010).
173 Serpe, L. *et al.* Influence of salivary washout on drug delivery to the oral cavity using coated microneedles: An in vitro evaluation. *Eur J Pharm Sci* **93**, 215-223, doi:10.1016/j.ejps.2016.08.023 (2016).
174 Oh, Y. J. *et al.* Ovalbumin and cholera toxin delivery to buccal mucus for immunization using microneedles and comparison of immunological response to transmucosal delivery. *Drug Deliv Transl Res*, doi:10.1007/s13346-021-00964-z (2021).
175 Nolan, T. *et al.* Safety and immunogenicity of an inactivated thimerosal-free influenza vaccine in infants and children. *Influenza Other Respir Viruses* **3**, 315-325, doi:10.1111/j.1750-2659.2009.00108.x (2009).
176 Thakur, R. R. *et al.* Rapidly dissolving polymeric microneedles for minimally invasive intraocular drug delivery. *Drug Deliv Transl Res* **6**, 800-815, doi:10.1007/s13346-016-0332-9 (2016).
177 Watkinson, A. C., Kearney, M. C., Quinn, H. L., Courtenay, A. J. & Donnelly, R. F. Future of the transdermal drug delivery market--have we barely touched the surface? *Expert Opin Drug Deliv* **13**, 523-532, doi:10.1517/17425247.2016.1130034 (2016).
178 Quinn, H. L., Kearney, M. C., Courtenay, A. J., McCrudden, M. T. & Donnelly, R. F. The role of microneedles for drug and vaccine delivery. *Expert Opin Drug Deliv* **11**, 1769-1780, doi:10.1517/17425247.2014.938635 (2014).
179 McCrudden, M. T. *et al.* Microneedle applications in improving skin appearance. *Exp Dermatol* **24**, 561-566, doi:10.1111/exd.12723 (2015).
180 Richter-Johnson, J., Kumar, P., Choonara, Y. E., du Toit, L. C. & Pillay, V. Therapeutic applications and pharmacoeconomics of microneedle technology. *Expert Rev Pharmacoecon Outcomes Res* **18**, 359-369, doi:10.1080/14737167.2018.1485100 (2018).
181 Ansaldi, F., de Florentiis, D., Durando, P. & Icardi, G. Fluzone(®) Intradermal vaccine: a promising new chance to increase the acceptability of influenza vaccination in adults. *Expert Rev Vaccines* **11**, 17-25, doi:10.1586/erv.11.154 (2012).
182 Frenck, R. W. *et al.* Comparison of the immunogenicity and safety of a split-virion, inactivated, trivalent influenza vaccine (Fluzone®) administered by intradermal and intramuscular route in healthy adults. *Vaccine* **29**, 5666-5674, doi:10.1016/j.vaccine.2011.06.010 (2011).
183 Lutton, R. E. *et al.* A novel scalable manufacturing process for the production of hydrogel-forming microneedle arrays. *Int J Pharm* **494**, 417-429, doi:10.1016/j.ijpharm.2015.08.049 (2015).
184 Larrañeta, E. *et al.* A facile system to evaluate in vitro drug release from dissolving microneedle arrays. *Int J Pharm* **497**, 62-69, doi:10.1016/j.ijpharm.2015.11.038 (2016).
185 Ripolin, A. *et al.* Successful application of large microneedle patches by human volunteers. *Int J Pharm* **521**, 92-101, doi:10.1016/j.ijpharm.2017.02.011 (2017).
186 Rouphael, N. G. *et al.* The safety, immunogenicity, and acceptability of inactivated influenza vaccine delivered by microneedle patch (TIV-MNP 2015): a randomised, partly blinded, placebo-controlled, phase 1 trial. *Lancet* **390**, 649-658, doi:10.1016/S0140-6736(17)30575-5 (2017).

187 Caffarel-Salvador, E. *et al.* A microneedle platform for buccal macromolecule delivery. *Science Advances* **7**, eabe2620, doi:10.1126/sciadv.abe2620 (2021).

Chapter 3. IN SITU 3D PATTERNING OF ELECTROSPUN FIBERS USING TWO-LAYER COMPOSITE MATERIALS

Adapted from: **Creighton, R.**, Phan, J., Woodrow, K.A. In situ 3D patterning of electrospun fibers using two-layer composite materials. Scientific Reports (2020) 10, 7949.

3.1 ABSTRACT

Polymeric electrospun nanofibers have extensive applications in filtration, sensing, drug delivery, and tissue engineering that often require the fibers to be patterned or integrated with a larger device. Here, we describe a highly versatile *in situ* strategy for three-dimensional electrospun fiber patterning using collectors with an insulative surface layer and conductive recessed patterns. We show that two-layer collectors with pattern dimensions down to 100-micrometers are easily fabricated using available laboratory equipment. We use finite element method simulation and experimental validation to demonstrate that the fiber patterning strategy is effective for a variety of pattern dimensions and fiber materials. Finally, the potential for this strategy to enable new applications of electrospun fibers is demonstrated by incorporating electrospun fibers into dissolving microneedles for the first time. These studies provide a framework for the adaptation of this fiber patterning strategy to many different applications of electrospun fibers.

3.2 INTRODUCTION

Electrospun fibers are a unique material with broad capabilities in filtration, sensing, drug delivery, and tissue engineering due to the versatility of materials that can be processed. Because of their interconnected pores, which create a tortuous path for particles, electrospun fibers have been developed for commercial use in air and liquid filtration.[1-4] This filtration function

combined with mechanical strength and breathability has also made electrospun fibers ideally suited to act as protective textiles for chemical or biological toxins.[5] Electrospun polymers with fluorescent or colorimetric activity have also been used as sensors for various environmental hazards like mercury ions and health hazards like organic solvents.[6-8] Electrospun fibers are useful in many different biological applications including tissue engineering and drug delivery because of the wide range of biocompatible materials that can be electrospun and the variety of strategies for incorporating physicochemically diverse agents.[9-11] Additionally, the mechanical and chemical properties of electrospun polymeric fibers can be simultaneously engineered through polymer selection, fiber alignment, and biologic incorporation.[12] These engineered electrospun fibers have been a useful tool for supporting cell viability in engineered tissues and for studying the effect of mechanical and chemical cues on cell phenotype.[13-15]

For these applications, electrospun fibers need to be patterned on various length scales for optimal function or for device integration. This is often achieved by electrospinning fibers in large sheets that are then mechanically cut into pieces with dimensions down to 5 mm and positioned within devices.[16,17] Bulk mechanical patterning has been used to layer electrospun fibers between microfluidic channels for portable and lightweight dialysis systems.[16] Fibers have also been cut and layered within the core of stimuli-responsive hydrogels for controlled drug delivery, but in this application the mechanical fiber patterning strategy resulted in uncontrolled diffusion at the device edges.[17] Mechanical fiber patterning is not generalizable because it can lead to poor control over device dimensions at small length scales,[17] and it is not feasible for complex device designs such as micro-scale grids or microfluidic channels containing discreet micro-scale fiber regions.[8,18,19] Furthermore, mechanical patterning and integration strategies can lead to fiber deformation and alteration of the fiber mat porosity, which is critical to its function

for filtration, drug delivery, and tissue engineering.[1] Therefore, there is a need for alternative fiber patterning strategies that preserve fiber structure and function, improve fiber function in existing applications, and enable new applications.

Several alternative fiber patterning strategies currently exist. Processes like photolithography and ultraviolet and femtosecond laser ablation have enabled precise fiber integration within microfluidic channels,[18,20] and have been used to increase cell infiltration and isolate cells within fiber mats.[21-23] However, many of these patterning processes are incompatible with fibers intended for biological applications, and these processes can alter polymer fiber molecular weight, reduce tensile strength, and introduce debris into the final fiber structure.[21,23] Because of these limitations, *in situ* fiber patterning strategies like near field electrospinning and electrostatic manipulation are better suited for applications requiring preservation of fiber morphology and biological reagents.[24-27] Near field electrospinning enables precise control over the deposition of single fibers to generate pattern dimensions between 25 μm and 1 mm, which is useful for characterization of fiber properties such as piezoelectricity,[28] but the process is low throughput and not ideal for large scale devices.[24] Electrostatic based fiber patterning using electric field lenses or patterned collectors has high throughput, biological compatibility, and preserves fiber morphology. However, electric field lenses can only control fiber deposition on the centimeter scale,[29] and existing patterned collectors lack versatility because the fiber patterning effect requires a particular polymer or a specific pattern design and dimension.[25-27] Taken together, the current state of the field suggests a need for an *in situ* fiber patterning strategy with more versatility in terms of fiber material, pattern complexity, and pattern dimensions.

Here, we describe a highly versatile *in situ* strategy for three-dimensional electrospun fiber patterning based on two-layer collectors with an insulative surface and conductive recessed patterns. Using finite element method simulations, we evaluated the effect of various collector design factors on the predicted fiber patterning. Key findings from these simulations were then verified experimentally. This strategy is compatible with different fiber materials and pattern dimensions, which will enable use in a broad range of future applications. To demonstrate one potential application of this new fiber patterning strategy, electrospun fibers were integrated into dissolving microneedles for the first time, and the microneedle mechanical properties were evaluated.

3.3 Results and Discussion

3.3.1 *Rapid fabrication of complex electrospun fiber patterns using two-layer collectors*

Previous studies have demonstrated that electrospun fibers are extremely sensitive to minor changes in electric field and collector dielectric properties.[29] Fiber deposition has been focused into centimeter scale spot sizes through manipulation of the electric field,[29] and fiber collection density has been modified on the micrometer scale by micropatterned collectors.[25,26] However, no single *in situ* electrospun fiber patterning strategy has demonstrated generalizability from micrometer to centimeter length scales for a variety of relevant fiber materials. Additionally, existing *in situ* fiber patterning strategies are not capable of patterning in three dimensions on a range of length scales, which could prove valuable for integrating fibers within drug delivery systems, sensors, or microfluidic channels.[16,17]

We investigated the ability of collectors with an insulative surface layer and conductive recessed patterns to generate three-dimensional patterned fibers on a range of length scales. To

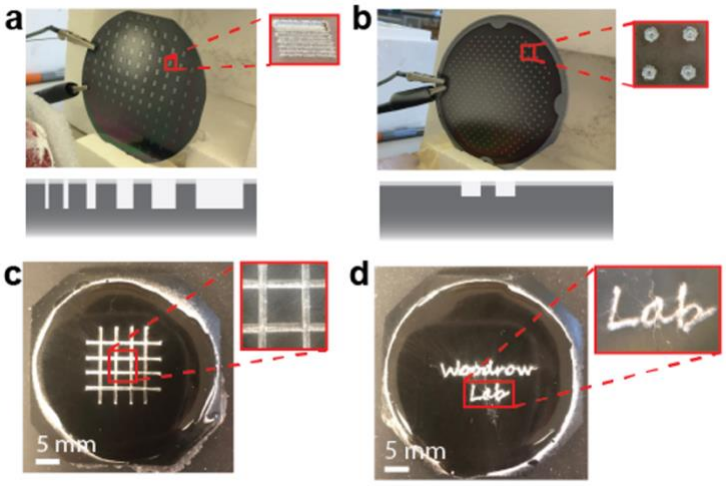

Figure 3.1. Rapid fabrication of complex electrospun fiber patterns using two-layer collectors.

(A) Trench and (B) doughnut micropatterns were created in silicon using traditional microfabrication techniques. Schematic (not to scale) of the collector cross-sections depict the trench pattern depth (150 µm) and range of widths (500 to 5 µm) and the doughnut pattern depth (50 µm). The 2 µm thick photoresist layer was left on the silicon wafers to act as the insulative surface layer. (C-D) Patterns that were approximately 500 µm wide and 500 µm deep were created in a carbon black-PDMS composite material with an approximately 600 µm thick PDMS insulative surface layer using a CO2 laser cutter. On all of these collectors, polyvinyl alcohol (PVA) fibers deposited densely in the micropatterns compared to the collector surface.

evaluate this concept, we first created micropatterned collectors in silicon. Trench patterns with 150-µm depth and doughnut patterns with 50-µm depth were created in silicon wafers using standard photolithographic patterning and deep reactive ion etching. The approximately 2-µm thick polymeric photoresist was left on the wafer after etching, creating a two-layer patterned collector with an insulative surface layer (Figure 3.1a, 3.1b). Poly(vinyl alcohol) (PVA) fibers were readily deposited over the majority of the collector, and fibers deposited more densely in the silicon patterns than on the photoresist-coated collector surface (Figure 3.1a, 3.1b). We expected that the insulative photoresist layer caused an increase in electric potential at the collector surface, leading to fiber repulsion from the surface and deposition in the conductive recessed patterns.

To explore the constraints of this fiber patterning strategy on a larger scale, we created poly(dimethyl siloxane) (PDMS)-based collectors. PDMS is easy to manipulate on a range of length scales using either additive or subtractive methods.[30-32] Additionally, PDMS can be made conductive by incorporating high concentrations of conductive particulates such as carbon black.[33] We first created a conductive mixture of carbon black and PDMS (C-PDMS), then added an approximately 600-μm thick layer of insulative PDMS on the surface. Use of this material enabled rapid fabrication of complex patterns on the scale of hundreds of micrometers using a CO_2 laser. Similar to the silicon collectors, PVA fibers deposited more densely within the patterns compared to the collector surface (Figure 3.1c, 3.1d). Together, these preliminary experiments demonstrated that patterned conductive collectors with an insulative surface layer could be used to generate patterned electrospun fibers on a range of length scales.

3.3.2 *Finite element method simulations following statistically designed experiments for collector geometry designs*

We sought to evaluate the design space of our fiber patterning strategy using a series of two-dimensional finite element method simulations. The first set of simulations followed a two-level, five factor, full factorial design to determine collector design factors that would have the most significant effect on electrospun fiber patterning. Factors of interest included insulative layer thickness and feature spacing, width, height and geometry (Figure 3.2a). The primary response output was the difference between the electric field at the bottom of the pattern and the electric field at the collector surface (ΔE). Assuming the deposition of the electrospun fibers is primarily driven by the force of the electric field, a ΔE greater than 0 would predict more fiber deposition in the patterns compared to the collector surface.

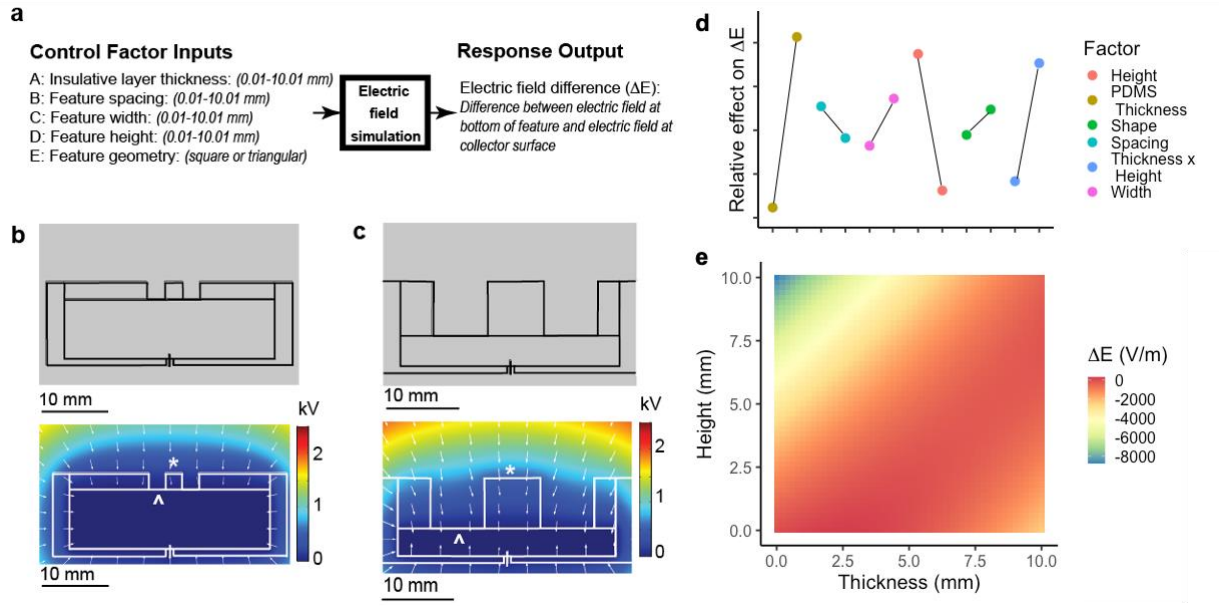

Figure 3.2. Finite element method simulations following statistically designed experiments for collector geometry designs.

(A) P-diagram of the design of experiments, including the five different control factor inputs and the primary response output. Factors were varied from 2.51 mm to 7.51 mm in the initial full factorial design, then were varied from 0.01 mm to 10.01 mm for the central composite design. Representative images from two distinct simulations for square feature geometry with (B) 2.51 mm width, height, spacing, and thickness, and (C) 7.51 mm width, height, spacing, and thickness. These images show the starting geometry, the calculated electric potential (color gradient, scale in kV), and electric field (arrow vectors). Annotations indicate the location of the collector surface (*) and bottom of the pattern (^) used to calculate the ΔE response output. (D) Means plot showing the relative effect of each factor at each level. The largest effect was observed for the insulative layer thickness, feature height, and the interaction of these two factors. (E) The heat map of ΔE from the quadratic model indicates that ΔE is maximized by limiting feature height to 5 mm and increasing the insulative layer thickness proportionally with increasing feature height.

Each simulation calculated the potential and electric field for geometries, materials, and electrostatic conditions matching actual experimental setups to be used in later studies (Figure 3.2b, 3.2c). Two sample simulations for small scale (2.5 mm width, height, spacing, and thickness) and large scale (7.5 mm width, height, spacing, and thickness) square patterns computed a ΔE of -143 V/m for the small scale pattern and a higher ΔE of 105 V/m for the large scale pattern (Figure 3.2b, 3.2c). To determine the factor or factors that were driving this result, the main effect size for each factor was calculated. The main effect for each factor is defined as the difference between the average ΔE at its high and low levels holding all other factors

constant. For this set of experiments, the insulative layer thickness and feature height had the largest effect on ΔE (effect size= 1,615 and -1,632 V/m, respectively) (Figure 3.2d). These results indicate that an increase in insulative layer thickness or a decrease in feature height would result in an increased ΔE, which predicts increased fiber deposition in the pattern. Calculation of two- and three-factor interactions showed that only the interaction of insulative layer thickness and feature height had an appreciable effect on ΔE (effect size= -1,424 V/m). Because these two factors interact, their effect should be considered by the interaction term rather than the individual main effects. Statistical analysis showed that all of the evaluated factors and the thickness-height interaction factor had a significant effect on ΔE (Table 3.1). However, it was also clear from this analysis that ΔE is primarily determined by the thickness-height interaction. These results suggest that appropriate selection of just feature height and insulative layer thickness could yield electrospun fiber patterns of a variety of widths, spacing, and shape with high selectivity.

Table 3.1. Statistical analysis of finite element method simulations

Full Factorial Design					
	Sum of Squares	*df*	*Mean Square*	*F Value*	*p-value, Prob > F*
Model	6.05E7	6	1.00E7	228	1.37E-20
A-PDMS thickness	2.08E7	1	2.08E7	472	9.34E-18
B-Spacing	6.18E5	1	6.18E5	14.0	9.56E-04
C-Width	6.39E5	1	6.39E5	14.4	8.15E-04
D-Height	2.13E7	1	2.13E7	482	7.26E-18
E-Shape	8.59E5	1	8.59E5	19.4	1.70E-04
AD	1.62E7	1	1.62E7	367	1.81E-16
Central Composite Design					
	Sum of Squares	*df*	*Mean Square*	*F Value*	*p-value, Prob > F*
Model	4.24E7	7	6.06E6	737	1.38E-24
A-PDMS Thickness	1.32E7	1	1.32E7	1611	4.49E-22
B-Spacing	1.91E5	1	1.91E5	23.3	7.92E-05
C-Width	1.52E5	1	1.52E5	18.5	2.85E-04
D-Height	1.77E7	1	1.77E7	2158	1.87E-23
AD	7.13E6	1	7.13E6	868	3.56E-19
A^2	2.44E6	1	2.44E6	297	2.83E-14
D^2	1.98E6	1	1.98E6	241	2.39E-13

To further explore factor interactions and to evaluate a larger range of pattern dimensions, we conducted another set of simulations following a central composite experimental design. Shape was omitted as a factor to simplify the design and because the full factorial design indicated that it was not one of the main factors affecting ΔE. The results were similar to the results from the full-factorial design, with the largest and most significant effects observed for insulative layer thickness, feature height, and the interaction of these two factors (Table 3.1). A quadratic model based on the results was then used to construct a heat map of the interaction between insulative layer thickness and feature height for intermediate values of spacing (5 mm) and width (5 mm). This heat map indicated that to maximize ΔE for the dimensions evaluated here, feature height should be limited to 5 mm and insulative layer thickness should be increased proportionally as feature height increases (Figure 3.2e). Importantly, ΔE can be increased for feature heights greater than 5 mm by further increasing the insulative layer thickness beyond the range of these simulations. For example, ΔE of 2,581 V/m was calculated for a triangular feature with 5.01 mm width, 15 mm height, 5.01 mm spacing, and 20 mm insulative layer thickness. Applications that require larger feature sizes will require additional simulations centered around the dimensions of interest to ensure accurate prediction of ΔE. Together these simulations suggest that this fiber patterning strategy can be used over a wide range of length scales.

3.3.3 *Rapid and inexpensive collector prototyping by subtractive and additive processes using a PDMS-based composite material*

To experimentally evaluate the collector design features predicted to affect fiber deposition in the simulations, we modified the PDMS based materials and collector fabrication process used for our proof-of-concept collectors. In the first iteration of these collectors, the 12.5% w/v C-PDMS was highly viscous, making it difficult to mix and mold the material. To

address this challenge, we incorporated carbon black into the PDMS at a lower concentration (7.5 wt%), then poured it into a mold and placed it on a rotating platform shaker to generate turbulence in the mixture and increase the settling velocity of the carbon black particles.[34] The settling of the carbon black was observed qualitatively by electrospinning PVA fibers onto the bottom (Figure 3.3a) and top (Figure 3.3b) of the C-PDMS after 15 hours of shaking followed by curing. Fiber deposition was uniform across the bottom of the material, likely due to concentration of the carbon black particles (Figure 3.3a). In comparison, fiber deposition was sparse and uneven on the top of the material where the particles were likely more dilute (Figure 3.3b). Although the shaking step adds time to the collector fabrication process, it enables uniform fiber collection with carbon black concentrations below the 10 wt% threshold needed to achieve conductivity ($5*10^{-3}$ $(ohm*cm)^{-1}$) in carbon black-PDMS mixtures and below previously reported concentrations for electrospinning collectors (12.5% w/v).[27,33,35] The small reduction of carbon black concentration reduces the viscosity of the mixture approximately 6-fold, from 148,000 cP to 24,000 cP. This reduction facilitates easy mixing and molding of the material.[33]

We incorporated this modification of the C-PDMS processing into both subtractive and additive fabrication methods. As described previously, the subtractive process starts with

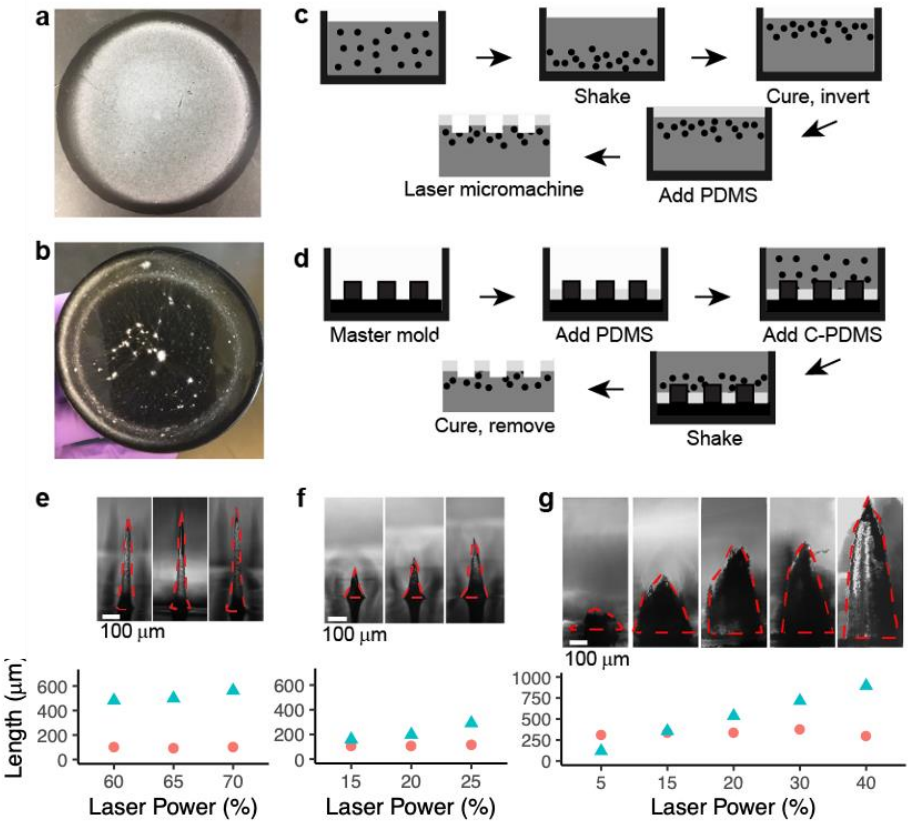

Figure 3.3. Rapid and inexpensive collector prototyping by subtractive and additive processes using a PDMS-based composite material.

(A) PVA fibers electrospun onto the side of the cured carbon black-PDMS mixture with concentrated carbon black particles, showing uniform fiber deposition. (B) PVA fibers electrospun onto the carbon black-PDMS mixture with diffuse carbon black particles, showing minimal and highly irregular fiber deposition. Schematic of the (C) subtractive procedure starting with adding the 7.5 wt% carbon black in PDMS to a mold, then shaking the mixture. This mixture is cured and inverted, then a layer of PDMS is added to the surface and cured. The two-layer material is then patterned using a CO_2 laser. (D)The additive fabrication procedure starts with a master mold. PDMS is added and cured, then C-PDMS is added and the entire mold is placed on a plate shaker. The C-PDMS is then cured, and the completed collector removed from the mold. Representative optical images and measurements of base (●) and height (◢) dimensions of conical features cast from a PDMS collector laser cut with (E) a point pattern, (F) a circle pattern (diameter: 0.06 mm), or (G) a helix pattern (diameter: 0.25 mm, 10 turns). All features used a variable laser power and constant laser speed (95%).

preparation and curing of the C-PDMS, followed by addition of PDMS. This completed two-layer material is then micromachined using a CO_2 laser system (Figure 3.3c). While the subtractive process used in the proof-of-concept collectors was well suited to relatively shallow patterns (feature depth less than 1 mm), fabrication of deeper patterns required multiple passes of the laser. Therefore, we evaluated an additive process that is better suited to larger patterns. For

the additive process (Figure 3.3d), an appropriate volume of PDMS is first added to a master mold to achieve the desired thickness and cured. Next, the C-PDMS mixture is added to the mold, shaken, and cured. For the experimental studies used to verify the simulation results, we chose to use the subtractive fabrication method to create conical features in the two-layer PDMS-based material with diameters ranging from 98 to 378 μm and heights ranging from 159 to 895 μm (Figure 3.3e- 3.3g).

From start to finish, both collector fabrication processes require approximately 30 minutes of active time over 2 days. The entire collector fabrication process is completed with inexpensive materials and laboratory equipment that is readily available. While potential alternative collector materials systems such as silicon have higher stiffness and higher conductivity, this PDMS based system is favorable for proof-of-concept studies, rapid collector design iteration, or for settings where a cleanroom for silicon processing is not available.

3.3.4 *Electrospun fiber conformation to 3D collector pattern depends on insulative layer thickness and feature height*

After identifying key factors predicted to affect fiber deposition patterns and developing a strategy for rapidly prototyping different collector patterns, we set out to experimentally validate our simulation results. The first goal of the experimental evaluation was to assess the effect of the insulative surface layer compared to a fully conductive patterned collector. An additive strategy was used to generate millimeter-scale patterns (3 mm diameter, 3.25 mm height, and 5.5 mm spacing) in a collector with and without a 600-μm thick insulative PDMS layer (Figure 3.4a, 3.4b). PVA fibers deposited only on the surface of the fully conductive collector with-out the insulative layer, but fibers deposited densely in the patterns on the insulated two-layer collector (Figure 3.4a, b). These results agree with the simulations, which calculated a 330 V/m higher ΔE

for the collector with the insulative PDMS layer. These studies experimentally demonstrate the function of an insulative surface layer to achieve fiber deposition within recessed patterns.

The PDMS-based collectors were then scaled down by approximately 10-fold to verify that the patterning effect was valid at smaller length scales (conical pattern: 269 ± 5 μm diameter, 522 ± 6 μm height, 1400 μm spacing, 400 μm insulative PDMS layer thickness). Although the simulations calculated a ΔE value less than 0 V/m (-119 V/m), we observed a

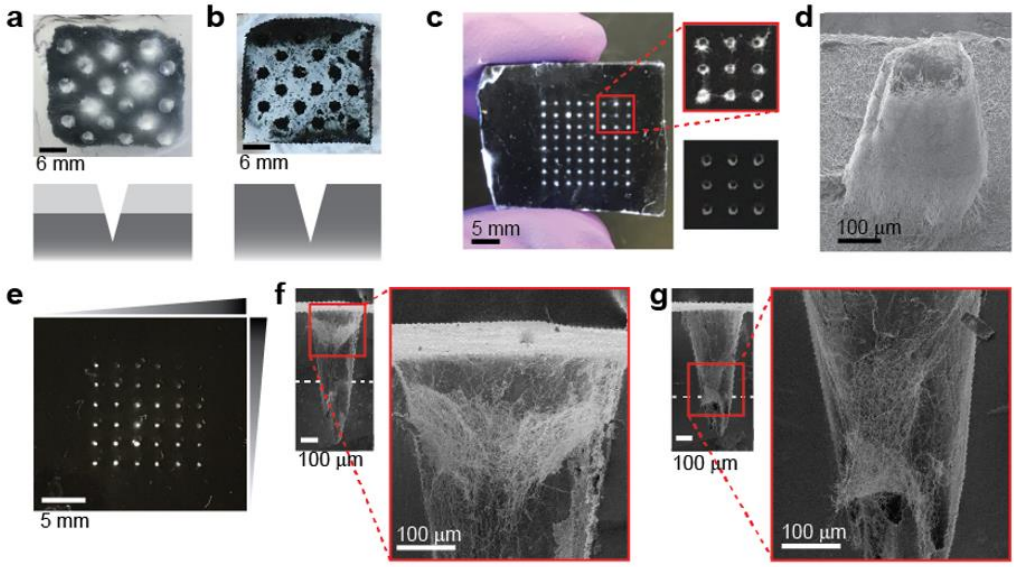

Figure 3.4. Electrospun fiber conformation to 3D collector pattern depends on insulative layer thickness and feature height.

PVA fiber collection on millimeter-scale PDMS-based patterned collectors (A) with and (B) without a 600 μm thick PDMS surface layer demonstrates the need for the insulative layer to achieve fiber deposition in the micropatterns. Conical patterns had diameter 3 mm, 3.25 mm height, and 5.5 mm spacing. (C) Micro-scale PDMS-based collector with (top inset) and without (bottom inset) PVA fiber deposition. Collector had 400 μm PDMS thickness and conical patterns with 269±5 μm diameter, 522±6 μm height, 1400 μm spacing. (D) SEM image of fibers carefully removed from micro-scale collector demonstrates fiber patterning in three dimensions. (E) Top-down view of micropatterned collector with gradient PDMS layer thickness containing PVA electrospun fibers. This collector contained conical patterns with 364±16 μm diameter, 777±20 μm height, 1600 μm spacing, and a PDMS layer that ranged from 400 to 580 μm. Fiber deposition is less visible in areas of the collector with thicker PDMS layer. (F) Cross-sectional SEM image of the gradient PDMS thickness micropatterned collector at a region with 400 μm PDMS thickness and (G) a region with 500 μm PDMS thickness containing PVA electrospun fibers. The approximate location of the insulative layer is denoted by the white dashed line. These SEM images were processed in Adobe Photoshop to improve visibility of fibers. Contrast was set to 100 and exposure offset was set to -0.1. For all electrospinning experiments, the needle-collector separation distance was 10 cm. The solution flow rate varied between 1.5-5 μL/min and the applied voltage varied between 7.5-8.5 kV because of the differences in solution properties. For millimeter scale collectors, fibers were electrospun for approximately 5 minutes, and for microscale collectors, fibers were electrospun for 1-2 minutes.

similar patterning effect for this microscale collector, with fibers deposited densely within the patterns in 1-2 minutes and little to no deposition on the collector surface (Figure 3.4c). These results suggest that experimental fiber patterning is possible at a wider range of ΔE values than those predicted by the simulations. To verify that we were not simply observing fibers bridging over the patterns, we increased the electrospinning time to create a fiber mat strong enough to be removed from the collector. We then imaged the fibers with scanning electron microscopy and observed that the fibers conformed to the patterned collector in three dimensions (Figure 3.4d). Coupled with the results for the millimeter-scale collector, these results confirm that with appropriate selection of feature height and insulative layer thickness, the fiber patterning strategy is feasible on a range of length scales.

To better understand the effect of insulative layer thickness on fiber deposition, we fabricated a microscale collector with a gradient insulative PDMS layer thickness and constant feature geometry, dimensions, and spacing. This collector contained conical patterns (364 ± 16 μm diameter, 777 ± 20 μm height, 1600 μm spacing), and an insulative PDMS layer that ranged from 400 to 580 μm. Our simulations calculated that the ΔE was 48 V/m higher for the 580 μm PDMS thickness compared to the 400 μm PDMS thickness. PVA fibers were deposited densely in the patterns over a majority of the collector in 1-2 minutes, with more visible fibers in the patterns with a thinner insulative PDMS layer and fewer visible fibers visible in patterns with a thicker insulative PDMS layer (Figure 3.4e). When cross-sections of this fiber-containing collector were inspected by SEM, we observed that the fiber deposition depth was modulated by the insulative PDMS thickness. Fibers deposited near the openings of the patterns with a 400-μm thick PDMS layer (Figure 3.4f), while fibers appeared to be deposited toward the bottom of the pattern for a 500 μm-thick PDMS layer (Figure 3.4g). The deeper fiber deposition in patterns

with a thicker insulative PDMS layer is possibly related to the increased ΔE compared to patterns with a thinner insulative PDMS layer.

Overall, the experimental evaluation of our two-layer collectors for *in situ* fiber patterning agreed with the predictions of the finite element method simulations. Electrospun fibers deposited into patterns with a range of feature heights from 3.25 mm to 522 μm through appropriate selection of insulative layer thickness, corroborating a key finding from the simulations. Because the simulations do not capture some key factors related to fiber material and electrospinning dynamics,[36,37] they cannot be used alone to precisely determine fiber deposition patterns. However, agreement in trends between the experiments and the simulations suggests that the simulation results can be used as a guide to direct the design of two-layer collectors for three-dimensional patterning of electrospun fibers.

3.3.5 *In situ patterning strategy shows versatility for physicochemically diverse polymers*

Another desirable feature of our patterning strategy is its ability to accommodate *in situ* electrospinning of a variety of fiber materials with different physicochemical properties. We evaluated this experimentally since the properties of the fibers and their behavior in the electric field were too complex to simulate accurately. We chose to demonstrate patterning of polycaprolactone (PCL) and poly(lactic-co-glycolic acid) (PLGA) here because they are widely used in drug delivery and tissue engineering, and organic solutions of these polymers have very different properties than the aqueous PVA solution used in our original experimental validation studies.[4,13,23,38] Because the PDMS-based collectors are much less conductive than standard metal collectors used for electrospinning, the low polarity polyester solutions required

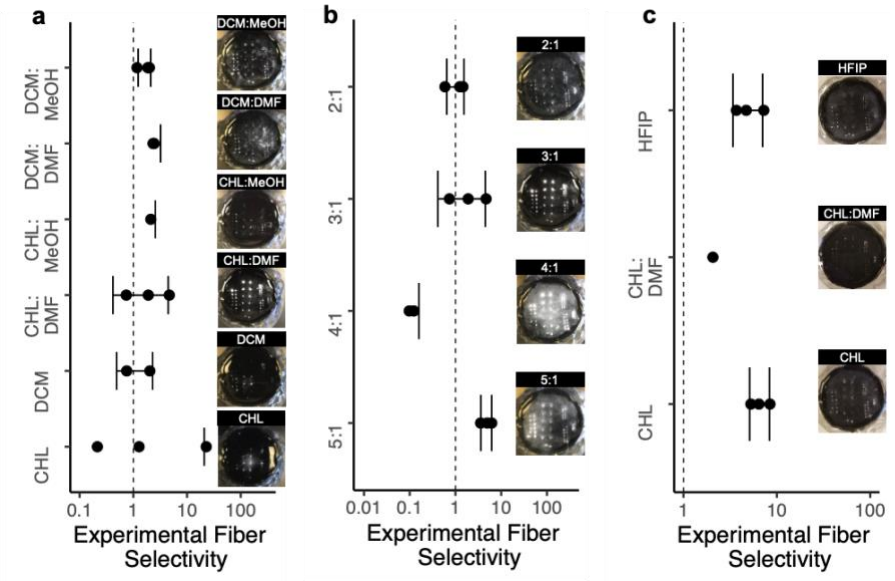

Figure 3.5. In situ patterning strategy shows versatility for physicochemically diverse polymers.

Ratio of fiber mass in the micropatterns to fiber mass on the collector surface and representative top-down images of fibers on micropatterned collectors for (A) PCL fibers electrospun from different solvents, (B) PCL fibers electrospun from different CHL:DMF ratios, (C) PLGA fibers electrospun from different solvents. (n=3, error bars represent standard deviations). The same collector with conical micropatterns of base diameter 364±16 μm, height 777±20 μm, spacing ranging from 0.5 mm to 4 mm, and insulative layer thickness 0.4 mm was used for all electrospinning experiments. PCL fibers were electrospun at a voltage of 17 kV, while PLGA fibers were electrospun at a voltage of 18 kV. All fiber samples were electrospun at a 5 μL/min flow rate and 25 cm tip to collector distance for 2 minutes.

experimentation to identify formulations with reproducible results, high yield, and selectivity for the pattern. For each polyester, we measured solution properties and fiber output from electrospinning (2 minutes) onto a collector containing five 2x6 arrays of conical patterns (364±16 μm diameter, 777±20 μm height, 500-4000 μm spacing, 500 μm insulative layer thickness). We also calculated the yield and the experimental fiber selectivity (S_E), defined here as the ratio of fiber mass deposited in the patterns to fiber mass deposited on the collector surface (Table 3.2, Figure 3.5a).

To improve the *in situ* patterning of PCL fibers, we first prepared PCL solutions at 12 wt% in various solvents and solvent mixtures with different conductivity and viscosity, factors that are known to affect fiber morphology and deposition patterns.[24,26,36,37] In general, higher fiber yield was observed for PCL solutions with higher viscosity and lower conductivity (chloroform (CHL), 3:1 chloroform: dimethylformamide (CHL: DMF)) (Table 3.2). The CHL: DMF mixture was prioritized for further studies because of its high S_E combined with its high yield and uniform deposition across the collector (Figure 3.5a). In the next iteration of PCL solution development, we tuned the solution conductivity by changing the ratio of CHL:DMF rather than through addition of salts because of the poor yield and S_E of the highest conductivity solutions in the initial solvent evaluation (Table 3.2). The best yield (100.8%) and S_E (4.9) were observed for the PCL solution in 5:1 CHL: DMF, which had approximately 30% lower conductivity and approximately 20% higher viscosity than the starting 3:1 CHL: DMF solution (Figure 3.5b). While the yield of this solution still varied between replicates, S_E was reproducible. Ultimately, a 12 wt% solution of PCL in 5:1 CHL: DMF was identified to be best suited for our *in situ* patterning, producing a nearly 20-fold increase in fiber yield and nearly 50-fold increase in S_E compared to the worst performing solution. A similar approach was used to

identify a formulation with high yield and S_E for PLGA fibers. Here, we found that a 10% PLGA solution in CHL provided the best yield (111%) and S_E (6.71) (Figure 3.5c).

Table 3.2. Polymer solution properties for patterned electrospun fibers

	Solvent	Conductivity (μS/cm)	Viscosity (Pa*s)	Output (mg)[a, b]	Yield (%) [a]	S_E
PCL Solvent Selection[c]	CHL	0.00	6.66	0.55±0.32	45.8±26.6	8.09
	DCM	0.00	3.45	0.1±0.01	8.3±0.8	1.39
	DCM: DMF	0.59	5.54	0.35±0.25	29.1±20.8	2.38
	DCM: MeOH	0.81	2.64	0.14±0.07	11.6±5.8	1.67
	CHL: MeOH	0.56	2.58	0.07±0.04	5.8±3.3	2.11
	CHL: DMF	0.24	4.56	0.83±0.39	69.1±32.5	2.43
PCL Conductivity Evaluation[c]	2:1 CHL: DMF	0.22	3.91	0.57±0.32	47.5±26.6	1.09
	4:1 CHL: DMF	0.20	5.33	0.76±0.26	63.3±21.6	0.10
	5:1 CHL: DMF	0.17	5.36	1.21±0.49	100.8±40.8	4.90
PLGA Solvent Selection[d]	CHL	0.00	2.03	1.11±0.16	111±16	6.71
	CHL: DMF	0.36	3.72	0.17±0.08	17±8	2.06
	HFIP	0.09	10.84	1.04±0.40	104±40	5.21

[a]Mean ± standard deviation of n=3 electrospinning replicates, [b] Output is reported as total fiber mass on the collector after 2 minutes of electrospinning, [c] All PCL solutions were prepared at 12 wt%, [d] All PLGA solutions were prepared at 10 wt%

Performance of PLGA solutions followed similar trends to the PCL solutions, with higher viscosity and lower conductivity solutions producing the highest S_E and yield (Table 3.2). This effect is potentially caused by the increased net charge density of electrospun fibers produced from higher conductivity solutions.[39] These fibers may not completely discharge after deposition on the collector, leading to repulsion of incoming fibers.[25,40] Therefore, future studies attempting to pattern fibers containing high concentrations of conductive agents could encounter reduced fiber yield or compromised fiber pattern quality. However, these studies could explore the use of AC potentials or a modified collector material to reduce surface charge accumulation and

overcome this challenge.[25,40] Overall, the polymer solution development performed here provides a framework for adapting virtually any fiber formulation containing active agents, other additives, or different fiber materials for use with our patterning strategy.

3.3.6 *Fabrication of mechanically robust integrated fiber microneedles*

As a demonstration of one application of this fiber patterning strategy, we used it to integrate electrospun fibers with dissolving microneedles. Here, we generated a two-layer collector in the shape of a microneedle array, deposited electrospun fibers within the collector patterns, and filled the collectors with a polymer solution to create a dissolvable matrix around the electrospun fibers and a backing layer (Figure 3.6b).[41-43] In a cross-sectional image of the completed integrated fiber microneedle device, we observed an interconnected network of electrospun fibers dispersed throughout the polymer matrix material along the entire length of the needle (Figure 3.6b inset). This data suggests that the 3D-pattern of the electrospun fibers is maintained after the addition of polyacrylic acid. Based on previous studies of polyacrylic acid microneedles, we anticipate that the matrix material will dissolve rapidly on contact with the interstitial fluid in the skin to deliver a 3D network of electrospun fibers.[41-43]

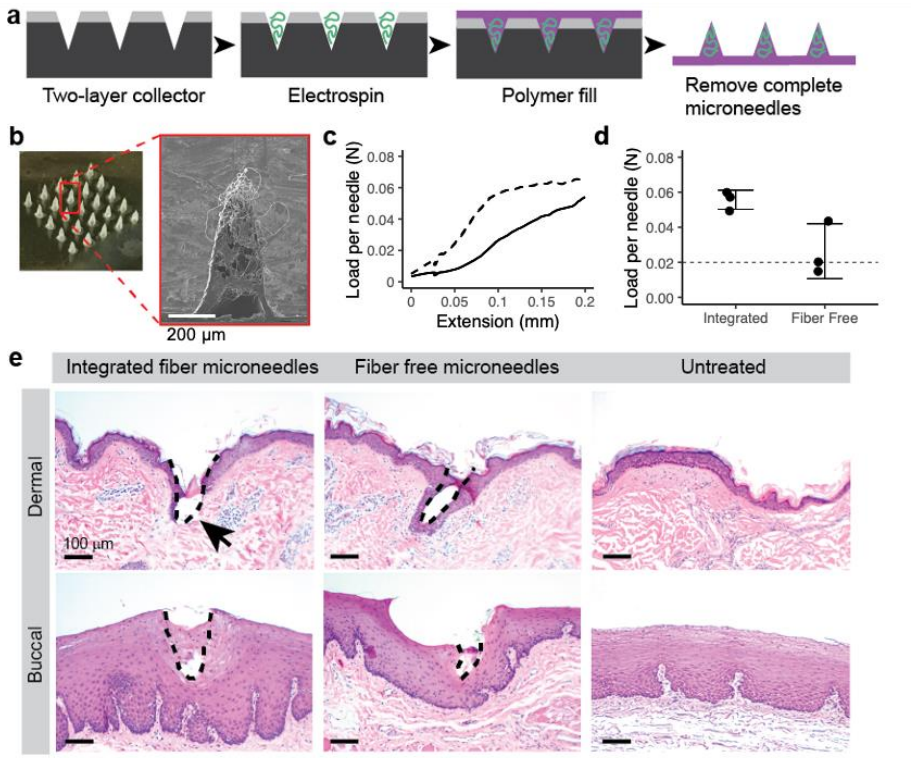

Figure 3.6. Fabrication of mechanically robust integrated fiber microneedles.

(A) Integrated fiber microneedle fabrication approach. (B) Optical microscope image of a completed integrated fiber microneedle array and (inset) SEM image of a single integrated fiber microneedle cross-section reveals an interconnected network of electrospun fibers dispersed throughout the polymer matrix material. (C) Graph of load and extension per needle for compression of microneedle arrays between two steel plates using an Instron universal testing system. Curve represents the mean of three integrated fiber microneedle arrays (dashed line) and fiber free microneedles (solid line) from separate PDMS-based collectors. Error bars omitted for graph clarity. (D) Failure forces per needle for integrated fiber microneedles compared to fiber free microneedles. For all samples measured with this method, the failure force was taken as the load at 0.1 mm extension (n=3, error bars represent standard deviations). (E) Optical microscopy of dermal and buccal tissue treated with fiber free microneedles or integrated fiber microneedles demonstrating integrated fiber microneedle disruption of the dermal stratum corneum and viable epidermis and fiber free microneedle and integrated fiber microneedle access to the epithelium of buccal tissue. Untreated dermal and buccal tissue controls are provided to demonstrate the native structure of both tissues.

Because the primary function of microneedles is their ability to puncture tissue,[44] mechanical characterization of the integrated fiber microneedles was prioritized for these proof-of-concept studies. The integrated fiber microneedles used for these studies consisted of PCL fibers electrospun from the optimized solution described in the previous section onto a collector with conical patterns (364±16 µm diameter, 777±20 µm height, 1000 µm spacing, 500 µm insulative layer thickness). After electrospinning for 2 minutes, an aqueous solution of

poly(acrylic acid) was applied to the collector to give the integrated fiber microneedles mechanical strength and to create a dissolvable backing layer (Figure 3.6b). Compressive testing of microneedle arrays indicated that integrated fiber microneedles were stiffer than microneedles without fibers fabricated by the same process (Figure 3.6c). Integrated fiber microneedle failure forces exceeded previously established targets for tissue puncture,[45] with an average failure force per needle of 0.055 N (Figure 3.6d). In contrast, conventional matrix microneedles without fibers failed at a lower force of 0.027 N/needle. This observation could be related to the microarchitecture of the integrated fiber microneedle device (Figure 3.6b). In previous studies, a similar microarchitecture enabled efficient transfer of compressive force from the matrix material to the fiber reinforcement material, resulting in improved compressive mechanical properties.[46,47] The failure force of the integrated fiber microneedles was reproducible, suggesting a consistent fabrication process. Since the predicted force per needle for tissue insertion is approximately 0.02 N, these needles have a factor of safety of nearly 3, meaning that they should reliably and completely puncture tissue.[44]

To validate that the integrated fiber microneedle patch could effectively puncture tissue, we applied the patch to non-human primate dermal and buccal tissue *ex vivo*. These tissues are of interest for drug and vaccine delivery and possess different mechanical properties.[48,49] The results indicate that only integrated fiber microneedles penetrated both the stratum corneum and the viable epidermis of dermal tissue (Figure 3.6e). In buccal tissue, the integrated fiber microneedles penetrated to a depth of approximately 240 μm, 30% of the needle height. Conventional matrix microneedles without fibers penetrated approximately 130 μm in the buccal tissue, potentially because they are mechanically weaker than the integrated fiber microneedles. In previous studies, penetration depths of 30-50% of the microneedle height have been sufficient

to achieve both bolus and sustained delivery with approximately 30% delivery efficiency.[50,51] As such, we expect to see comparable delivery with a 30% penetration depth of our microneedles in buccal tissue. Future studies applying integrated fiber microneedles for specific drug delivery applications could alter microneedle dimensions or application force to achieve the desired penetration depth.[52,53]

Integrated fiber microneedles could provide an alternative delivery modality for electrospun fibers, and they could expand the functionality of existing dissolving microneedles by enabling localized and tunable release from the fiber scaffolds. Future studies with these microneedles could iterate on the needle geometry or dimensions to optimize the mechanical stiffness or tissue penetration depths. This example application illustrates how this fiber patterning strategy could enable the development of new device architectures not possible with currently available fiber patterning methods.

3.4 CONCLUSION

In this work, we demonstrated an *in situ* strategy for three-dimensional patterning of electrospun fibers using two-layer patterned collectors. Using a combination of finite element method simulations and experimental validation, we have established that the patterning effect is primarily dependent on the pattern height and insulative layer thickness. Furthermore, our simulations and experiments indicate that three-dimensional fiber patterning is possible for pattern dimensions ranging from hundreds of micrometers to the centimeter scale. This pattern dimension range bridges the gap of pattern dimensions achievable using existing *in situ* fiber patterning strategies. This fiber patterning strategy could be used to fabricate 3D cell culture scaffolds, drug delivery devices, or microfluidic devices in future work. We demonstrated that

this fiber patterning strategy can be used to integrate electrospun fibers into microneedles for the first time.

3.5 MATERIALS AND METHODS

3.5.1 *COMSOL simulation setup and parameters*

The effect of various two-layer patterned collector designs on the electric field near the collector was evaluated using finite element method simulations (COMSOL Multiphysics version 5.1). The 2D schematic of the collector and the electrospinning setup for each simulation was prepared in AutoCAD (Autodesk AutoCAD 2015). For every simulation, the tip to collector distance was set to 10 cm. The geometry included a boundary around the entire setup. The materials assigned to each geometry in the simulation matched the materials used in experimental evaluations. Charge conservation was maintained in the simulation, and the zero-charge boundary condition was assigned to the outer boundary of the geometry. The initial value for electric potential was set to zero across the entire geometry. The applied voltage of 7.5 kV was assigned to the geometry representing the needle in the electrospinning setup. This is an actual voltage that was used for the experimental evaluation. The geometry representing the collector was grounded. Geometries were rendered with an extra fine physics-controlled mesh. The electric field at different points relative to the collector was calculated using the potential computed by the simulation.

3.5.2 *Statistical analysis of simulations*

All simulation experimental design and statistical analysis was performed using Design Expert software (version 9.0.4, Stat-Ease Inc.). The central composite design included factorial points matched to the full factorial design, 5 center points, and 9 star points (α=2.5). Results from

both experimental designs were analyzed using ANOVA and the F-test. The results of the central composite design were used to construct a quadratic model (R^2=0.9958) that can be used to predict ΔE for any given set of control factor inputs (Equation 3.1):

$$\Delta E = 63 + 231 * thickness - 35 * spacing + 31 * width - 455 * height + 106 * thickness * height - 46 * thickness^2 - 42 * height^2 \quad (3.1)$$

Results from the factorial design were tested for normality using the Shapiro-Wilk test, which resulted in a W-value of 0.967 and a p-value of 0.561, indicating that terms not selected for the model were normally distributed. The central composite design results were tested for normality by inspecting the normal probability plot for linearity.

3.5.3 *Design and preparation of two-layer patterned collectors*

To prepare the millimeter-scale two-layer patterned collectors, first an array of cones was designed in Autodesk Inventor and 3D printed in poly(lactic acid) with a FlashForge Finder at the University of Washington CoMotion Makerspace. A layer of PDMS (mixed at 1:10 ratio curing agent: pre-polymer, Sylgard 184, Dow Corning) was added to the array and cured at room temperature for 24 hours. C-PDMS was prepared by first incorporating 7.5wt% carbon black (Vulcan XC 72R, particle size 50 nm, Fuel Cell Store) into the PDMS pre-polymer using an overhead stirrer (IKA Eurostar) with a propeller attachment at 250 rpm. When all the carbon black was incorporated, the PDMS curing agent (1:10 ratio to the pre-polymer) was added and mixed for 5 minutes at 250 rpm. The completed C-PDMS mixture was added to the master cone array until the cone tips were completely covered. The entire mold was then placed on a rotating platform shaker at the highest setting for 15 hours. The C-PDMS was then cured in an oven at 37°C for 24 hours, and the completed collector was removed from the master mold. To prepare the micro-scale two-layer patterned collectors, first the complete C-PDMS mixture was added to

a 40 mm square plastic weigh boat, placed on a rotating platform shaker at the highest setting for 15 hours, and cured in an oven at 37°C for 24 hours. The C-PDMS material was then inverted, and PDMS (0.4 mL) was added to the surface. After this two-layer material was fabricated, the conical patterns were created in the material using a VLS 3.60 CO_2 laser system (Universal Laser Systems) in vector mode with the enhance feature selected. To create the 364-μm diameter base and 777-μm height conical patterns used for the microneedle application, a helix pattern with 10 turns and a diameter of 0.25 mm was plotted using the laser cutter. Laser power was set to 40% and speed was set to 90%.

3.5.4 *Rheology*

Viscosity of carbon black-PDMS mixtures was measured using a TA-Instruments Rheometer (Model ARG2) with a 40 mm diameter, 2º steel cone geometry. Data were collected in frequency sweep oscillation mode with constant small strain of 4%. Viscosity was calculated by dividing G" by the angular frequency. Viscosity values are reported at an angular frequency of 1 rad/s.

3.5.5 *Polymer solution preparation and electrospinning*

Solutions of polyester materials were prepared by combining PCL (Sigma Aldrich, average M_n 80,000) or PLGA (Lactel Absorbable Polymers, 50:50 L:G ester terminated, 0.55-0.75 dL/g inherent viscosity in HFIP) in appropriate solvents, followed by stirring overnight on a rotisserie style shaker at room temperature. All PCL solutions were prepared at 12 wt%, and all PLGA solutions were prepared at 10 wt%. Solutions of PVA (Spectrum Chemical, M_w~105 kDa, P1180) were prepared in water at 10 wt% by stirring overnight with gentle heating. Polymer solution conductivity was determined using a conductivity meter (Thermo Scientific Orion Star

A212) and viscosity was measured on a rheometer (TA Instruments AR-G2). Polymer solutions were loaded in a glass syringe fitted with a 22G blunt tipped needle. The polymer solution was dispensed from the syringe using a syringe pump (New Era Pump Systems, Inc.) at a 2 μL/min flow rate. The patterned collector of interest was fixed to a custom holder that inserted copper wires to the back of the collector. The wires were pierced through a polyethylene foam block to hold the collector at the proper height and to prevent fiber deposition on objects other than the collector. The ground from the power source (Gamma High Voltage Research) was attached to these wires and the positive lead was attached to the base of the needle. The applied voltage varied between 7.5 and 18 kV depending on the polymer solution and the tip to collector distance. Fiber samples were electrospun for 1-5 minutes.

3.5.6 *Microscopy*

All optical microscope images were obtained with a Nikon Eclipse Ti microscope with a Nikon Digital Sight DS-Fi2 camera. After fiber deposition on the patterned collectors, fibers were carefully removed with clear packaging tape and mounted on glass microscope slides for imaging. Images were captured at 20X magnification. The same contrast and brightness settings were used for all images to enable unbiased threshold analysis. SEM imaging of electrospun fibers on the two-layer patterned collectors, patterned fibers alone, and completed microneedles was performed on a JEOL JSM7400F cold field emission scanning electron microscope. All samples were coated with a 3 nm layer of gold-palladium prior to SEM imaging.

3.5.7 *Image analysis and calculation of experimental fiber selectivity*

All image analysis was performed in ImageJ. The percent area of the collector surface covered with fibers within the microscope image field was determined by converting an optical

microscope image to 8-bit, applying an auto-threshold to make all fibers appear completely black, and measuring percent area. This calculation was repeated for images from four different locations on the collector surface, and an average percent area was calculated. Fiber diameters were measured from at least 50 different fibers in SEM images. The percent area from the threshold analysis and the fiber diameter were used to estimate the volume of fibers covering the collector surface. The volume value was then multiplied by a scaling factor to estimate the fiber volume across the entire collector surface. Assuming the density of the fibers was equal to reported density of the raw polymer material, we calculated the mass of fibers on the collector surface. The mass of fibers in the patterns was then determined by subtracting the calculated mass of fibers on the collector surface from the measured total fiber mass on the collector. Finally, the ratio of fiber mass in the patterns to fiber mass on the collector surface was calculated.

3.5.8 *Microneedle fabrication*

After electrospinning, the microneedle mold two-layer collectors were filled with an aqueous PAA solution (8.75 wt%) by centrifugation at 1000x g for 1 hour. Excess PAA was removed from the collector surface and a higher concentration PAA solution (35 wt%) was added to the collector to create a strong backing layer. Microneedles were dried at room temperature for 2 days, and then the complete integrated fiber microneedle patch was gently removed from the collector. Once the collector is fabricated, the integrated fiber microneedle patches can be fabricated with an active time of approximately 1 hour over two days.

3.5.9 *Microneedle mechanical characterization*

Compression testing of microneedle arrays was performed on an Instron Universal Testing System (Model 5943). An array size of 5x5 was used for all groups and replicates. Prior to testing, arrays were inspected and needles that were broken or damaged during storage were not included in the calculation of force per needle. The microneedle array was mounted to a microscope slide with double-sided tape, and the slide was then secured to the fixed base plate with double-sided tape. A flat stainless-steel disc adapter was attached to the load cell. The load cell moved toward the fixed base plate at a rate of 20 μm/s. The instrument began collecting data when the measured load exceeded 0.08 N. The experiment ended either when the load reached 25 N or when the length of the experiment reached 45 seconds.

3.5.10 *Tissue puncture and histology*

Rhesus macaque buccal and dermal tissue was obtained from the Washington National Primate Research Center tissue donor program. Freshly excised buccal tissue was briefly dried with a Kimwipe, then either fiber free microneedles or integrated fiber microneedles were applied to the tissue using forceps for 30 seconds, followed by incubation at 37°C for 5 minutes to allow for microneedle patch dissolution. Dermal tissue from the arm was shaved before harvesting and treated in the same way. Tissues were rinsed with PBS, and then fixed in formalin overnight. Tissue processing and staining was performed by the Pathology Research Services Laboratory at the University of Washington School of Medicine Department of Pathology. Fixed tissues were embedded in paraffin, and 5 μm thick sections were obtained using a microtome. Tissue microarchitecture was visualized using hematoxylin and eosin staining.

3.6 ACKNOWLEDGEMENTS

The authors would like to thank Dr. Josh Buser for his consultation and assistance in troubleshooting the laser cutting process and Dr. Mark Morgan for the preparation of the silicon micropatterned two-layer collectors. SEM imaging was conducted at the Washington Nanofabrication Facility, a National Nanotechnology Coordinated Infrastructure (NNCI) site at the University of Washington, which is supported in part by funds from the Molecular Engineering & Sciences Institute, the Clean Energy Institute, the Washington Research Foundation, the M. J. Murdock Charitable Trust, the National Science Foundation and the National Institutes of Health. This work was supported by NIH/NIHCD grant DP2HD075703 to KAW. RC was supported by an NSF Graduate Research Fellowship (DGE-1256082) and by the STD & AIDS Research Training Fellowship Program (NIH 2T32AI007140-41).

3.7 REFERENCES

1 Gopal, R. *et al.* Electrospun nanofibrous filtration membrane. *Journal of Membrane Science* **281**, 581-586, doi:10.1016/j.memsci.2006.04.026 (2006).

2 Leung, W. W. F., Hung, C. H. & Yuen, P. T. Effect of face velocity, nanofiber packing density and thickness on filtration performance of filters with nanofibers coated on a substrate. *Separation and Purification Technology* **71**, 30-37, doi:10.1016/j.seppur.2009.10.017 (2010).

3 Gibson, P., Schreuder-Gibson, H. & Rivin, D. Transport properties of porous membranes based on electrospun nanofibers. *Colloids and Surfaces a-Physicochemical and Engineering Aspects* **187**, 469-481, doi:10.1016/s0927-7757(01)00616-1 (2001).

4 Stoddard, R. J., Steger, A. L., Blakney, A. K. & Woodrow, K. A. In pursuit of functional electrospun materials for clinical applications in humans. *Ther Deliv* **7**, 387-409, doi:10.4155/tde-2016-0017 (2016).

5 Schreuder-Gibson, H. *et al.* Protective textile materials based on electrospun nanofibers. *Journal of Advanced Materials* **34**, 44-55 (2002).

6 Wang, X. Y. *et al.* Electrospun nanofibrous membranes for highly sensitive optical sensors. *Nano Letters* **2**, 1273-1275, doi:10.1021/nl020216u (2002).

7 Yoon, J., Jung, Y. S. & Kim, J. M. A Combinatorial Approach for Colorimetric Differentiation of Organic Solvents Based on Conjugated Polymer-Embedded

Electrospun Fibers. *Advanced Functional Materials* **19**, 209-214, doi:10.1002/adfm.200800963 (2009).

8 Yu, G. F. *et al.* Patterned, highly stretchable and conductive nanofibrous PANI/PVDF strain sensors based on electrospinning and in situ polymerization. *Nanoscale* **8**, 2944-2950, doi:10.1039/c5nr08618c (2016).

9 Jing, Z. *et al.* Biodegradable electrospun fibers for drug delivery. *Journal of Controlled Release* **92**, 227-231, doi:10.1016/S0168-3659(03)00372-9 (2003).

10 Luu, Y. K., Kim, K., Hsiao, B. S., Chu, B. & Hadjiargyrou, M. Development of a nanostructured DNA delivery scaffold via electrospinning of PLGA and PLA-PEG block copolymers. *J Control Release* **89**, 341-353 (2003).

11 Rujitanaroj, P. O., Wang, Y. C., Wang, J. & Chew, S. Y. Nanofiber-mediated controlled release of siRNA complexes for long term gene-silencing applications. *Biomaterials* **32**, 5915-5923, doi:10.1016/j.biomaterials.2011.04.065 (2011).

12 Zhang, Y. Z., Su, B., Venugopal, J., Ramakrishna, S. & Lim, C. T. Biomimetic and bioactive nanofibrous scaffolds from electrospun composite nanofibers. *Int J Nanomedicine* **2**, 623-638 (2007).

13 Li, W., Laurencin, C., Caterson, E., Tuan, R. & Ko, F. Electrospun nanofibrous structure: A novel scaffold for tissue engineering. *Journal of Biomedical Materials Research* **60**, 613-621, doi:10.1002/jbm.10167 (2002).

14 Yang, F., Murugan, R., Wang, S. & Ramakrishna, S. Electrospinning of nano/micro scale poly(L-lactic acid) aligned fibers and their potential in neural tissue engineering. *Biomaterials* **26**, 2603-2610, doi:10.1016/j.biomaterials.2004.06.051 (2005).

15 Yang, Y. *et al.* Promotion of skin regeneration in diabetic rats by electrospun core-sheath fibers loaded with basic fibroblast growth factor. *Biomaterials* **32**, 4243-4254, doi:10.1016/j.biomaterials.2011.02.042 (2011).

16 Lee, K. H., Kim, D. J., Min, B. G. & Lee, S. H. Polymeric nanofiber web-based artificial renal microfluidic chip. *Biomedical Microdevices* **9**, 435-442, doi:10.1007/s10544-007-9047-5 (2007).

17 Yang, H. F., Hong, W. & Dong, L. A controlled biochemical release device with embedded nanofluidic channels. *Applied Physics Letters* **100**, doi:10.1063/1.4704143 (2012).

18 Wallin, P. *et al.* A method to integrate patterned electrospun fibers with microfluidic systems to generate complex microenvironments for cell culture applications. *Biomicrofluidics* **6**, doi:10.1063/1.4729747 (2012).

19 Yang, D. Y. *et al.* Electrospun Nanofibrous Membranes: A Novel Solid Substrate for Microfluidic Immunoassays for HIV. *Advanced Materials* **20**, 4770-+, doi:10.1002/adma.200801302 (2008).

20 Carlberg, B., Wang, T. & Liu, J. Direct Photolithographic Patterning of Electrospun Films for Defined Nanofibrillar Microarchitectures. *Langmuir* **26**, 2235-2239, doi:10.1021/la9045447 (2010).

21 Dong, Y. X., Yong, T., Liao, S., Chan, C. K. & Ramakrishna, S. Degradation of electrospun nanofiber scaffold by short wave length ultraviolet radiation treatment and its potential applications in tissue engineering. *Tissue Engineering Part A* **14**, 1321-1329, doi:10.1089/ten.tea.2007.0395 (2008).

22 Lee, B. L. *et al.* Femtosecond laser ablation enhances cell infiltration into three-dimensional electrospun scaffolds. *Acta Biomater* **8**, 2648-2658, doi:10.1016/j.actbio.2012.04.023 (2012).
23 Lim, Y. C. *et al.* Micropatterning and Characterization of Electrospun Poly(epsilon-Caprolactone)/Gelatin Nanofiber Tissue Scaffolds by Femtosecond Laser Ablation for Tissue Engineering Applications. *Biotechnology and Bioengineering* **108**, 116-126, doi:10.1002/bit.22914 (2011).
24 Sun, D. H., Chang, C., Li, S. & Lin, L. W. Near-field electrospinning. *Nano Letters* **6**, 839-842, doi:10.1021/nl0602701 (2006).
25 Ding, Z., Salim, A. & Ziaie, B. Selective Nanofiber Deposition through Field-Enhanced Electrospinning. *Langmuir* **25**, 9648-9652, doi:10.1021/la901924z (2009).
26 Dempsey, D. K. *et al.* Micropatterning of Electrospun Polyurethane Fibers Through Control of Surface Topography. *Macromolecular Materials and Engineering* **295**, 990-994, doi:10.1002/mame.201000152 (2010).
27 Cheng, Q., Lee, B. L. P., Komvopoulos, K. & Li, S. Engineering the Microstructure of Electrospun Fibrous Scaffolds by Microtopography. *Biomacromolecules* **14**, 1349-1360, doi:10.1021/bm302000n (2013).
28 Liu, Z. H., Pan, C. T., Lin, L. W. & Lai, H. W. Piezoelectric properties of PVDF/MWCNT nanofiber using near-field electrospinning. *Sensors and Actuators a-Physical* **193**, 13-24, doi:10.1016/j.sna.2013.01.007 (2013).
29 Deitzel, J. M., Kleinmeyer, J. D., Hirvonen, J. K. & Tan, N. C. B. Controlled deposition of electrospun poly(ethylene oxide) fibers. *Polymer* **42**, 8163-8170, doi:10.1016/s0032-3861(01)00336-6 (2001).
30 Yu, H. & Zhou, G. Deformable mold based on-demand microchannel fabrication technology. *Sensors and Actuators B-Chemical* **183**, 40-45, doi:10.1016/j.snb.2013.03.117 (2013).
31 Tu, K. T. & Chung, C. K. Rapid prototyping of biodegradable microneedle arrays by integrating CO2 laser processing and polymer molding. *Journal of Micromechanics and Microengineering* **26**, doi:10.1088/0960-1317/26/6/065015 (2016).
32 Nejad, H. R., Sadeqi, A., Kiaee, G. & Sonkusale, S. Low-cost and cleanroom-free fabrication of microneedles. *Microsystems & Nanoengineering* **4**, doi:10.1038/micronano.2017.73 (2018).
33 Niu, X. Z., Peng, S. L., Liu, L. Y., Wen, W. J. & Sheng, P. Characterizing and Patterning of PDMS-Based Conducting Composites. *Advanced Materials* **19**, 2682-2686, doi:10.1002/adma.200602515 (2007).
34 Eaton, J. K. & Longmire, E. K. in *Multiphase Flow Handbook* (eds Efstathios E. Michaelides, Clayton T. Crowe, & John D. Schwarzkopf) Ch. 12, 729-752 (CRC Press, 2017).
35 Unger, M. A., Chou, H. P., Thorsen, T., Scherer, A. & Quake, S. R. Monolithic microfabricated valves and pumps by multilayer soft lithography. *Science* **288**, 113-116, doi:10.1126/science.288.5463.113 (2000).
36 Fong, H., Chun, I. & Reneker, D. Beaded nanofibers formed during electrospinning. *Polymer* **40**, 4585-4592, doi:10.1016/S0032-3861(99)00068-3 (1999).
37 Zong, X. *et al.* Structure and process relationship of electrospun bioabsorbable nanofiber membranes. *Polymer* **43**, 4403-4412, doi:10.1016/S0032-3861(02)00275-6 (2002).

38 Carson, D., Jiang, Y. & Woodrow, K. A. Tunable Release of Multiclass Anti-HIV Drugs that are Water-Soluble and Loaded at High Drug Content in Polyester Blended Electrospun Fibers. *Pharmaceutical Research* **33**, 125-136, doi:10.1007/s11095-015-1769-0 (2016).

39 Pillay, V. *et al.* A Review of the Effect of Processing Variables on the Fabrication of Electrospun Nanofibers for Drug Delivery Applications. *Journal of Nanomaterials* **2013**, doi:10.1155/2013/789289 (2013).

40 Kessick, R., Fenn, J. & Tepper, G. The use of AC potentials in electrospraying and electrospinning processes. *Polymer* **45**, 2981-2984, doi:10.1016/j.polymer.2004.02.056 (2004).

41 DeMuth, P. C., Min, Y., Irvine, D. J. & Hammond, P. T. Implantable Silk Composite Microneedles for Programmable Vaccine Release Kinetics and Enhanced Immunogenicity in Transcutaneous Immunization. *Advanced Healthcare Materials* **3**, 47-58, doi:10.1002/adhm.201300139 (2014).

42 DeMuth, P. C., Garcia-Beltran, W. F., Ai-Ling, M. L., Hammond, P. T. & Irvine, D. J. Composite Dissolving Microneedles for Coordinated Control of Antigen and Adjuvant Delivery Kinetics in Transcutaneous Vaccination. *Advanced Functional Materials* **23**, 161-172, doi:10.1002/adfm.201201512 (2013).

43 Johnson, A. R. *et al.* Single-Step Fabrication of Computationally Designed Microneedles by Continuous Liquid Interface Production. *PLoS One* **11**, e0162518, doi:10.1371/journal.pone.0162518 (2016).

44 Park, J. H., Allen, M. G. & Prausnitz, M. R. Biodegradable polymer microneedles: Fabrication, mechanics and transdermal drug delivery. *Journal of Controlled Release* **104**, 51-66, doi:10.1016/j.jconrel.2005.02.002 (2005).

45 Davis, S. P., Landis, B. J., Adams, Z. H., Allen, M. G. & Prausnitz, M. R. Insertion of microneedles into skin: measurement and prediction of insertion force and needle fracture force. *Journal of Biomechanics* **37**, 1155-1163, doi:10.1016/j.jbiomech.2003.12.010 (2004).

46 Kai, D. *et al.* Mechanical properties and in vitro behavior of nanofiber-hydrogel composites for tissue engineering applications. *Nanotechnology* **23**, 095705, doi:10.1088/0957-4484/23/9/095705 (2012).

47 Zhou, C. & Wu, Q. A novel polyacrylamide nanocomposite hydrogel reinforced with natural chitosan nanofibers. *Colloids Surf B Biointerfaces* **84**, 155-162, doi:10.1016/j.colsurfb.2010.12.030 (2011).

48 Goktas, S., Dmytryk, J. J. & McFetridge, P. S. Biomechanical behavior of oral soft tissues. *J Periodontol* **82**, 1178-1186, doi:10.1902/jop.2011.100573 (2011).

49 Moronkeji, K., Todd, S., Dawidowska, I., Barrett, S. D. & Akhtar, R. The role of subcutaneous tissue stiffness on microneedle performance in a representative in vitro model of skin. *J Control Release* **265**, 102-112, doi:10.1016/j.jconrel.2016.11.004 (2017).

50 Lee, J. W., Park, J. H. & Prausnitz, M. R. Dissolving microneedles for transdermal drug delivery. *Biomaterials* **29**, 2113-2124, doi:10.1016/j.biomaterials.2007.12.048 (2008).

51 McNeilly, C. L. *et al.* Microprojection arrays to immunise at mucosal surfaces. *J Control Release* **196**, 252-260, doi:10.1016/j.jconrel.2014.09.028 (2014).

52 Bal, S. M. *et al.* Influence of microneedle shape on the transport of a fluorescent dye into human skin in vivo. *J Control Release* **147**, 218-224, doi:10.1016/j.jconrel.2010.07.104 (2010).

53 Donnelly, R. F. *et al.* Optical coherence tomography is a valuable tool in the study of the effects of microneedle geometry on skin penetration characteristics and in-skin dissolution. *J Control Release* **147**, 333-341, doi:10.1016/j.jconrel.2010.08.008 (2010).

Chapter 4. QUANTITATIVE EVALUATION OF TWO-LAYER COLLECTORS FABRICATED FROM 3D-PRINTED MASTER MOLDS

4.1 ABSTRACT

Electrostatic patterning of electrospun fibers has been used to improve filtration, control drug release, and direct cell adhesion and proliferation. Often these functions are optimized by tuning the fiber material, pattern dimensions, or electrospinning settings, which results in micron-scale changes in the fiber pattern. While previous fiber patterning studies often include characterization of the diameter of single fibers the final fiber mat function, quantitative evaluation of the fiber pattern itself is not typical. However, this characterization is critical to understand the factors contributing to the fiber pattern and to understand the final function of the patterned fiber mat. Here, we develop a new two-layer collector fabrication process using 3D-printed master molds using a custom analysis pipeline to quantitatively evaluate the fiber pattern quality of each iteration. Using this approach, we quantify the effect of electrospinning setup, insulative layer thickness, and conductive particle concentration on fiber pattern quality and select the best design for three-dimensional fiber patterning. Through iterative experimentation, fiber yield was increased 3-fold, fiber selectivity for the patterns was increased more than 4-fold, and uniformity of the patterning was increased nearly 14-fold. This rational approach to patterned fiber development could be applied to virtually any method or pattern in the future to better understand fiber patterning processes and the resulting patterned fiber function.

4.2 INTRODUCTION

The deposition pattern of electrospun fibers can be controlled in two dimensions or three dimensions by manipulation of electrostatic forces. Previous studies have used either secondary electrodes or patterned collectors to manipulate these forces. Secondary electrodes have been used to control two-dimensional fiber deposition on the centimeter-scale.[1,2] In combination with specialized electrospinning parameters, two dimensional patterns on the millimeter-scale could be produced.[3] Patterned collectors fabricated from a single material such as a metal or nylon mesh have also been used to manipulate the electric field and control fiber deposition.[4-9] Alternatively, patterned collectors can be designed from composite materials such as an insulative base with a patterned electrolyte with specific electronic properties to specifically attract or repel fibers to different areas of the collector.[10-14]

Patterned electrospun fibers have previously been used for diverse applications including filtration,[15] cell patterning and alignment,[11,14,16] tissue engineering scaffolds,[6,17] and control of drug release rates.[4,5] For example, osteoblast attachment to three-dimensional honeycomb polycaprolactone scaffolds was dependent on pattern diameter and pattern wall height. Specifically, the relative cell density was two-fold greater for 360 μm diameter patterns compared to 80 μm or 160 μm diameter patterns, and selective cell attachment was only observed for a 40 μm wall height and not a 10 μm wall height.[16] In another study, cellulose acetate fibers loaded with Diclofenac sodium were collected on nylon meshes with opening sizes of 50 μm or 100 μm. Fibers collected on the 50 μm opening size mesh were more hydrophobic than those collected on the 100 μm opening size mesh, indicated by water contact angles of 134º and 117º, respectively. The increased hydrophobicity for fibers collected on the smaller opening size mesh led to a two-fold decrease in drug release rate.[4]

Although previous studies have evaluated different patterns, collector materials, and fiber materials, the effect on fiber patterning is most often described only qualitatively despite apparent quantitative differences.[7,9-11,16] For example, in a study evaluating fiber patterning using patterned electrolytes on insulating collectors, the apparent fiber yield varied for the different insulating collector materials evaluated.[11] Although it was not quantified in this study, fiber yield is an important consideration for fibers encapsulating valuable reagents or for scale-up of the electrospinning process.[18] In another study, the pattern spacing appeared to have an effect on the uniformity of the pattern across the fiber mat.[7] Uniformity and reproducibility are most commonly addressed in studies of large scale electrospinning.[19,20] However, non-uniformity could also confound functional studies of patterned electrospun fibers. Additionally, in a study of patterned fibers for osteoblast culture, the fiber material appeared to affect the density of fiber deposition within hexagonal shaped wells.[16] This could have contributed to the observed differences in cell attachment and proliferation for the two fiber materials, but the only fiber pattern characterization performed was measurement of the wall height. In general, development of robust fiber patterning methods and their application requires additional methods for quantitative characterization.

We have previously reported the development of two-layer patterned collectors for three-dimensional fiber patterning. Our previous work demonstrated the feasibility and basic capabilities of this technology using laser machined collectors.[13] Here, we develop collectors fabricated using 3D-printed master molds using a custom analysis pipeline to quantitatively evaluate fiber pattern quality. We evaluate the effect of different electrospinning setups on the fiber pattern quality achieved with patterned collectors for the first time. Additionally, we use an alternate conductive elastomer to improve the pattern quality of conductive fiber materials.

Together, these studies expand on our initial work to more fully characterize two-layer collectors for three-dimensional fiber patterning and identify next steps to extend the fiber patterning technology to additional fiber materials. Additionally, this work demonstrates how different quantitative fiber pattern characterization metrics can be combined to improve the function of a fiber patterning technology.

4.3 RESULTS AND DISCUSSION

4.3.1 *Two-layer collector fabrication strategy*

We previously reported a method to pattern electrospun fibers *in situ* using two-layer patterned collectors. In this original study, collectors were patterned on a micro-scale fabricated using laser micromachining. While this fabrication method enabled rapid iteration through different collector designs, fabrication time increased linearly with the number of collectors and the number of features (Figure 4.1a). Additionally, the laser machining process generated persistent dross in the collectors that contaminated the resulting structures and compromised their morphology (Figure 4.1b). Smooth and uniform surfaces were not possible for small aspect ratio features (Figure 4.1c), and other possible shapes like pyramids that are easily fabricated using a 3D printed master mold (Figure 4.1d) were not possible.

Because of these limitations, we pursued a fabrication process based on a 3D-printed positive master. After printing one master mold, we could cast many two-layer collectors for fiber patterning by first adding a layer of insulative PDMS and allowing it to cure, followed by adding a conductive mixture of carbon black and PDMS and allowing it to cure. To maximize the quality of the resulting fiber patterning, we performed several iterations on factors related to

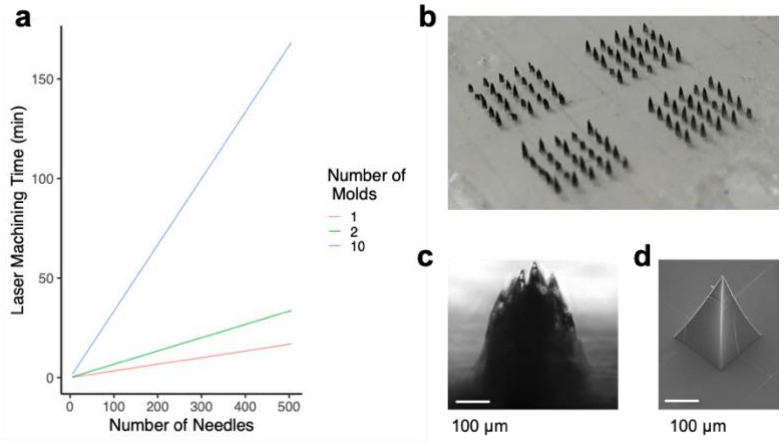

Figure 4.1. Motivation for the development of a collector fabrication method using 3D-printed master molds.

a) Plot of theoretical required laser machining time demonstrating a linear increase with the number of needles in the array and the number of molds. b) Completed microneedles removed from a laser machined mold appear black from the dross left in the mold. c) Optical microscope image of a microneedle cast from a laser machined mold demonstrates how low aspect ratio microneedle dimensions can yield non-uniform morphology. d) SEM image of a pyramidal microneedle fabricated using a 3D printed master mold, demonstrating alternative microneedle morphologies not possible with laser machining.

the electrospinning setup and collector design (Table 4.1). Factors were altered from their baseline level one at a time, while all other factors were kept constant.

For each iteration, we characterized fiber yield, uniformity, and the selectivity ratio, or mass of fibers in the pattern cavities compared to the collector surface. We analyzed the fiber integration by three different methods in an attempt to gain a complete characterization. The top-down image analysis of the collectors with fibers provides an accurate description of fiber deposition on the mold surface, but it is not indicative of three-dimensional integration with the mold. 3D characterization was therefore obtained for the evaluation of insulative layer thickness and carbon black-PDMS concentration by SEM imaging of the fibers after removal from the mold. However, in the removal process the fibers can be torn, collapsed, or deformed. Because of this limitation, we developed an additional characterization method that calculates the mass of fibers in the pattern cavities using microscopy and analysis of the fiber mass on the collector. We

expect that combining these different characterization methods enables a complete evaluation of fiber pattern quality.

Table 4.1. Description of factors varied during the development of the two-layer collector fabrication method based on master molds

	Copper Plate Electrode	Collector Edge Insulation	Insulative Layer Thickness (μm)	Carbon Black Concentration (% w/w)
Baseline Level	+	+	620	7.5
Other Evaluated Levels	-	-	387	5
			465	10
			562	

4.3.2 *Finite element method evaluation of electrospinning setup*

We first evaluated the effect of adding an auxiliary copper plate electrode around the needle dispensing the polymer solution and the effect of positioning foam insulation around the edges of the patterned collector using finite element method simulations (Figure 4.2a, 4.2b). The collector contained three triangular features with opening width 900 μm, height 2370 μm, and insulative layer thickness 470 μm. The primary output from these simulations was ΔE, defined as the difference between the electric field at the bottom of the pattern and the collector surface. Interpretation of these simulations assumes spatial fiber deposition is determined by the force of the electric field. Therefore, fiber deposition in the patterns is expected for a ΔE value greater than 0 V/m. The simulation results indicated that the presence of the copper plate electrode creates a stronger potential close to the collector and a more evenly dispersed electric field (Figure 4.2c). Without the copper plate electrode, there was a high potential and electric field around the needle that rapidly decayed as the distance from the needle increased. The collector edge insulation did not appear to affect the potential or electric field lines in any of the

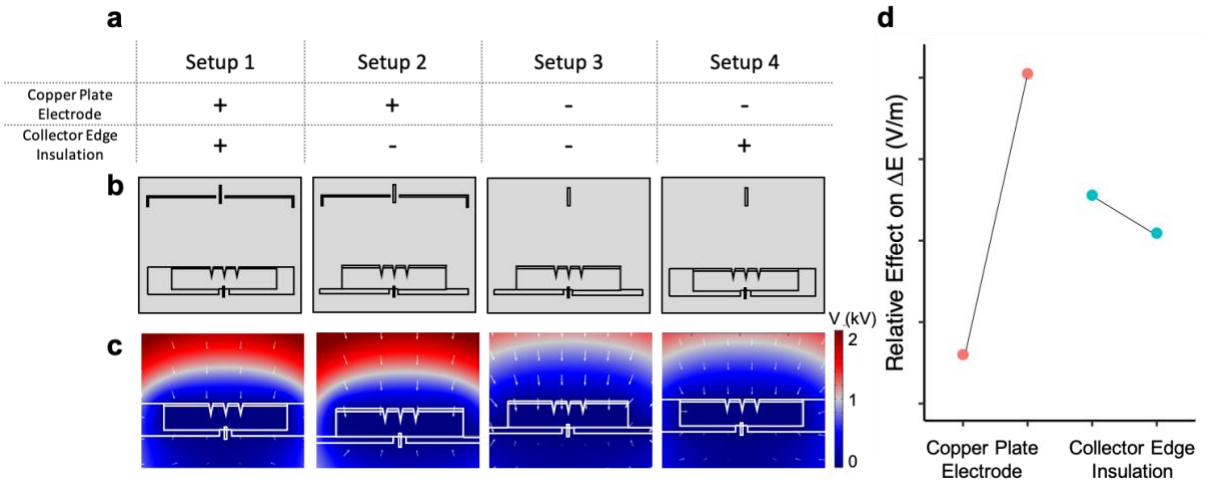

Figure 4.2. Simulations predict fiber patterning could be improved using an auxiliary electrode

a) Description of the four electrospinning setups evaluated using finite element method simulations. b) Schematics (not to scale) of the geometries used in the simulations. c) Simulation results of the potential (color gradient) and electric field (white arrows). The arrow length represents the logarithm of the magnitude of the electric field. The number of arrows was constant across all simulations. d) Means plot indicating the relative effect of each factor on ΔE holding the other factor constant.

simulations. These results are consistent with previous modeling performed by Yang et al which suggested that inclusion of an auxiliary plate electrode produces weaker electric field at the needle tip and a more uniform electric field between the needle and collector compared to a needle electrode alone.[20]

To understand the possible effect of the copper plate electrode and the collector edge insulation on predicted fiber patterning, the main effect of each factor independent of the other factor was calculated. The copper plate electrode had a much larger effect on ΔE (ΔE = 172 V/m) compared to the collector edge insulation (ΔE = -23 V/m) based on these simulations (Figure 4.2d). Overall, the electrospinning setup simulations suggested that the copper plate electrode could increase selective fiber deposition, but the collector edge insulation had a minimal effect on fiber deposition. However, because this simple static simulation is only designed to evaluate the electric field in the vicinity of the collector and not the actual movement of the fibers in the

electric field, both factors were also evaluated experimentally before selecting a setup to prioritize in later studies.

4.3.3 *Experimental evaluation of electrospinning setup*

When the setups were evaluated experimentally, we observed twice as much fiber mass on the collector for the setup with the copper plate electrode and the collector edge insulation compared to all of the other setups (Figure 4.3a). Setup 1 with the copper plate electrode and the collector edge insulation also resulted in a highly uniform fiber deposition pattern (CV= 3.6%) across the pattern array (Figure 4.3b). These results are consistent with previous studies in which auxiliary electrodes increased fiber production efficiency three-fold and increased fiber mat uniformity.[19] The collector edge insulation appeared to affect the location of fiber deposition in combination with the copper plate electrode, with very few fibers visible on the collector when the setup included the copper plate electrode but not the collector edge insulation (Setup 2). This could be due to fibers collecting on the exposed conductive areas on the sides of the collector rather than in the pattern cavities. Meanwhile, setups 3 and 4 without the auxiliary electrode resulted in unstable fiber formation and a variable pattern (Setup 3 CV = 49%, Setup 4 CV = 221%) independent of the presence of the collector edge insulation (Figure 4.3b). This result could be explained by the stronger electric field close to the needle observed in our simulations and previously described.[20] Previous studies suggest that a stronger electric field near the electrospinning nozzle results in a fiber with higher surface charge density. These more highly charged fibers are potentially more sensitive to the patterned collector, as observed by others,[16] resulting in fiber deposition in the patterns (observed in Setup 3) even without the collector edge insulation. However, higher fiber charge could also lead to incomplete fiber discharge after deposition on the collector, resulting in patterning of initially deposited fibers followed by

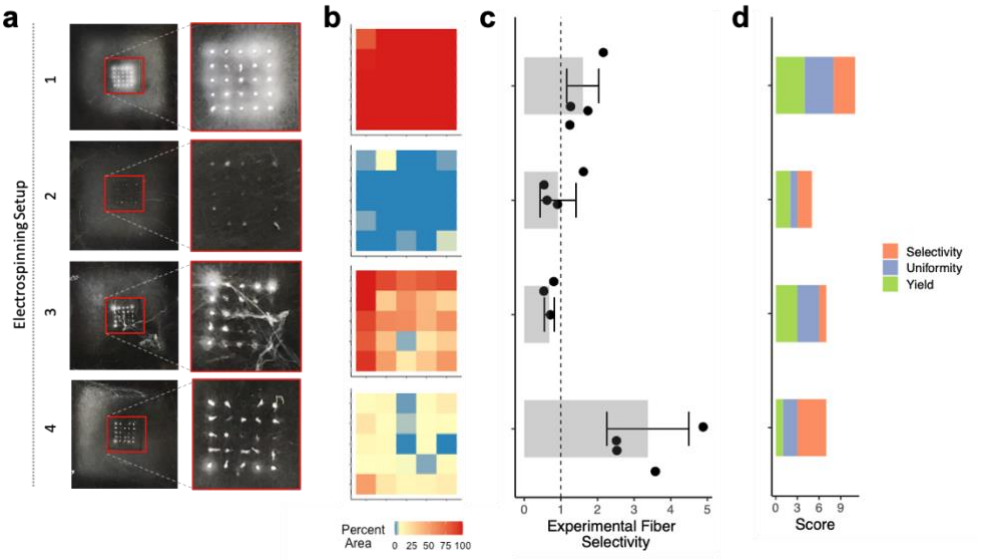

Figure 4.3. Electrospinning setup including auxiliary electrode and collector insulation yields highest pattern quality

a) Top-down images of PLGA fibers deposited on two-layer patterned collectors using different electrospinning setups. The same collector with 300 µm diameter, 800 µm height conical cavities, 7.5% w/w carbon black in the conductive layer, and a 620 µm thick insulative layer was used for each experiment. Images on the left show the entire collector area, while the inset is a closer image of the pattern area. b) Heat maps of the percent area around each section of the pattern filled with fibers, calculated using threshold analysis of the top-down fiber images. c) Ratio of fiber mass in the micropatterns to fiber mass on the collector surface. d) Aggregate fiber pattern quality scores calculated by ranking the yield, coefficient of variation of the percent area heat maps, and the experimental fiber selectivity for each electrospinning setup, then calculating the sum of each rank.

repulsion of additional incoming fibers.[7] This phenomenon is one possible explanation of the non-uniform fiber patterning observed for Setups 3 and 4.

The foam insulation influenced the fiber selectivity for the pattern cavities, with setups including the foam resulting in a higher selectivity (Setup 1 S_E = 1.6; Setup 4 S_E = 3.37) compared to setups without the foam (Setup 2 S_E = 0.92, Setup 3 S_E = 1.4) (Figure 4.3c). Although the selectivity of Setup 1 (S_E = 1.6) with the copper plate electrode was less than Setup 4 (S_E = 3.37), this result could be due to the higher fiber mass collected with Setup 1. Because the volume of the pattern cavities is finite, as fiber yield increases beyond the capacity of the cavities, more fibers are deposited on the collector surface, resulting in reduced selectivity. If needed in future studies, the selectivity of Setup 1 could likely be increased by reducing the

electrospinning time. When yield, uniformity, and selectivity were considered together, Setup 1 had the highest overall fiber quality score (Figure 4.3d). Together, the simulation and experimental results led to the use of a copper plate electrode and collector edge insulation in the electrospinning setup.

4.3.4 *Effect of insulative layer thickness on fiber pattern quality*

Next, we evaluated the effect of the insulative layer thickness on *in situ* fiber patterning. Two-layer collectors were fabricated using different volumes of PDMS ranging from 0.25 mL to 0.4 mL to generate theoretical PDMS layer thicknesses ranging from 387 to 620 µm. Variation of fiber yield between the collectors (98% – 147%) was within error, but the location of the fiber

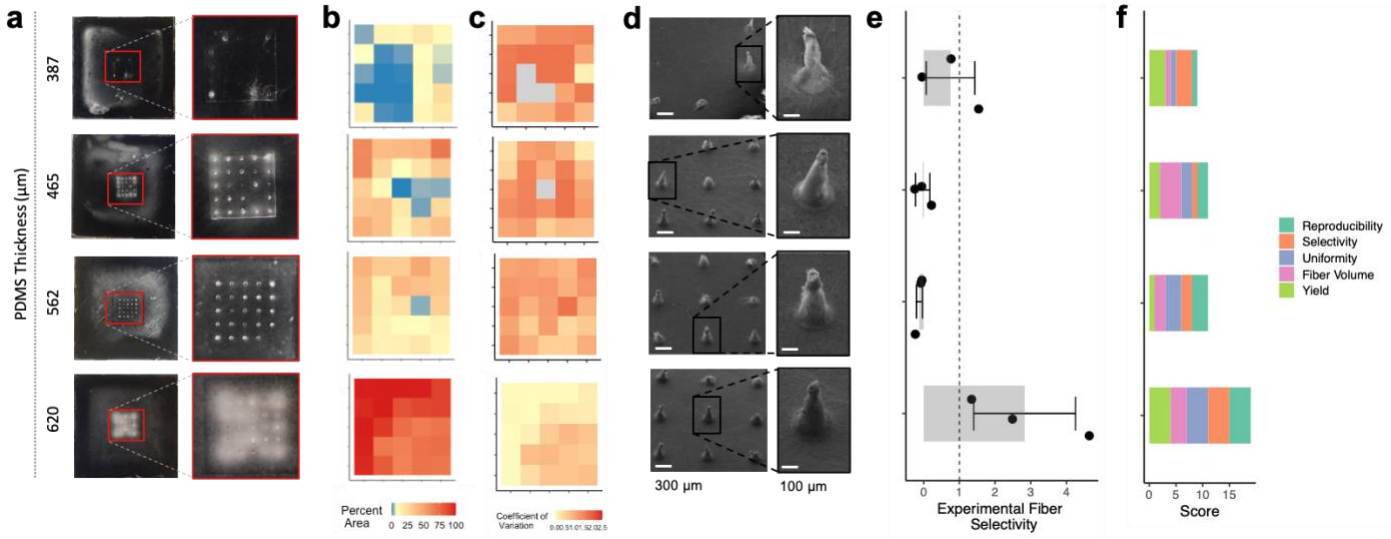

Figure 4.4. Increased insulative layer thickness improves fiber pattern quality

a) Top-down images of PLGA fibers deposited on two-layer patterned collectors with different insulative layer thicknesses. Each collector contained 300 µm diameter, 800 µm height conical cavities and was fabricated using 7.5% w/w carbon black in the conductive layer and electrospinning was performed using a setup with an auxiliary electrode and collector insulation for each experiment. Images on the left show the entire collector area, while the inset is a closer image of the pattern area. b) Heat maps of the percent area around each section of the pattern filled with fibers, calculated using threshold analysis of the top-down fiber images. c) Heat maps of the coefficient of variation of the percent area value for each pattern section across three electrospinning replicates. d) SEM images of fibers removed from the collectors used for measurement of patterned fiber volume. e)Ratio of fiber mass in the micropatterns to fiber mass on the collector surface. Grey bars represent the mean and error bars represent the standard deviation of three electrospinning replicates. f) Aggregate fiber pattern quality scores calculated by ranking the yield, uniformity, reproducibility, fiber volume, and the experimental fiber selectivity for each collector, then calculating the sum of each rank.

deposition was more focused in the region of the pattern cavities for collectors with a thicker PDMS layer (Figure 4.4a).

Uniformity increased as the PDMS layer thickness increased, with the most uniform fiber deposition pattern observed for the collector with the thickest PDMS layer (CV = 16%) (Figure 4.4b). Reproducibility of the fiber pattern for independent electrospinning experiments followed the same trend, with the lowest coefficient of variation (CV = 35%) between electrospinning experiments measured for the collector with the thickest PDMS layer (Figure 4.4c). Based on SEM images of fibers removed from the collectors after electrospinning, fibers appeared to conform well to the conical cavities of the collector for all collectors with a PDMS thickness greater than 387 µm (Figure 4.4d). ImageJ analysis approximating the fiber volume from these images found that the fiber volume for the collector with 387 µm PDMS thickness was approximately an order of magnitude less than the volume for the other collectors. The highest fiber selectivity (S_E = 4.06) was measured for the collector with the thickest PDMS layer (Figure 4.4e). Although the collector with the thinnest PDMS layer had the next highest selectivity (S_E = 2.38), its low uniformity, reproducibility, and fiber volume led to the lowest overall fiber quality score (Figure 4.4f). Together, the high uniformity, reproducibility, and selectivity for the thickest PDMS layer (620 µm) led to the highest fiber quality score and prioritization of this thickness for future studies.

Although our previously developed two-layer collectors exhibited apparent high quality fiber patterning into features of similar dimensions with a 400-µm PDMS layer, it is likely that a larger volume of PDMS is required for collectors fabricated from master molds due to the high viscosity PDMS clinging to the walls and features of the mold.[21] Based on our previous simulation results, the collector with 387 µm PDMS thickness likely had such inferior fiber

patterning results because of an overall higher surface potential.[13] This higher potential enables more fiber deposition across the entire collector surface, leading to fewer fibers deposited in the patterns in a given time frame. Relative permittivity of collector materials has been shown to affect electrospun fiber alignment and two-dimensional spatial deposition in previous studies.[12,22] However, no previous group has modified collector material properties to achieve three-dimensional fiber patterning. These results could be used in combination with our previously published simulation results to direct the adaptation of this fiber patterning approach to other pattern dimensions, geometries, or conductive materials.

4.3.5 *Effect of carbon black concentration on fiber pattern quality*

Finally, we evaluated the effect of carbon black concentration on the electrospun fiber patterning quality. Carbon black concentration in the conductive PDMS layer of the collectors was varied from 5 wt% to 10 wt%. The fiber yield for each of these collectors was approximately equal (107% - 119%), but there was a distinct difference in the uniformity and reproducibility of the fiber deposition for these collectors (Figure 4.5a-c). The fiber deposition pattern for the 5 wt% carbon black collector was highly irregular with fibers appearing to deposit asymmetrically. The 7.5 wt% carbon black collector resulted in the most uniform (CV = 35%) and reproducible (CV between 3 electrospinning replicates = 92%) fiber deposition (Figure 4.5b, 4.5c). The 10 wt% carbon black collector performed similarly (CV = 39%, CV between 3 electrospinning replicates = 103%), but with more non-specific fiber deposition on the collector surface (Figure 4.5a-c).

Complete conformation to the collector was only observed for the 7.5 wt% and 10 wt% carbon black collectors, and the volume of these fibers was approximately equal (Figure 4.5d). Some three-dimensional patterning was observed for the 5 wt% carbon black collector, but the

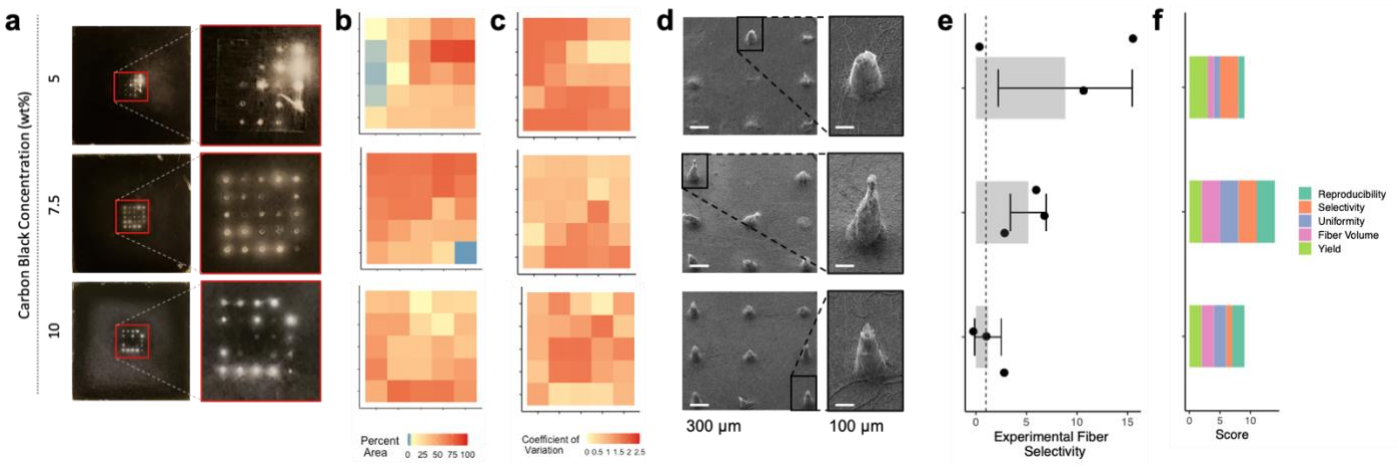

Figure 4.5. Intermediate carbon black concentration produces highest fiber pattern quality

a) Top-down images of PLGA fibers deposited on two-layer patterned collectors with different carbon black concentrations in the conductive layer. Each collector contained 300 µm diameter, 800 µm height conical cavities, and was fabricated using a 620 µm insulative layer thickness. Electrospinning was performed using a setup with an auxiliary electrode and collector insulation for each experiment. Images on the left show the entire collector area, while the inset is a closer image of the pattern area. b) Heat maps of the percent area around each section of the pattern filled with fibers, calculated using threshold analysis of the top-down fiber images. c) Heat maps of the coefficient of variation of the percent area value for each pattern section across three electrospinning replicates. d) SEM images of fibers removed from the collectors used for measurement of patterned fiber volume. e)Ratio of fiber mass in the micropatterns to fiber mass on the collector surface. Grey bars represent the mean and error bars represent the standard deviation of three electrospinning replicates. d) Aggregate fiber pattern quality scores calculated by ranking the yield, uniformity, reproducibility, fiber volume, and the experimental fiber selectivity for each collector, then calculating the sum of each rank.

volume of the fibers was an order of magnitude less than the other two collectors. Although the 5 wt% collector demonstrated a high experimental selectivity (S_E = 12.74) because of the near complete exclusion of fiber deposition from the collector surface, the results were too variable to prioritize for later studies (Figure 4.5e). The 7.5 wt% carbon black concentration was prioritized for future studies because its uniform and reproducible fiber deposition combined with its high selectivity (S_E = 7.75) resulted in the highest fiber quality score (Figure 4.5f).

These results were surprising because we expected that a higher carbon black concentration would lead to a stronger electric field force and more fiber deposition in the pattern cavities. While this was true when the concentration was increased from 5% to 7.5%, but we did not observe any additional benefit when the concentration was increased further to 10%. Additionally, we observed a reduction in selectivity and uniformity for the 10% carbon black

collector compared to the 7.5% carbon black collector. The reduction in selectivity was likely due to the observed increased fiber deposition on the collector surface (Figure 4.5a). Future studies could evaluate potential improvement in fiber patterning quality for this carbon black concentration with increased insulative layer thickness. Meanwhile, it is possible that the reduced uniformity of the collector fabricated with 10% carbon black in the conductive layer was caused by incomplete mixing or carbon black particle aggregation during the mixing process. This could potentially be addressed in future studies through modifications to the mixing process such as increased mixing time or increased shear force. Future work could also use alternative materials for the conductive layer of the collectors, as described in the next section.

4.3.6 *Evaluation of liquid metal elastomer composite as conductive layer material*

Carbon black is an inexpensive and non-toxic additive to fabricate conductive elastomers. However, carbon black-PDMS mixtures are difficult to mix at high concentrations because the mixture viscosity increases as the concentration increases.[13] Additionally, at high carbon black concentrations, the composite can become brittle and difficult to handle.[23] At the lower carbon black concentrations for which we have observed high quality fiber patterning, we also previously observed that the fiber deposition pattern and selectivity was sensitive to the precursor solution conductivity. In our previous studies, precursor solutions with lower conductivities have resulted in superior fiber patterning[13] potentially because these fibers carry less surface charge, leading to more complete electrical discharge after deposition on the collector and less repulsion of incoming fibers.[7,24] If this is true, we could expect that an elastomer composite with higher conductivity would result in improved yield and pattern quality for high conductivity fiber precursor solutions.

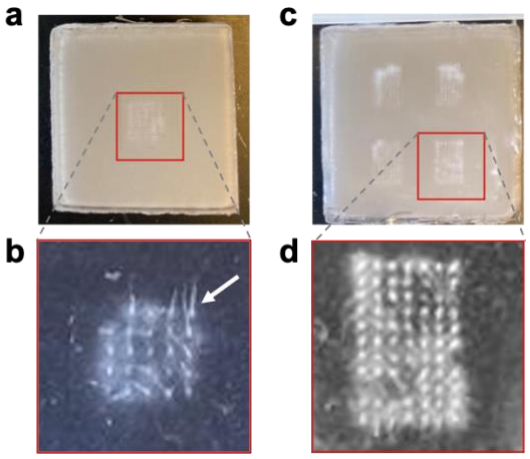

Figure 4.6. Evaluation of a liquid metal elastomer composite as the conductive layer

a, c) Top-down images of PVA fibers deposited on two-layer patterned collectors with two different dimensions using a 30% v/v mixture of eutectic gallium indium and PDMS conductive layer. a) The collector with 800 µm length cavities was fabricated using a 775 µm insulative layer thickness, and c) the collector with 300 µm length cavities was fabricated using a 390 µm insulative layer thickness. Electrospinning was performed using a setup without the auxiliary electrode and with collector insulation. The top images show the entire collector area with PVA fibers deposited on the collectors, while the bottom images b) and d) show a closer image of fibers after removal from the collectors. The white arrow in b) indicates fibers that were deposited in the collector cavities that were deformed upon removal from the collector.

A strength of fabricating two-layer collectors from 3D printed master molds is the ability to evaluate alternative conductive elastomer composites that are incompatible with laser machining. To demonstrate the feasibility of replacing the carbon black-PDMS composite with an alternative conductive elastomer, we evaluated a composite of eutectic gallium indium (EGaIn) and PDMS as the conductive material in the two-layer patterned collectors. The thickness of the insulative layer was increased by 25% based on preliminary studies demonstrating highly productive electrospinning on two-layer collectors with EGaIn-PDMS. The EGaIn-PDMS composite was prepared at 30% v/v, previously demonstrated to result in a 4-fold increase in the dielectric constant of PDMS.[25] We observed selective deposition of PVA fibers into conical cavities with 800 µm length and into pyramidal cavities with 300 µm length (Figure 4.6). Conical fiber structures formed through conformation to the collector were visible after fiber removal (Figure 4.6b, white arrow). This work demonstrates the tunability of this fiber

patterning and collector fabrication process. Because the conductivity of EGaIn ($\sigma = 3.4 * 10^4$ S/cm)[26] is much higher than carbon black ($\sigma = 10^{-2}$-10^1 S/cm),[27] it will be interesting in future work to quantitatively evaluate how this increase in conductive particle conductivity changes the patterning quality of different fiber formulations.

4.4 Conclusion

In these studies, we developed two-layer collectors fabricated from 3D-printed master molds using a custom fiber pattern analysis pipeline to quantitatively characterize the effect of electrospinning setup, insulative layer thickness, and conductive particle concentration on fiber pattern quality. Using a series of experiments, fiber yield was increased 3-fold, fiber selectivity for the patterns was increased more than 4-fold, and uniformity of the patterning was increased nearly 14-fold for the best-performing electrospinning setup and collector design compared to the worst-performing. We also demonstrated how an alternative conductive elastomer composite can be directly incorporated into the two-layer collector fabrication method, which demonstrates the tunability of this approach and could be evaluated in the future to further improve fiber patterning. We anticipate that the quantitative analysis performed here could be adapted to any fiber patterning strategy and any pattern to facilitate rational method development and to better understand the function of patterned fibers in future experiments.

4.5 Materials and Methods

4.5.1 *Collector fabrication*

Master molds with an array of 25 conical features with 300 µm diameter and 800 µm height or with an array of 77 pyramidal features with 100 µm base width and height and 300 µm height were designed in Autodesk Inventor and 3D printed using IP-S resin on an indium tin oxide

coated glass substrate using the Nanoscribe Photonic Professional GT2 using a 25X objective lens in shell mode. After developing the resist according to the manufacturer's instructions, completed master molds were placed within an outer mold 3D printed in poly(lactic acid) with a FlashForge Finder at the University of Washington CoMotion Makerspace. The completed master was then coated with silane (trichloro(1H,1H,2H,2H-perfluorooctyl)silane, Sigma Aldrich) to prevent adhesion of cast molds. The desired volume of PDMS (mixed at 1:10 ratio curing agent: pre-polymer, Sylgard 184, Dow Corning) was added to the master mold and cured at room temperature for 24 hours. C-PDMS was prepared by incorporating 7.5wt% carbon black (Vulcan XC 72R, particle size 50 nm, Fuel Cell Store) into the PDMS pre-polymer and curing agent by manual mixing with a spatula, and then 3 milliliters of the completed C-PDMS mixture was added to the master mold. The entire mold was then placed on a rotating platform shaker at the highest setting for 15 hours. The C-PDMS was then cured in an oven at 37°C for 24 hours, and the completed collector was removed from the master mold.

4.5.2 *Finite element method simulations*

The effect of various electrospinning setups on the electric field near the collector was evaluated using finite element method simulations (COMSOL Multiphysics version 5.1). The 2D schematic of the collector and the electrospinning setup for each simulation was prepared in AutoCAD (Autodesk AutoCAD 2015). The collector contained three triangular features with opening width 900 µm, height 2400 µm, and insulative layer thickness 470 µm. Some simulations included a copper plate electrode 20 cm wide. For each simulation, the tip to collector distance was set to 10 cm. The geometry included a boundary around the entire setup. Charge conservation was maintained in the simulation, and the zero-charge boundary condition was assigned to the outer boundary of the geometry. The initial value for electric potential was

set to zero across the entire geometry. The applied voltage of 7.5 kV was assigned to the geometry representing the needle in the electrospinning setup. For setups including a copper plate electrode, the copper electrode was also assigned an applied voltage of 7.5 kV to match experimental conditions. The geometry representing the collector was grounded. Geometries were rendered with an extra fine physics-controlled mesh. The electric field at different points relative to the collector was calculated using the potential computed by the simulation.

4.5.3 *Polymer solution preparation and electrospinning*

Electrospinning precursor solutions were prepared by dissolving PLGA (Lactel Absorbable Polymers, 50:50 L:G ester terminated, 0.55-0.75 dL/g inherent viscosity in HFIP) at 14% w/v in HFIP, followed by stirring overnight on a rotisserie style shaker at room temperature. Polymer solutions were loaded in a glass syringe fitted with a 22G blunt tipped needle. The polymer solution was dispensed from the syringe using a syringe pump (New Era Pump Systems, Inc.) at a 1 μL/min flow rate. The patterned collector of interest was fixed to a custom holder that inserted copper wires to the back of the collector. The wires were pierced through a polyethylene foam block to hold the collector at the proper height and to prevent fiber deposition on objects other than the collector. The ground from the power source (Gamma High Voltage Research) was attached to these wires and the positive lead was attached to the base of the needle. The applied voltage varied between approximately 15 and 18 kV depending on the relative humidity in the lab. Fiber samples were electrospun for 2 minutes.

4.5.4 *Uniformity and reproducibility analysis*

Fiber pattern uniformity and reproducibility were both evaluated through ImageJ analysis of top-down images of collectors with fibers. To analyze a collector, an array of identical 1 mm x

1 mm square regions of interest was overlaid on the image and aligned with the pattern array. The image was then converted to 8-bit, and an auto-threshold was applied to make all fibers appear completely black. The percent area within each region of interest was then calculated. The theoretical ideal percent area was calculated as 7% assuming the ideal fiber deposition pattern would result in visible fibers in the entire pattern opening area of 0.07 mm^2. Heatmaps of the percent area values for each region of interest were plotted with a scale relative to the theoretical ideal percent area. Uniformity was determined by first calculating the mean percent area for each individual region of interest for three independent electrospinning replicates, then calculating the coefficient of variation between each region of interest across the array. Reproducibility was determined by calculating the coefficient of variation for each individual region of interest for three independent electrospinning replicates, then calculating the average coefficient of variation between each region of interest across the array.

4.5.5 *SEM imaging and fiber volume analysis*

SEM imaging of patterned electrospun fibers removed from the collectors was performed on a JEOL JSM7400F cold field emission scanning electron microscope. All samples were coated with a 3 nm layer of gold-palladium prior to SEM imaging. The approximate volume of a 3x3 array of conical fiber patterns was calculated from diameter and height measurements for each sample.

4.5.6 *Image analysis and calculation of experimental fiber selectivity*

All image analysis was performed in ImageJ. The percent area of the collector surface covered with fibers within the microscope image field was determined by converting an optical microscope image to 8-bit, applying an auto-threshold to make all fibers appear completely

black, and measuring percent area. This calculation was repeated for images from four different locations on the collector surface, and an average percent area was calculated. Fiber diameters were measured from at least 10 different fibers in microscope images. The percent area from the threshold analysis and the fiber diameter were used to estimate the volume of fibers covering the collector surface. The volume value was then multiplied by a scaling factor to estimate the fiber volume across the entire collector surface. Assuming the density of the fibers was equal to reported density of the raw polymer material, we calculated the mass of fibers on the collector surface. The mass of fibers in the patterns was then determined by subtracting the calculated mass of fibers on the collector surface from the measured total fiber mass on the collector. Finally, the ratio of fiber mass in the patterns to fiber mass on the collector surface was calculated.

4.5.7 *Calculation of aggregate score describing fiber pattern quality*

Aggregate fiber pattern quality scores were determined by ranking the fiber mass output, uniformity, reproducibility, fiber volume, and selectivity of comparable collectors. Individual ranks for each factor were added to result in an aggregate score for each collector.

4.6 ACKNOWLEDGEMENTS

Nanoscribe 3D printing and SEM imaging were conducted at the Washington Nanofabrication Facility, a National Nanotechnology Coordinated Infrastructure (NNCI) site at the University of Washington, which is supported in part by funds from the Molecular Engineering & Sciences Institute, the Clean Energy Institute, the Washington Research Foundation, the M. J. Murdock Charitable Trust, the National Science Foundation and the National Institutes of Health. Liquid metal elastomer composites were prepared by Mohammad

Malakooti, Professor of Mechanical Engineering at the University of Washington. This work was supported by NIH/NIHCD grant DP2HD075703 to KAW. RC was supported by an NSF Graduate Research Fellowship (DGE-1256082) and by the STD & AIDS Research Training Fellowship Program (NIH 2T32AI007140-41).

4.7 REFERENCES

1 Bellan, L. M. & Craighead, H. G. Control of an electrospinning jet using electric focusing and jet-steering fields. *Journal of Vacuum Science & Technology B* **24**, 3179-3183, doi:10.1116/1.2363403 (2006).

2 Nurfaizey, A. H. *et al.* Control of Spatial Deposition of Electrospun Fiber Using Electric Field Manipulation. *Journal of Engineered Fibers and Fabrics* **9**, 155-164 (2014).

3 Neubert, S. *et al.* Focused deposition of electrospun polymer fibers. *Journal of Applied Polymer Science* **125**, 820-827, doi:10.1002/app.35578 (2012).

4 Adepu, S. *et al.* Effect of micropatterning induced surface hydrophobicity on drug release from electrospun cellulose acetate nanofibers. *Applied Surface Science* **426**, 755-762, doi:10.1016/j.apsusc.2017.07.197 (2017).

5 Kakunuri, M., Wanasekara, N. D., Sharma, C. S., Khandelwal, M. & Eichhorn, S. J. Three-dimensional electrospun micropatterned cellulose acetate nanofiber surfaces with tunable wettability. **134**, doi:10.1002/app.44709 (2017).

6 Liverani, L. *et al.* Electrospun patterned porous scaffolds for the support of ovarian follicles growth: a feasibility study. *Scientific Reports* **9**, doi:10.1038/s41598-018-37640-1 (2019).

7 Ding, Z., Salim, A. & Ziaie, B. Selective Nanofiber Deposition through Field-Enhanced Electrospinning. *Langmuir* **25**, 9648-9652, doi:10.1021/la901924z (2009).

8 Wu, Y., Dong, Z., Wilson, S. & Clark, R. Template-assisted assembly of electrospun fibers. *Polymer* **51**, 3244-3248, doi:10.1016/j.polymer.2010.04.039 (2010).

9 Zucchelli, A., Fabiani, D., Gualandi, C. & Focarete, M. L. An innovative and versatile approach to design highly porous, patterned, nanofibrous polymeric materials. *Journal of Materials Science* **44**, 4969-4975, doi:10.1007/s10853-009-3759-2 (2009).

10 Kim, G. H., Nam, H., Choi, W., An, T. & Lim, G. Electrospinning Nanofiber on an Insulating Surface with a Patterned Functional Electrolyte Electrode. *Advanced Materials Interfaces*, 1701204, doi:10.1002/admi.201701204 (2018).

11 Park, S. M. *et al.* Direct fabrication of spatially patterned or aligned electrospun nanofiber mats on dielectric polymer surfaces. *Chemical Engineering Journal* **335**, 712-719, doi:10.1016/j.cej.2017.11.018 (2018).

12 Lavielle, N. *et al.* Structuring and Molding of Electrospun Nanofibers: Effect of Electrical and Topographical Local Properties of Micro-Patterned Collectors. *Macromolecular Materials and Engineering* **297**, 958-968, doi:10.1002/mame.201100327 (2012).

13 Creighton, R. L., Phan, J. & Woodrow, K. A. In situ 3D-patterning of electrospun fibers using two-layer composite materials. *Scientific Reports* **10**, doi:10.1038/s41598-020-64846-z (2020).

14 Liu, Y. W. *et al.* Electrospun Fibrous Mats on Lithographically Micropatterned Collectors to Control Cellular Behaviors. *Langmuir* **28**, 17134-17142, doi:10.1021/la303490x (2012).

15 Ying, T., Su, J., Jiang, Y., Ke, Q. & Xu, H. A pre-wetting induced superhydrophilic/superlipophilic micro-patterned electrospun membrane with self-cleaning property for on-demand emulsified oily wastewater separation. *Journal of Hazardous Materials* **384**, 121475, doi:10.1016/j.jhazmat.2019.121475 (2020).

16 Nedjari, S. *et al.* Electrospun Honeycomb as Nests for Controlled Osteoblast Spatial Organization. *Macromolecular Bioscience* **14**, 1580-1589, doi:10.1002/mabi.201400226 (2014).

17 Kang, Y. *et al.* Tissue-Engineered Trachea Consisting of Electrospun Patterned sc-PLA/GO-g-IL Fibrous Membranes with Antibacterial Property and 3D-Printed Skeletons with Elasticity. *Biomacromolecules* **20**, 1765-1776, doi:10.1021/acs.biomac.9b00160 (2019).

18 Persano, L., Camposeo, A., Tekmen, C. & Pisignano, D. Industrial Upscaling of Electrospinning and Applications of Polymer Nanofibers: A Review. *Macromolecular Materials and Engineering* **298**, 504-520, doi:10.1002/mame.201200290 (2013).

19 Wu, D. *et al.* Enhanced Deposition Uniformity via an Auxiliary Electrode in Massive Electrospinning. *Nanomaterials* **6**, doi:10.3390/nano6070135 (2016).

20 Yang, Y. *et al.* Effect of electric field distribution uniformity on electrospinning. *Journal of Applied Physics* **103**, doi:10.1063/1.2924439 (2008).

21 Schneider, F., Draheim, J., Kamberger, R. & Wallrabe, U. Process and material properties of polydimethylsiloxane (PDMS) for Optical MEMS. *Sensors and Actuators A: Physical* **151**, 95-99, doi:10.1016/j.sna.2009.01.026 (2009).

22 Yan, H., Liu, L. & Zhang, Z. Alignment of electrospun nanofibers using dielectric materials. *Applied Physics Letters* **95**, doi:10.1063/1.3242378 (2009).

23 Niu, X. Z., Peng, S. L., Liu, L. Y., Wen, W. J. & Sheng, P. Characterizing and Patterning of PDMS-Based Conducting Composites. *Advanced Materials* **19**, 2682-2686, doi:10.1002/adma.200602515 (2007).

24 Kessick, R., Fenn, J. & Tepper, G. The use of AC potentials in electrospraying and electrospinning processes. *Polymer* **45**, 2981-2984, doi:10.1016/j.polymer.2004.02.056 (2004).

25 Pan, C. *et al.* A Liquid-Metal–Elastomer Nanocomposite for Stretchable Dielectric Materials. *Advanced Materials* **31**, 1900663, doi:10.1002/adma.201900663 (2019).

26 Dickey, M. D. *et al.* Eutectic Gallium-Indium (EGaIn): A Liquid Metal Alloy for the Formation of Stable Structures in Microchannels at Room Temperature. *Advanced Functional Materials* **18**, 1097-1104, doi:10.1002/adfm.200701216 (2008).

27 Spahr, M. E., Gilardi, R. & Bonacchi, D. in *Fillers for Polymer Applications* (ed Roger Rothon) 375-400 (Springer International Publishing, 2017).

Chapter 5. FORMULATION OF INTEGRATED FIBER MICRONEEDLES FOR VACCINE DELIVERY

Portions adapted from: **Creighton, R.**, Phan, J., Woodrow, K.A. In situ 3D patterning of electrospun fibers using two-layer composite materials. Scientific Reports (2020) 10, 7949.

5.1 ABSTRACT

Electrospun fibers can be formulated for many different drug and vaccine delivery applications through incorporation of small molecules, proteins, or nucleic acids. However, delivery of fiber materials *in vivo* is currently limited to topical delivery or surgical implantation. Delivery via the topical route is limited by the diffusion barrier of skin, and while surgical implantation can overcome this barrier, it is highly invasive. Here, we integrate electrospun fibers encapsulating a model small molecule, protein, or nucleic acid into microneedle molds using *in situ* fiber patterning. Protein fibers were formulated to meet loading requirements and nucleic acid fiber formulations incorporating different transfection reagents were explored. Fiber pattern quality of each fiber formulation was quantitatively evaluated. Compared to conventional matrix microneedles, integrated fiber microneedles exhibited superior small molecule drug loading and release and mechanical properties more independent of protein loading. These studies demonstrate the compatibility of our *in situ* fiber patterning technology with diverse fiber formulations and motivate the use of integrated fiber microneedles as a new dosing modality to address limitations of electrospun fibers and conventional matrix microneedles.

5.2 INTRODUCTION

Electrospun fibers are a unique material for drug and vaccine delivery. Virtually any natural or synthetic material can be electrospun, such as chitosan,[1] ethyl cellulose,[2] polyesters,[3-7] and pH-responsive materials.[8,9] Hydrophilic[1,3] and hydrophobic[1,2] small molecule drugs have been incorporated into electrospun fibers with total drug loading of 40%.[10] Additionally, emulsion electrospinning has been used to encapsulate and preserve the bioactivity of proteins such as growth factors, enzymes, and vaccine antigens.[5,7,9] Nucleic acids have also been incorporated into electrospun fibers by coaxial electrospinning,[11] direct mixing with polymer solutions containing block copolymers,[12] or by emulsion electrospinning.[13]

Electrospun fibers are currently delivered through two primary modalities: topical delivery and surgical implantation. Electrospun fibers have been applied orally for antibacterial drug delivery,[10] vaginally for delivery of microbicides or contraceptives,[14] transdermally for delivery of vitamins,[1,3] and in open wounds to accelerate healing.[4,8] However, in each of these examples the pharmaceutical agent was limited to small molecules that can effectively diffuse through tissue. Additionally, transdermal delivery requires the use of adhesives to retain the fibers at the desired delivery site for the duration of drug release,[3] but it is common for these adhesives or the active pharmaceutical ingredient to cause irritation at the site of delivery,[15] which could reduce user compliance. Electrospun fibers can also be surgically implanted to overcome barriers to topical delivery like tissue diffusion and material retention.[16-19] For example, electrospun fibers have been surgically implanted to provide controlled release of mesoporous silica particles loaded with siRNA.[18] Electrospun fibers have also been evaluated as antibacterial drug delivery devices to treat periodontal infection.[19] In some applications, surgical administration is required for specific local delivery or tissue regeneration.[16,17] However, when

the primary function of the fibers is systemic or superficial drug delivery, a less invasive method of administration would be advantageous.

To overcome these challenges, we integrated electrospun fibers containing a variety of model pharmaceutical agents with microneedles. Microneedles have been extensively studied for drug and vaccine delivery.[20-25] They can be delivered dermally and at mucosal surfaces including the gastrointestinal,[22] oral,[23,24] and vaginal mucosa.[25] Microneedles can effectively penetrate tissue to overcome diffusion barriers associated with topical delivery, and they are painless and minimally invasive in contrast to surgical implantation.[26,27] Microneedles can also be specifically designed for microneedle tip implantation, achieving sustained release for up to 16 days without the use of adhesives typically required for sustained topical delivery.[28,29] Therefore, integrated fiber microneedles are a new fiber delivery modality that could be expected to bridge the gap between topical delivery and surgical implantation of electrospun fibers.

We previously developed two-layer micropatterned collectors capable of fiber integration into recessed patterns. Here, we demonstrate *in situ* integration of fiber formulations containing a model small molecule, protein, or nucleic acid into two-layer microneedle molds. We also provide data directly comparing the release kinetics and mechanical properties of integrated fiber microneedles and conventional matrix microneedles, which suggests potential advantages of the integrated fiber microneedles. Together, these studies demonstrate the potential for many different applications of integrated fiber microneedles and provide a starting point for future optimization and application.

5.3 Results and Discussion

5.3.1 *Patterning quality of small molecule-loaded fibers*

First, we evaluated the patterning quality of fibers loaded with a model small molecule, dapivirine (DPV). Poly-L-lactic acid fibers without drug and with 30 wt% DPV had similar output and yield. Electrospinning of fibers with 15 wt% DPV was highly productive, effectively filling the microneedle cavities in half the time required for the no drug and 30 wt% drug formulations (Table 5.1). Uniformity varied slightly between the different formulations, with the 30 wt% DPV samples exhibiting the most uniform fiber patterning (CV = 48%) and the 15 wt% DPV samples exhibiting the least uniform fiber patterning (CV = 85%) (Figure 5.1a-c). The 30% DPV samples also had approximately twice the area of visible fibers compared to the no drug and 15% DPV samples. The reproducibility, quantified as the coefficient of variation between independent electrospinning replicates, was approximately 40% for all fiber formulations.

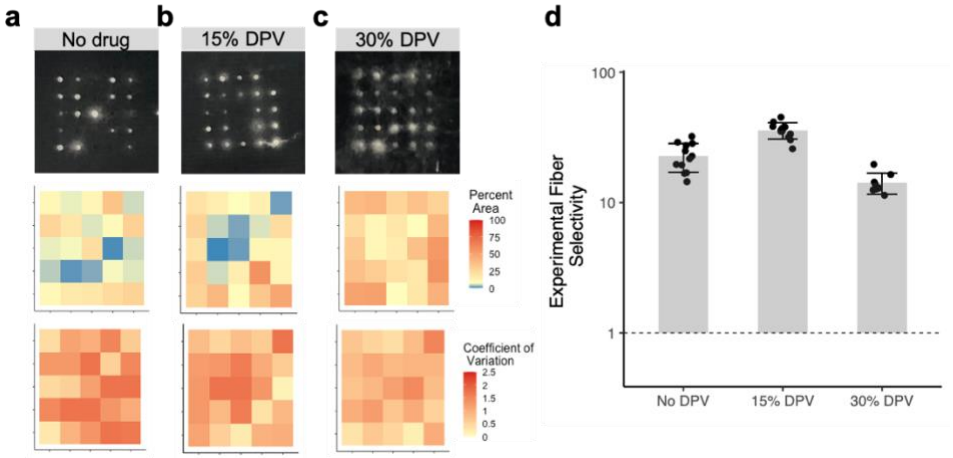

Figure 5.1. Integration of dapivirine-loaded fibers into two-layer microneedle mold collectors.

Top-down images of a) drug-free PLLA fibers, b) 15 wt% dapivirine-loaded PLLA fibers, and c) 30 wt% dapivirine-loaded PLLA fibers deposited on a two-layer microneedle mold collector with 300 µm diameter, 800 µm height conical cavities, 620 µm insulative layer thickness, and 7.5 wt% carbon black conductive layer. Heat maps of the percent area around each section of the pattern filled with fibers, calculated using threshold analysis of the top-down fiber images, were used to characterize pattern uniformity. Heat maps of the coefficient of variation of the percent area value for each pattern section across three electrospinning replicates were used to characterize pattern reproducibility. d) Ratio of fiber mass in the micropatterns to fiber mass on the collector surface. Grey bars represent the mean and error bars represent the standard deviation of 4 measurements from 3 independent electrospinning replicates.

Selectivity followed a similar trend, with the highest selectivity (S_E = 35.68) measured for the 15 wt% DPV formulation followed by the drug free formulation (S_E = 23.27) and the 30 wt% DPV formulation (S_E = 14.21) (Figure 5.1d).

It is likely that differences in solution conductivity is responsible for the changes in fiber patterning quality for different small molecule drug loading. Although we did not measure the solution conductivity here, previous studies have reported that addition of small molecule drugs can increase solution conductivity approximately 100-fold.[30] These results are consistent with our previous observation that fiber patterning quality improved as the solution conductivity increased from 0.0 µS/cm to 0.17 µS/cm, but a further increase to 0.22 µS/cm reduced fiber selectivity approximately 5-fold.[31] Future studies requiring high dapivirine loading could explore alternative solvents or precursor solution additives to tune the solution properties and further increase fiber selectivity. Overall, in these studies we demonstrated that fibers with up to 30 wt% DPV loading can be selectively integrated into microneedles using our two-layer collector technology without any specialized formulation.

Table 5.1. Electrospinning results for drug loaded and blank PLLA fibers

Dapivirine Loading (wt%)[a]	Output (mg)[b]	Yield (%)[b]	S_E
0	0.17 [c]	96	23.27
15	0.11 [d]	127	35.68
30	0.16 [c]	71	14.21

[a] All solutions were prepared at 15% w/v PLLA, [b] Mean of at least n=2 electrospinning replicates, [c] Output is reported as total fiber mass on the collector after 1 minute or [d] 30 seconds of electrospinning

5.3.2 *Release kinetics of small molecule-loaded iFMDs compared to conventional matrix microneedles*

We next evaluated dapivirine release kinetics from integrated fiber microneedles compared to conventional matrix microneedles. Conventional matrix microneedles without fibers loaded at 30 wt% dapivirine resulted in Ostwald ripening of the drug into large particles and needle deformation (Figure 5.2a-c). Because these microneedles were not suitable for further evaluation, integrated fiber microneedles and conventional matrix microneedles were prepared at a lower 15 wt% dapivirine loading for use in release studies. After an initial burst of approximately 5%, dapivirine release from the integrated fiber microneedles was linear over time with an approximate rate of 0.1% per day and 0.2% per day for 15 wt% and 30 wt% dapivirine loading, respectively. In contrast, the control group of conventional matrix microneedles with 15 wt% dapivirine loading showed negligible release before one week (Figure 5.2f-g). We observed during the release experiment that the drug loaded conventional matrix microneedles became white and opaque compared to a control group of conventional matrix microneedles without drug (Figure 5.2d-e). The observed opacity is likely caused by drug crystallization in the release conditions, which could also explain the slow release rate.[32] The release data for dapivirine

suggests that small molecule active pharmaceuticals could be incorporated in the integrated fiber microneedle device and released at controlled rates. In the context of vaccine delivery, controlled release of adjuvants has increased humoral immune responses up to 19-fold and cellular immune responses up to 10-fold in previous studies.[33-36] Additionally, the ability to incorporate dapivirine at higher percent loading than conventional matrix microneedles is an advantageous feature of the integrated fiber microneedle device, motivating continued development and evaluation of the device.

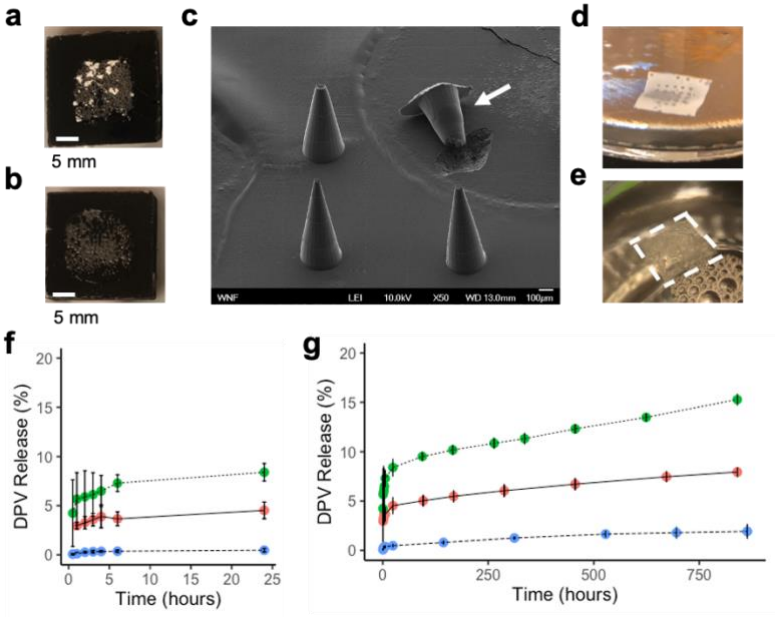

Figure 5.2. Integrated fiber microneedles enable formulation and release of dapivirine.

Preparation of PLLA microneedles (a) with 30 wt% dapivirine resulted in Ostwald ripening of the drug into large particles compared to (b) PLLA microneedles without drug. (c) SEM inspection of drug loaded PLLA microneedles revealed defects due to the particle formation (denoted by white arrow). During the release experiment, (d) dapivirine loaded conventional matrix microneedles became opaque, while (e) conventional matrix microneedles without drug remained transparent. The boundary of the conventional matrix microneedles without drug is denoted with a white dashed line to improve visibility. Percent dapivirine release over time was evaluated for integrated fiber microneedles at 15% (w/w) loading (red circles) and 30% (w/w) loading (green circles) and conventional matrix microneedles at 15% (w/w) loading (blue circles). (f) The first 24 hours of dapivirine release, and (g) dapivirine release over 33 days. Data represents the mean ± standard deviation of at least n=2 replicates.

5.3.3 *Development of a protein-fiber formulation with high loading*

While proteins have previously been incorporated into electrospun fibers, a majority of these studies evaluated fibers containing growth factors for tissue engineering.[5-7,37] These applications require low protein loading in the range of 0.01 wt% to 0.2 wt%.[6,37] To achieve a modest protein vaccine dose of 30 µg in a 25-needle integrated fiber microneedle array (typical integrated fiber mass of 0.3 mg), the minimum required protein loading in the fibers is 10 wt%. Therefore, the first objective in formulating protein in electrospun fibers for the integrated fiber microneedle device was maximizing the protein loading and burst release. We used a base emulsion formulation consisting of 20% v/v aqueous phase containing 40 mg/mL protein with 0.2% v/v Tween 20 surfactant and 50 wt% PEG (relative to polyester mass) dissolved in the aqueous phase. The maximum protein loading for this formulation was 3.8 wt%.

First, we tuned the aqueous phase percent from 10 to 30% v/v to observe the effect on protein burst release. For this experiment, we incorporated the same mass of protein in each sample, resulting in a theoretical loading ranging from 2.9 wt% to 3.8 wt%. We observed an increase in protein burst release from 25% to 75% when the aqueous phase percent was increased from 10% to 30% (Figure 5.3a). This trend is consistent with the results from previously published studies, where increasing the volume of aqueous phase from 70% to 90% resulted in a 20% increase of protein burst release.[38] Because a higher percent aqueous phase enables a higher theoretical protein loading, we attempted to further increase the aqueous phase percent to 40% v/v. However, this emulsion was unstable and did not produce fibers. To increase the spinnability of fiber formulations containing a high aqueous phase percent, we replaced PEG with PVA as the hydrophilic excipient. With PVA in the aqueous phase, we were able to electrospin fibers with 40% v/v aqueous phase and a theoretical loading of 16 wt% protein. With

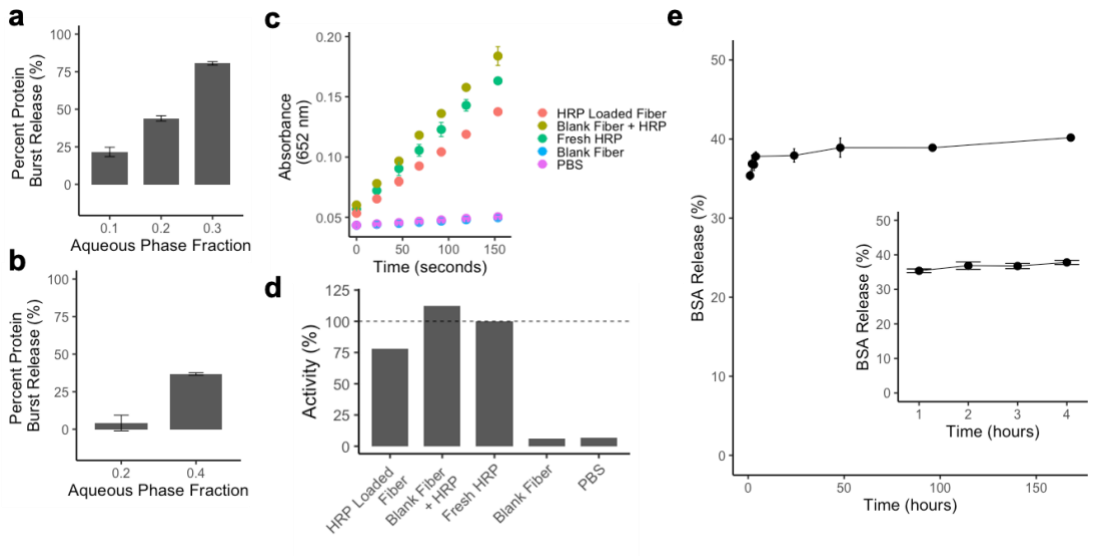

Figure 5.3. Development and evaluation of polyester fibers highly loaded with protein.

a) Percent of bovine serum albumin released from emulsion electrospun polyester fibers prepared using different aqueous phase fractions. Polyethylene glycol was included in the aqueous phase at 50% w/w relative to the mass of the polyesters. b) Percent of bovine serum albumin released from emulsion electrospun polyester fibers prepared using different aqueous phase fractions. Polyvinyl alcohol was included in the aqueous phase at 10% w/v. All fibers were prepared using 80:20 PLGA:PCL in the organic phase and release was measured after 24 hours of incubation in water at 4ºC. Reported percent release was calculated based on the theoretical protein loading. c) Kinetic enzymatic activity of horseradish peroxidase extracted from PLGA electrospun fibers prepared with a 40% v/v aqueous phase containing 5% w/v polyvinyl alcohol compared to fresh protein control. d) Percent activity was calculated relative to the activity of the fresh horseradish peroxidase control. Activity measurements were repeated at least three times. e) Release kinetics of bovine serum albumin from PLGA electrospun fibers prepared with a 40% v/v aqueous phase containing 5% w/v polyvinyl alcohol. Percent release was calculated by extracting protein remaining in the fibers after the final time point. Data for a, b, and g are represented as the mean ± standard deviation of technical replicates of the BCA assay.

this formulation, we observed a burst release of 36% in 24 hours (Figure 5.3b). Therefore, through a series of iterations, we increased the theoretical protein loading more than 4-fold and increased the mass of protein burst release more than 3-fold.

After increasing the protein theoretical loading and burst release, the next objective of the fiber-protein formulation was to evaluate the protein activity after encapsulation in the fibers and protein release kinetics. Similar to previous studies,[38-40] we observed that horseradish peroxidase extracted from protein-loaded fibers retained 75% of its bioactivity compared to a fresh dilution of the protein (Figure 5.3c,d). Fibers loaded with bovine serum albumin exhibited an initial burst of approximately 35%, followed by a sustained released at a rate of approximately 0.3% per day

(Figure 5e). The slow sustained protein release rate we observed is similar to values reported from previous studies of protein-loaded polyester electrospun fibers.[5,38,40] We expect based on previous studies that the release rate can be tuned in the future through the selection of polyester material or by changing the ratio of hydrophilic excipients in the formulation.[38]

5.3.4 *Patterning quality of protein-loaded fibers*

Next, we evaluated the patterning quality of the lead candidate protein-loaded fiber formulation with both high (125 µg) and low (12.5 µg) protein loading. Fiber output and yield were 2-fold higher for the formulation with low protein loading compared to high protein loading. During the electrospinning process, the formulation with high protein loading exhibited some unstable fiber formation and fiber bundling (Figure 5.4a). Quantitatively, patterning of the formulation with low protein loading was more uniform (CV = 57%) compared to the formulation with higher protein loading (CV = 93%), but the two formulations had approximately equal reproducibility (Figure 5.4a-b). Both fiber formulations were deposited in the microneedle cavities with high selectivity, although selectivity of fibers with low loading (S_E = 59.1) was slightly higher than fibers with low loading (S_E = 40.0) (Figure 5.4c).

Similar to the results we observed for integration of small molecule loaded fibers, it is likely that the differences in fiber patterning quality observed for different protein loading is due to differences in the precursor solution properties. Previous studies have reported that incorporation of different amounts of protein can alter the stability of electrospinning and the resulting fiber diameter.[7,9] Future studies requiring equivalent fiber patterning with different

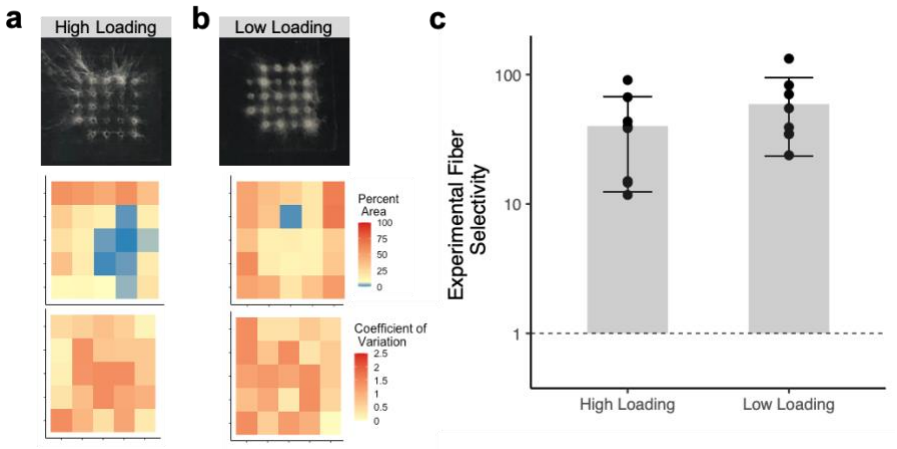

Figure 5.4. Electrospun fibers loaded with different concentrations of a model protein are effectively integrated into two-layer microneedle mold collectors

a) Top-down images of PLGA fibers with high (125 µg) or b) low (12.5 µg) loading of bovine serum albumin deposited on a two-layer microneedle mold collector with 300 µm diameter, 800 µm height conical cavities, 620 µm insulative layer thickness, and 7.5 wt% carbon black conductive layer. Heat maps of the percent area around each section of the pattern filled with fibers, calculated using threshold analysis of the top-down fiber images, were used to characterize pattern uniformity. Heat maps of the coefficient of variation of the percent area value for each pattern section across three electrospinning replicates were used to characterize pattern reproducibility. c) Ratio of fiber mass in the micropatterns to fiber mass on the collector surface. Grey bars represent the mean and error bars represent the standard deviation of 4 measurements from 3 independent electrospinning replicates.

fiber protein loading could explore the use of different polymer concentrations to tune solution viscosity and the use of alternate solvents or salts to decrease or increase solution conductivity, respectively.

5.3.5 *Mechanical properties of protein-loaded microneedles*

In a previous study of solid microneedles coated with pharmaceutical agents, an increase in agent loading from 20 to 35 ng resulted in changes to microneedle tip geometry, which led to a reduction in delivery efficiency from ~80% to ~20%.[41] In a separate study of dissolving polymer matrix microneedles, loading of propranolol was limited to 10 wt% because higher concentrations of drug resulted in insufficient needle mechanical properties.[42] Additionally, an evaluation of calcein-loaded PLGA microneedles demonstrated a two-fold reduction in microneedle failure force when only 2% w/w drug was loaded.[43] When the loading was

increased to a modest 10% w/w, the failure force of the needles was less than the force required for tissue penetration, suggesting that the needles would fracture before insertion.[43] Integrated fiber microneedles can be designed to incorporate active agents only into the fibers, maintaining the mechanical properties of the surrounding polymer matrix material. We therefore anticipated that integrated fiber microneedles with different protein loading would display more consistent mechanical properties compared to conventional matrix microneedles.

We first prepared conventional matrix microneedles with high (125 µg per needle) or low (12.5 µg per needle) loading of a model protein bovine serum albumin (BSA). Matrix microneedles with high protein loading demonstrated brittle fracture compared to a 10-fold lower protein loading, based on the shape of the load vs. extension curves and SEM inspection of the failed microneedles (Figure 5.5a-d). The tips of the highly loaded matrix microneedles appear to have fractured during failure (Figure 5.5c), while the tips of matrix microneedles with low

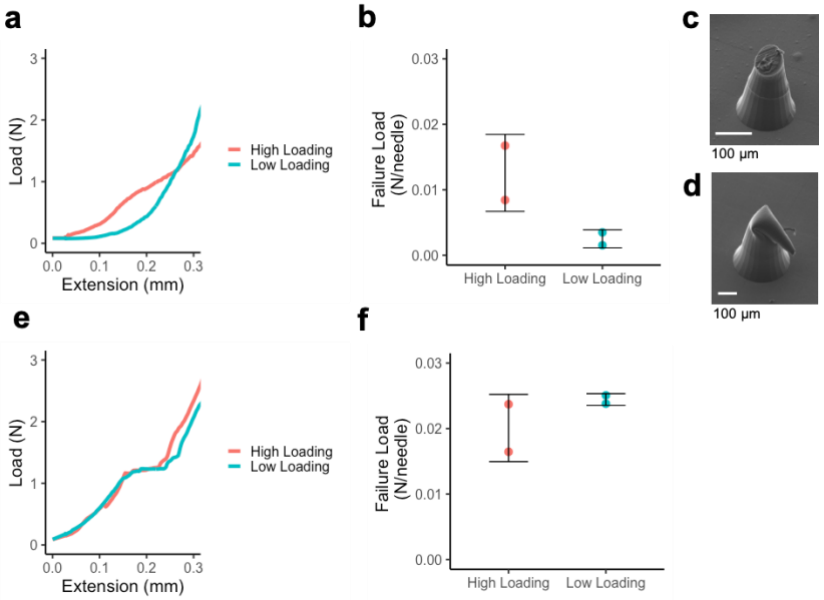

Figure 5.5. Integrated fiber microneedles decouple protein loading from mechanical properties

a) Representative graph of load and extension for compression of conventional matrix microneedle arrays and e) integrated fiber microneedle arrays with high (125 µg) or low (12.5 µg) loading of bovine serum albumin between two steel plates using an Instron universal testing system. b) Failure forces per needle for conventional matrix microneedles and f) integrated fiber microneedles with high (125 µg) or low (12.5 µg) loading of bovine serum albumin. For all samples measured with this method, the failure force was taken as the load at 0.1 mm extension (n=2, error bars represent standard deviations). c) SEM image of conventional matrix microneedles with high (125 µg) or d) low (12.5 µg) loading of bovine serum albumin after failure.

loading appear to have bent (Figure 5.5d). Additionally, matrix microneedles with low loading failed at an average force of 0.003 N per needle, while matrix microneedles with high loading failed at a 4-fold higher average force of 0.012 N per needle (Figure 5.5b). Meanwhile, integrated fiber microneedles with high and low BSA loading demonstrated similar force v. extension curves and the difference in failure force was only 0.004 N per needle (Figure 5.5e-f). We anticipate that the slight difference in failure force observed here could have been caused by differences we previously observed for fiber patterning and integration of fibers containing different protein loading (see section 5.3.4). If this is true, even more consistent mechanical properties could likely be obtained with further tuning of the protein-fiber electrospinning process. The decoupling of protein loading from mechanical properties observed here suggests the integrated fiber microneedle system could be more suitable than conventional matrix microneedles for evaluating dose dependent effects on drug activity or immune responses while minimizing the potentially confounding effect of differences in needle penetration efficiency or penetration depth.

5.3.6 *Development of a DNA-fiber formulation with potential for high loading and compatibility with different condensing agents*

While there are several reports of DNA encapsulation in electrospun fibers in the literature, no reported formulation had demonstrated compatibility with different DNA transfection reagents, specifically commercial lipid-based reagents.[12,44-46] Additionally, several published DNA-fiber formulations rely on specialized block copolymers to facilitate DNA release,[12,45] and previous formulations reported low DNA loading of 0.1 wt%.[45] Taken together, the results from previous studies motivated us to explore DNA-fiber formulations with simple

fabrication procedures compatible with different transfection reagents, and with potential for high loading.

We performed a back of the envelope calculation to identify DNA loading requirements for potential proof-of-concept studies in mice. Based on preliminary fiber output data of approximately 1.2 µg of fibers per microneedle for a mouse-scale integrated fiber microneedle device and delivery of two arrays with a maximum size of 30x30 microneedles (3 mm x 3 mm array dimensions), we estimated that a maximum of 2.3 mg of fibers could be delivered in the mouse oral mucosa. Based on these estimates, a loading of 0.4 wt% would be required to achieve a relevant DNA dose of 10 µg in a mouse model.[47-49] After preliminary data indicated that it was possible to incorporate DNA with cationic polymer or lipid condensing agents using a simple emulsion method, we planned a four factor, two-level full factorial experiment to evaluate

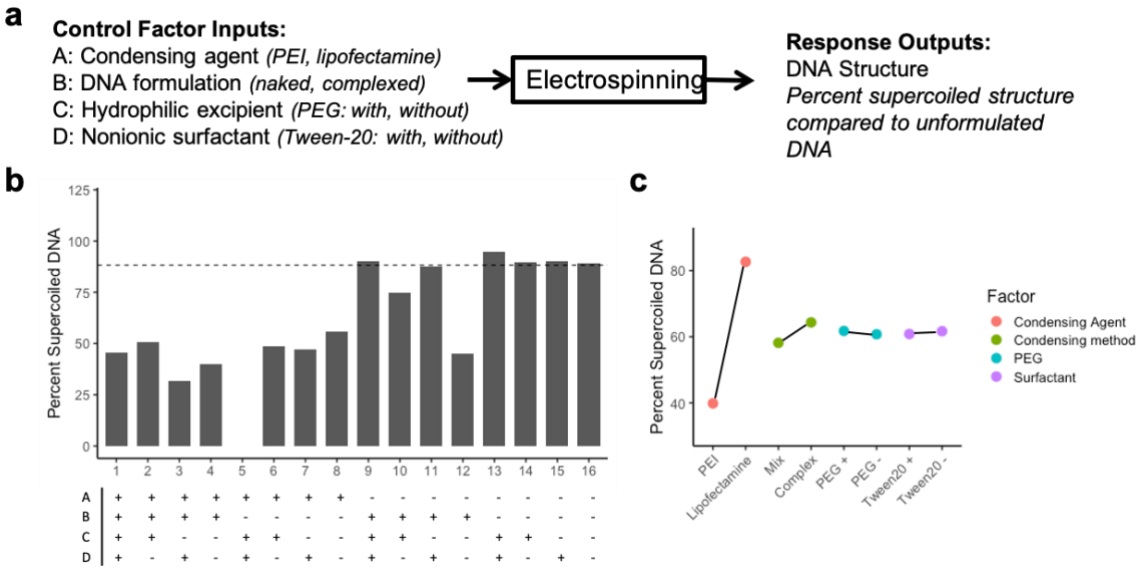

Figure 5.6. Evaluation of fiber formulation factors on the structure of formulated plasmid DNA.

a) P-diagram of the design of experiments, including the four different control factor inputs and the primary response output. b) Structure of DNA extracted from each fiber formulation evaluated using gel electrophoresis. The proportion of supercoiled DNA to relaxed DNA was calculated for each sample and compared to control unformulated DNA (dashed line). The table below the graph denotes the level of each factor for each fiber formulation. c) Means plot showing the effect of each factor at each level on the proportion of supercoiled DNA extracted from the fiber formulations.

the effect of condensing agent, DNA loading method, excipients, and surfactants on DNA structure after formulation in electrospun fibers (Figure 5.6a). These factors were selected because they had a demonstrated effect on DNA loading, structure, or release in published studies.[44-46]All samples were prepared using a simple emulsion method with 10% w/v 80:20 PLGA:PCL in HFIP as the organic phase. After preparing each DNA-loaded fiber formulation, DNA was extracted from the fibers and the DNA structure was evaluated using gel electrophoresis. The proportion of supercoiled DNA to relaxed DNA was calculated for each sample and compared to control unformulated DNA (Figure 5.6b).

The main effects table shows the difference between the average percent supercoiled DNA for each factor at its high and low levels holding all other factors constant. The main effects table for the DNA structure outcome shows that the commercial lipofectamine condensing reagent resulted in 48.5% more DNA in supercoiled structure than PEI (Figure 5.6c). The condensing method also had a notable effect on the DNA structure, where condensing the DNA before incorporating it into the polymer emulsion for electrospinning resulted in 17.4% more DNA in supercoiled structure than directly mixing naked DNA into the emulsion with the condensing agent. Based on the main effects plot, the inclusion of hydrophilic excipients or a surfactant had a minimal effect on supercoiled DNA structure. However, for lipofectamine mixed with naked DNA in the emulsion, the data suggested that the supercoiled structure of the DNA was completely preserved when PEG and the surfactant were included in the formulation (Figure 5.6b, formulation number 9). This trend was not observed for formulations with PEI as the condensing agent or in formulations in which the DNA was condensed before formulation in the emulsion.

All samples in the designed experiment were prepared at a loading of 0.05 wt% because of the loading limitation of prepared DNA-condensing agent complexes, which must be prepared in dilute conditions. However, we anticipate that loading of unformulated DNA in the emulsion aqueous phase with the condensing agent in the organic phase could enable at least a 10-fold increase in loading to meet the required minimum 0.4 wt% loading. A previous study of emulsion electrospun fibers containing DNA in the aqueous phase and PEI as a DNA condensing agent in the organic phase of the emulsion observed formation of DNA-condensing agent complexes after release which were able to transfect cells.[45] Future studies could further evaluate this method of DNA incorporation, specifically determining the maximum loading possible and altering the fiber formulation process to better preserve DNA structure.

5.3.7 *Patterning quality of DNA-loaded fibers*

Initial evaluation of the patterning quality of DNA-loaded fibers resulted in unstable fiber formation and poor uniformity (CV = 133%) (Figure 5.7a). Previous experiments evaluating different polymer electrospinning solutions indicated that the selectivity of fiber deposition in microneedle cavities could be improved by reducing the conductivity of the polymer solution.[31] Therefore, as a first step to improve DNA-fiber microneedle integration, we modified the DNA-fiber formulation and prepared the DNA complexes in salt-free conditions. This modification reduced the intercollector CV approximately two-fold to 63% (Figure 5.7b).

While removing the salt from the DNA-fiber formulation improved the stability of fiber formation and uniformity, the fiber selectivity was relatively low compared to selectivity of small molecule loaded fibers and protein loaded fibers. Therefore, to further improve DNA fiber microneedle integration, we increased the polymer concentration and evaluated changes in fiber yield, uniformity, reproducibility, and selectivity. We observed that fiber output increased from 0.26 mg to 0.80 mg and yield increased from 66.7% to 134% when polymer concentration was increased from 10% to 15%. The increased polymer concentration did not result in a notable difference in uniformity or reproducibility (Figure 5.7b-c). However, fiber selectivity for the microneedle cavities approximately tripled with an increase in polymer concentration from 10% (S_E = 5.05) to 15% (S_E = 16.76) (Figure 5.7d). Based on its improved yield and selectivity, we

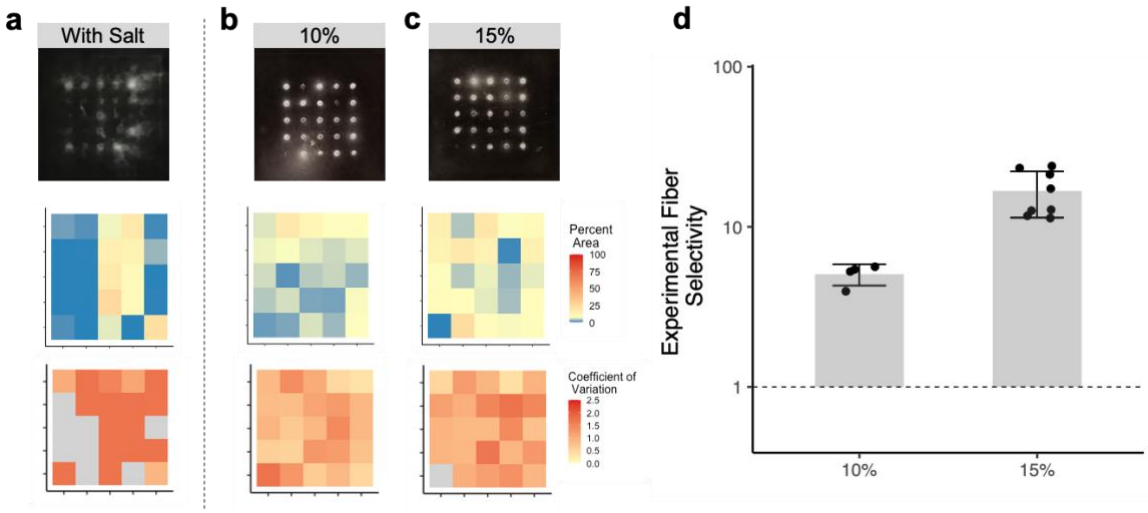

Figure 5.7. Integration of DNA-loaded fibers into two-layer microneedle mold collectors improved by reducing salt and increasing polymer concentration.

Top-down images of DNA-loaded 80:20 PLGA:PCL fibers deposited on a two-layer microneedle mold collector with 300 µm diameter, 800 µm height conical cavities, 620 µm insulative layer thickness, and 7.5 wt% carbon black conductive layer. a) DNA was complexed with PEI in buffered saline, then re-suspended in aqueous solution with polyethylene glycol and emulsified with a 10% w/v polyester solution. b-c) DNA was complexed with PEI in salt-free buffer, then re-suspended in aqueous solution with polyethylene glycol and emulsified with b) a 10% w/v polyester solution or c) a 15% w/v polyester solution. Heat maps of the percent area around each section of the pattern filled with fibers, calculated using threshold analysis of the top-down fiber images, were used to characterize pattern uniformity. Heat maps of the coefficient of variation of the percent area value for each pattern section across three electrospinning replicates were used to characterize pattern reproducibility. d) Ratio of fiber mass in the micropatterns to fiber mass on the collector surface. Grey bars represent the mean and error bars represent the standard deviation of 4 measurements from 3 independent electrospinning replicates.

selected the 15% PLGA concentration for future studies. Together, these data demonstrate the compatibility of DNA-loaded fibers with the *in situ* fiber patterning and microneedle integration process with appropriate design of the fiber formulation.

5.4 CONCLUSION

In these experiments, we developed fiber formulations to achieve feasible loading of active pharmaceutical ingredients in integrated fiber microneedles and demonstrated the compatibility of these different fiber formulations with our *in situ* fiber patterning method. Successful integration of diverse fiber formulations with dissolving microneedles suggests that integrated fiber microneedles are a feasible alternative delivery modality for electrospun fibers, with potential to combine the simple and non-invasive application of topical delivery with the delivery efficiency and sustained delivery capabilities of surgical implantation. We also performed experiments to directly compare the small molecule loading and release and the dependence of protein loading on needle mechanical properties of integrated fiber microneedles to conventional matrix microneedles. These studies demonstrated that integrated fiber microneedles can enable stable loading and release of small molecules at higher loading than conventional matrix microneedles and that integrated fiber microneedle mechanical properties are decoupled from protein loading. These studies provide two examples of potential advantages of integrated fiber microneedles over conventional matrix microneedles.

5.5 MATERIALS AND METHODS

5.5.1 *Preparation of drug loaded integrated fiber microneedles*

The electrospinning precursor solution was prepared by dissolving poly(L-lactide) (PLLA, Lactel Absorbable Polymers, ester terminated, inherent viscosity 0.9-1.2 dL/g) at 15%

w/v in a 50:50 mixture of chloroform and hexafluoro isopropanol. Dapivirine (DPV, provided by the International Partnership for Microbicides) was then added to this solution at 30% (w/w) or 15% (w/w) relative to the mass of the polymer. The precursor solution was loaded in a glass syringe fitted with a 22G blunt tipped needle. The polymer solution was dispensed from the syringe using a syringe pump (New Era Pump Systems, Inc.) at a 1 μL/min flow rate. The microneedle mold collector (conical patterns with 300 μm diameter, 800 μm height, 1000 μm spacing, 620 μm insulative layer thickness) was fixed to a custom holder that inserted copper wires to the back of the collector and held the collector at the same height as the needle. The ground from the power source (Gamma High Voltage Research) was attached to the copper wires and the positive lead was attached to the base of the needle. A voltage of 17 kV was applied, and the samples were electrospun for 30 seconds. After electrospinning, 100 μL of a 30% (w/v) solution of polyvinylpyrrolidone (PVP, average molecular weight 10 kDa, Sigma Aldrich) in water was added to the microneedle mold collector. The mold was then placed in a vacuum chamber for a total of 2 minutes. Then 100 μL of a 10% (w/v) solution of polyvinyl alcohol (product P1180, 85-89% hydrolyzed, Spectrum Chemical) in water was added, and the mold was placed in a vacuum chamber for one minute. After this vacuum step, an additional 100 μL of PVA solution was added to the mold. The microneedles were then dried at room temperature overnight.

5.5.2 *Preparation of drug loaded conventional matrix microneedles*

Drug loaded conventional matrix microneedles without fibers were prepared from a 15% (w/v) solution of PLLA in a 50:50 mixture of chloroform and HFIP without drug and with 15 wt% or 30 wt% dapivirine. 100 μL of this solution was applied to a microneedle mold (300 μm

needle diameter, 800 μm needle height, 1000 μm needle spacing), then placed in a vacuum chamber for a total of 2 minutes. An additional 100 μL of the same polymer solution was added to the mold, followed by 1 minute of vacuum. Conventional matrix microneedles were dried at room temperature overnight, then under vacuum to remove residual solvent.

5.5.3 *Measurement of dapivirine release kinetics*

Release studies were performed in phosphate buffered saline (pH 7.4) containing 1% cremophor. The volume of release media was adjusted to ensure sink conditions, defined as 10 times the solubility limit of dapivirine. Release was performed in a rotating shaker at 37ºC. At predetermined timepoints, 200 μL samples of release media were collected for HPLC analysis and replaced with an equal volume of fresh release media. Drug content was quantified using a Shimadzu Prominence UV-HPLC with a C18 column at 30ºC column temperature, 10 μL injection volume, 10 minute run time, and UV detection at 310 nm. A mixture of 65% acetonitrile and 35% 10 mM ammonium acetate in water was used as the mobile phase. A dapivirine standard curve was prepared in a 50:50 mixture of PBS and DMSO to enable quantification of drug in the release media. Percent release was calculated as the percent of the theoretically encapsulated drug.

5.5.4 *Formulation of protein loaded electrospun fibers*

Fibers for initial fiber development were prepared using an organic phase of 10% (w/v) 80:20 PLGA:PCL in HFIP. Immediately prior to electrospinning, 0.2% Tween 20 was added to the organic polymer solution and vortexed for 5 seconds. The aqueous phase was prepared in a separate tube by dissolving bovine serum albumin (BSA, Sigma Aldrich) in water at 40 mg/mL. Formulations included either PEG (100 kDa, Sigma Aldrich) at 50% w/w relative to the

polyesters or PVA (P1180, Spectrum Chemical) at 5% or 10% w/v in the aqueous phase. To prepare the emulsion, the aqueous phase was added dropwise to the organic phase while vortexing. The completed emulsion was electrospun onto an aluminum collector using a 20 μL/min flow rate, needle tip to collector distance of 10 cm, and 15 kV voltage.

5.5.5 *Preparation of protein loaded integrated fiber microneedles*

The organic phase was prepared by dissolving poly(lactic-co-glycolic acid) (50:50 PLGA, Lactel Absorbable Polymers, ester terminated, inherent viscosity 0.55-0.75 dL/g in HFIP) at 10% w/v in hexafluoro isopropanol. The aqueous phase was prepared by dissolving polyvinyl alcohol (P1180, Spectrum Chemical) at 5% w/v in water. Bovine serum albumin (BSA, Sigma Aldrich) was then added to this solution at a concentration of 40 mg/mL (high loading) or 4 mg/mL (low loading). Immediately prior to electrospinning, 0.2% Tween 20 was added to the organic phase and vortexed for 5 seconds. The aqueous phase was then added dropwise with vortexing. The completed emulsion was electrospun onto a microneedle mold collector (conical patterns with 300 μm diameter, 800 μm height, 1000 μm spacing) using a 1 μL/min flow rate and an applied voltage of 13.5 kV. Fibers with high protein loading were electrospun for 1 minute, and fibers with low protein loading were electrospun for 30 seconds. After electrospinning, 100 μL of a 30% (w/v) solution of polyvinylpyrrolidone (PVP, average molecular weight 10 kDa, Sigma Aldrich) in water was added to the microneedle mold collector. The mold was then placed in a vacuum chamber for a total of 2 minutes. Then 100 μL of a 10% (w/v) solution of polyvinyl alcohol (product P1180, 85-89% hydrolyzed, Spectrum Chemical) in water was added, and the mold was placed in a vacuum chamber for one minute. After this vacuum step, an additional 100 μL of PVA solution was added to the mold and then dried.

5.5.6 *Preparation of protein-loaded conventional matrix microneedles*

Loading of protein loaded conventional matrix microneedles was calculated to match the protein loading in the microneedle tips to the protein loading in the electrospun fibers of the integrated fiber microneedles. Microneedles were prepared by adding 200 µL of polyvinylpyrrolidone (10 kDa, 15% w/v solution in water) containing bovine serum albumin (13.1 mg for high dose, 1.31 mg for low dose) to microneedle molds and applying vacuum in two separate cycles for 1 minute per cycle. After gently agitating the mold to remove any visible bubbles, 200 µL of polyvinyl alcohol (P1180 Spectrum Chemical, 5% w/v solution in water) containing bovine serum albumin (13.1 mg for high dose, 1.31 mg for low dose) was added to the mold and vacuum was applied for 1 minute. Finally, 10% w/v polyvinyl alcohol in water was added to the mold and then dried.

5.5.7 *Measurement of protein release and activity*

Protein burst release was evaluated by first weighing protein-loaded fibers and adding them to 10 mL of MilliQ water in a conical tube. After 24 hours of incubation at 4ºC, protein concentration in the release media was measured using the Micro BCA Protein Assay Kit (Thermo Scientific) according to the manufacturer's instructions for the microplate procedure. Protein release kinetics were evaluated at 37ºC in a rotating incubator with PBS (pH 7.4) as the release media. At each time point, a 500 µL aliquot of the release media was removed to a clean tube and replaced with fresh PBS. After 7 days of release, all protein remaining in the fiber samples was extracted. Extraction was performed by adding chloroform to the tubes of release media with fiber samples, vortexing to dissolve the fibers, then centrifuging the tubes for 20 minutes to separate the aqueous and organic phases. Extraction efficiency was determined using a blank fiber sample spiked with protein. Protein content from the aqueous phase of this

extraction method and all release time points were measured using the Micro BCA Protein Assay Kit (Thermo Scientific) according to the manufacturer's instructions for the microplate procedure. Percent release was calculated using the extracted protein content. Protein activity was evaluated by preparing fibers loaded with horseradish peroxidase (HRP). Two days after electrospinning, HRP was extracted from electrospun fibers as described above and the protein concentration was determined using the Micro BCA Protein Assay. The protein was diluted to 5 ng/mL and a fresh dilution of HRP was prepared in PBS at 5 ng/mL. Extracts from blank fibers, extracts from blank fiber spiked with 5 ng/mL HRP, and PBS were included as controls. 100 µL of samples and controls were added to a clear 96-well plate followed by addition of 50 µL of TMB substrate (BioLegend). Absorbance was read at 650 nm immediately after TMB substrate addition and approximately every 20 seconds for 3 minutes. Protein bioactivity was calculated by comparing the increase in absorbance over time for HRP formulated in fibers to fresh HRP.

5.5.8 *Evaluation of protein loaded microneedle mechanical properties*

Compression testing of microneedle arrays was performed on an Instron Universal Testing System (Model 5943). An array size of 5x5 was used for all groups and replicates. The microneedle array was mounted to a microscope slide with double-sided tape, and the slide was then secured to the fixed base plate with double-sided tape. A flat stainless-steel disc adapter was attached to the load cell. The load cell moved toward the fixed base plate at a rate of 20 µm/s. The instrument began collecting data when the measured load exceeded 0.08 N. The experiment ended either when the load reached 25 N or when the length of the experiment reached 45 seconds.

5.5.9 *Preparation of DNA loaded electrospun fibers*

All fibers were prepared using a 10% (w/v) solution of 80:20 PLGA:PCL in HFIP and a theoretical loading of 0.05 wt%. For formulations incorporating DNA-condensing agent complexes, complexes were prepared the day before electrospinning. Lipofectamine-DNA complexes were prepared according to the manufacturer's instructions. To prepare PEI-DNA complexes, first 10 µg of DNA was added to 200 µL HEPES buffer and in a separate tube, 30 µg PEI was added to 200 µL HEPES buffer. Solutions were equilibrated for 5 minutes. The PEI dilution was added to the DNA dilution dropwise, then vortexed for 5 seconds and incubated for 15 minutes at room temperature. Complexes were stabilized using sucrose at a final concentration of 5%, then frozen and lyophilized overnight. Prepared complexes or DNA and condensing agent were suspended in the aqueous phase of the emulsion. Some formulations contained poly(ethylene glycol) (4 kDa, Sigma Aldrich) in the aqueous phase at a concentration of 10 mg/mL. Some formulations also contained Tween 20 in the organic phase at 0.2% v/v. The emulsion aqueous phase was added dropwise to the organic phase while vortexing. The completed emulsion was electrospun onto an aluminum collector using a 20 µL/min flow rate, needle tip to collector distance of 10 cm, and 15 kV voltage.

5.5.10 *DNA extraction and analysis*

DNA-loaded fibers were dissolved with approximately 10 µL of chloroform per milligram of fiber. An equal volume of 10 mg/mL heparin in TE buffer was added to the dissolved fibers and vortexed until a uniform emulsion formed. The mixture was then incubated on a rotisserie shaker for 1 hour at room temperature. The tube was then centrifuged for 5 minutes at 10,000 rpm and the aqueous phase containing DNA was removed to a separate tube for further analysis. DNA concentration was measured by staining with Hoechst 33258 (Thermo

Scientific) and measurement on a NanoDrop 3300 Fluorospectrometer (Thermo Scientific) following the manufacturer's instructions. Structure of the extracted DNA was evaluated using agarose gel electrophoresis. The agarose gel was prepared at 1% with Tris-acetate EDTA buffer. DNA samples (4 μL) were mixed with loading buffer (20 μL) and loaded into the wells of the gel. A voltage of 100 V was applied to the gel for 30 min. After staining with SYBR Safe (Invitrogen) following the manufacturer's instructions, an image of the gel was captured (Gel Doc EZ System, Bio-Rad). DNA band intensity was quantified using Bio-Rad Image Lab software, and the percent supercoiled DNA was taken as the intensity of the supercoiled DNA band divided by the total band intensity for the specific lane.

5.5.11 *Integration of DNA loaded fibers with microneedles*

The organic phase was prepared by dissolving and 80:20 blend of poly(lactic-co-glycolic acid) (50:50 PLGA, Lactel Absorbable Polymers, ester terminated, inherent viscosity 0.55-0.75 dL/g in HFIP) and polycaprolactone at 10% w/v in hexafluoro isopropanol. The aqueous phase contained polyethylene glycol (4 kDa, Sigma Aldrich) at 10 wt% relative to the mass of the polymers in the organic phase. PEI-DNA complexes were prepared using the same protocol used for the initial DNA-fiber formulation development described above, then re-suspended in the aqueous phase. The aqueous phase was then added dropwise to the organic phase with vortexing. The completed emulsion was electrospun onto a microneedle mold collector (conical patterns with 300 μm diameter, 800 μm height, 1000 μm spacing, 620 μm insulative layer thickness) using a 2 μL/min flow rate and an applied voltage of 13 kV. Samples were electrospun for 2 minutes.

5.5.12 *Image analysis and calculation of experimental fiber selectivity*

All image analysis was performed in ImageJ. The percent area of the collector surface covered with fibers within the microscope image field was determined by converting an optical microscope image to 8-bit, applying an auto-threshold to make all fibers appear completely black, and measuring percent area. This calculation was repeated for images from four different locations on the collector surface, and an average percent area was calculated. Fiber diameters were measured from at least 10 different fibers in microscope images. The percent area from the threshold analysis and the fiber diameter were used to estimate the volume of fibers covering the collector surface. The volume value was then multiplied by a scaling factor to estimate the fiber volume across the entire collector surface. Assuming the density of the fibers was equal to reported density of the raw polymer material, we calculated the mass of fibers on the collector surface. The mass of fibers in the patterns was then determined by subtracting the calculated mass of fibers on the collector surface from the measured total fiber mass on the collector. Finally, the ratio of fiber mass in the patterns to fiber mass on the collector surface was calculated.

5.5.13 *Analysis of fiber pattern uniformity*

Fiber pattern uniformity was evaluated through ImageJ analysis of top-down images of collectors with fibers. To analyze a collector, an array of identical 1 mm x 1 mm square regions of interest was overlaid on the image and aligned with the pattern array. The image was then converted to 8-bit, and an auto-threshold was applied to make all fibers appear completely black. The percent area within each region of interest was then calculated. The theoretical ideal percent area was calculated as 7% assuming the ideal fiber deposition pattern would result in visible fibers in the entire pattern opening area of 0.07 mm. Heatmaps of the percent area values for

each region of interest were plotted with a scale relative to the theoretical ideal percent area. Uniformity was described as the coefficient of variation between each region of interest across the array.

5.6 ACKNOWLEDGEMENTS

SEM imaging was conducted at the Washington Nanofabrication Facility, a National Nanotechnology Coordinated Infrastructure (NNCI) site at the University of Washington, which is supported in part by funds from the Molecular Engineering & Sciences Institute, the Clean Energy Institute, the Washington Research Foundation, the M. J. Murdock Charitable Trust, the National Science Foundation and the National Institutes of Health. The authors would like to thank Barry Lutz for the use of the Gel Doc EZ System. This work was supported by NIH/NIHCD grant DP2HD075703 to KAW. RC would like to acknowledge additional support from the NSF Graduate Research Fellowship (DGE-1256082) and the University of Washington STD & AIDS Research Training Fellowship Program (NIH 2T32AI007140-41).

5.7 REFERENCES

1 Mendes, A., Gorzelanny, C., Halter, N., Schneider, S. & Chronakis, I. Hybrid electrospun chitosan-phospholipids nanofibers for transdermal drug delivery. *International Journal of Pharmaceutics* **510**, 48-56, doi:10.1016/j.ijpharm.2016.06.016 (2016).

2 Ball, C., Chou, S. F., Jiang, Y. & Woodrow, K. A. Coaxially electrospun fiber-based microbicides facilitate broadly tunable release of maraviroc. *Mater Sci Eng C Mater Biol Appl* **63**, 117-124, doi:10.1016/j.msec.2016.02.018 (2016).

3 Madhaiyan, K., Sridhar, R., Sundarrajan, S., Venugopal, J. & Ramakrishna, S. Vitamin B-12 loaded polycaprolactone nanofibers: A novel transdermal route for the water soluble energy supplement delivery. *International Journal of Pharmaceutics* **444**, 70-76, doi:10.1016/j.ijpharm.2013.01.040 (2013).

4 Preem, L. *et al.* Interactions between Chloramphenicol, Carrier Polymers, and Bacteria-Implications for Designing Electrospun Drug Delivery Systems Countering Wound Infection. *Molecular Pharmaceutics* **14**, 4417-4430, doi:10.1021/acs.molpharmaceut.7b00524 (2017).

5 Briggs, T. & Arinzeh, T. L. Examining the formulation of emulsion electrospinning for improving the release of bioactive proteins from electrospun fibers. *Journal of Biomedical Materials Research Part A* **102**, 674-684, doi:10.1002/jbm.a.34730 (2014).

6 Yang, Y. *et al.* Promotion of skin regeneration in diabetic rats by electrospun core-sheath fibers loaded with basic fibroblast growth factor. *Biomaterials* **32**, 4243-4254, doi:10.1016/j.biomaterials.2011.02.042 (2011).

7 Chew, S. Y., Wen, J., Yim, E. K. F. & Leong, K. W. Sustained Release of Proteins from Electrospun Biodegradable Fibers. *Biomacromolecules* **6**, 2017-2024, doi:10.1021/bm0501149 (2005).

8 Sang, Q. *et al.* Electrospun gelatin/sodium bicarbonate and poly(lactide-co-epsilon-caprolactone)/sodium bicarbonate nanofibers as drug delivery systems. *Materials Science & Engineering C-Materials For Biological Applications* **81**, 359-365, doi:10.1016/j.msec.2017.08.007 (2017).

9 Frizzell, H., Ohlsen, T. & Woodrow, K. Protein-loaded emulsion electrospun fibers optimized for bioactivity retention and pH-controlled release for peroral delivery of biologic therapeutics. *International Journal of Pharmaceutics* **533**, 99-110, doi:10.1016/j.ijpharm.2017.09.043 (2017).

10 Schkarpetkin, D. *et al.* Development of novel electrospun dual-drug fiber mats loaded with a combination of ampicillin and metronidazole. *Dental Materials* **32**, 951-960, doi:10.1016/j.dental.2016.05.002 (2016).

11 Saraf, A., Baggett, L. S., Raphael, R. M., Kasper, F. K. & Mikos, A. G. Regulated non-viral gene delivery from coaxial electrospun fiber mesh scaffolds. *Journal of Controlled Release* **143**, 95-103, doi:10.1016/j.jconrel.2009.12.009 (2010).

12 Luu, Y. K., Kim, K., Hsiao, B. S., Chu, B. & Hadjiargyrou, M. Development of a nanostructured DNA delivery scaffold via electrospinning of PLGA and PLA-PEG block copolymers. *J Control Release* **89**, 341-353 (2003).

13 Okuda, T., Tahara, Y., Kamiya, N., Goto, M. & Kidoaki, S. S/O-nanodispersion electrospun fiber mesh effective for sustained release of healthy plasmid DNA with the structural and functional integrity. *Journal of Biomaterials Science-Polymer Edition* **24**, 1277-1290, doi:10.1080/09205063.2012.755600 (2013).

14 Blakney, A. K., Krogstad, E. A., Jiang, Y. H. & Woodrow, K. A. Delivery of multipurpose prevention drug combinations from electrospun nanofibers using composite microarchitectures. *Int J Nanomedicine* **9**, 2967-2978, doi:10.2147/IJN.S61664 (2014).

15 Romita, P. *et al.* Contact dermatitis due to transdermal therapeutic systems: a clinical update. *Acta Biomed* **90**, 5-10, doi:10.23750/abm.v90i1.6563 (2018).

16 Zhang, Y. *et al.* An electrospun fiber-covered stent with programmable dual drug release for endothelialization acceleration and lumen stenosis prevention. *Acta Biomaterialia* **94**, 295-305, doi:10.1016/j.actbio.2019.06.008 (2019).

17 Liu, S. *et al.* Electrospun fibrous membranes featuring sustained release of ibuprofen reduce adhesion and improve neurological function following lumbar laminectomy. *Journal of Controlled Release* **264**, 1-13, doi:10.1016/j.jconrel.2017.08.011 (2017).

18 Pinese, C. *et al.* Sustained delivery of siRNA/mesoporous silica nanoparticle complexes from nanofiber scaffolds for long-term gene silencing. *Acta Biomater* **76**, 164-177, doi:10.1016/j.actbio.2018.05.054 (2018).

19 Passos, P. C. *et al.* Nanofibrous antibiotic-eluting matrices: Biocompatibility studies in a rat model. *Journal of Biomedical Materials Research Part B: Applied Biomaterials*, doi:10.1002/jbm.b.34389 (2019).
20 Prausnitz, M. R. Microneedles for transdermal drug delivery. *Adv Drug Deliv Rev* **56**, 581-587, doi:10.1016/j.addr.2003.10.023 (2004).
21 Prausnitz, M. R., Mikszta, J. A., Cormier, M. & Andrianov, A. K. Micro needle-based vaccines. *Current topics in microbiology and immunology* **333**, 369-393 (2009).
22 Traverso, G. *et al.* Microneedles for drug delivery via the gastrointestinal tract. *Journal of pharmaceutical sciences* **104**, 362-367 (2015).
23 McNeilly, C. L. *et al.* Microprojection arrays to immunise at mucosal surfaces. *J Control Release* **196**, 252-260, doi:10.1016/j.jconrel.2014.09.028 (2014).
24 Ma, Y. *et al.* Vaccine delivery to the oral cavity using coated microneedles induces systemic and mucosal immunity. *Pharm Res* **31**, 2393-2403, doi:10.1007/s11095-014-1335-1 (2014).
25 Mc Crudden, M. T. C. *et al.* Design, Formulation, and Evaluation of Novel Dissolving Microarray Patches Containing Rilpivirine for Intravaginal Delivery. *Advanced Healthcare Materials* **8**, 1801510, doi:10.1002/adhm.201801510 (2019).
26 Gill, H. S., Denson, D. D., Burris, B. A. & Prausnitz, M. R. Effect of microneedle design on pain in human subjects. *Clin J Pain* **24**, 585-594 (2008).
27 Davis, S. P., Landis, B. J., Adams, Z. H., Allen, M. G. & Prausnitz, M. R. Insertion of microneedles into skin: measurement and prediction of insertion force and needle fracture force. *Journal of Biomechanics* **37**, 1155-1163, doi:10.1016/j.jbiomech.2003.12.010 (2004).
28 DeMuth, P. C., Min, Y., Irvine, D. J. & Hammond, P. T. Implantable Silk Composite Microneedles for Programmable Vaccine Release Kinetics and Enhanced Immunogenicity in Transcutaneous Immunization. *Advanced Healthcare Materials* **3**, 47-58, doi:10.1002/adhm.201300139 (2014).
29 Chen, M. C., Huang, S. F., Lai, K. Y. & Ling, M. H. Fully embeddable chitosan microneedles as a sustained release depot for intradermal vaccination. *Biomaterials* **34**, 3077-3086, doi:10.1016/j.biomaterials.2012.12.041 (2013).
30 Krogstad, E. A. & Woodrow, K. A. Manufacturing scale-up of electrospun poly(vinyl alcohol) fibers containing tenofovir for vaginal drug delivery. *Int J Pharm* **475**, 282-291, doi:10.1016/j.ijpharm.2014.08.039 (2014).
31 Creighton, R. L., Phan, J. & Woodrow, K. A. In situ 3D-patterning of electrospun fibers using two-layer composite materials. *Scientific Reports* **10**, doi:10.1038/s41598-020-64846-z (2020).
32 Yu, L. Amorphous pharmaceutical solids: preparation, characterization and stabilization. *Advanced Drug Delivery Reviews* **48**, 27-42, doi:10.1016/s0169-409x(01)00098-9 (2001).
33 Tam, H. H. *et al.* Sustained antigen availability during germinal center initiation enhances antibody responses to vaccination. *Proceedings of the National Academy of Sciences*, doi:10.1073/pnas.1606050113 (2016).
34 Chen, M. C., Lai, K. Y., Ling, M. H. & Lin, C. W. Enhancing immunogenicity of antigens through sustained intradermal delivery using chitosan microneedles with a patch-dissolvable design. *Acta Biomaterialia* **65**, 66-75, doi:10.1016/j.actbio.2017.11.004 (2018).

35 Jewell, C. M., López, S. C. & Irvine, D. J. In situ engineering of the lymph node microenvironment via intranodal injection of adjuvant-releasing polymer particles. *Proc Natl Acad Sci U S A* **108**, 15745-15750, doi:10.1073/pnas.1105200108 (2011).

36 Kim, J. *et al.* Injectable, spontaneously assembling, inorganic scaffolds modulate immune cells in vivo and increase vaccine efficacy. *Nature Biotechnology* **33**, 64-U241, doi:10.1038/nbt.3071 (2015).

37 Schneider, A., Wang, X. Y., Kaplan, D. L., Garlick, J. A. & Egles, C. Biofunctionalized electrospun silk mats as a topical bioactive dressing for accelerated wound healing. *Acta Biomater* **5**, 2570-2578, doi:10.1016/j.actbio.2008.12.013 (2009).

38 Kim, T. G., Lee, D. S. & Park, T. G. Controlled protein release from electrospun biodegradable fiber mesh composed of poly(epsilon-caprolactone) and poly(ethylene oxide). *International Journal of Pharmaceutics* **338**, 276-283, doi:10.1016/j.ijpharm.2007.01.040 (2007).

39 Yang, Y., Li, X., Qi, M., Zhou, S. & Weng, J. Release pattern and structural integrity of lysozyme encapsulated in core–sheath structured poly(dl-lactide) ultrafine fibers prepared by emulsion electrospinning. *European Journal of Pharmaceutics and Biopharmaceutics* **69**, 106-116, doi:10.1016/j.ejpb.2007.10.016 (2008).

40 Ji, W. *et al.* Fibrous scaffolds loaded with protein prepared by blend or coaxial electrospinning. *Acta Biomaterialia* **6**, 4199-4207, doi:10.1016/j.actbio.2010.05.025 (2010).

41 Chen, Y., Chen, B. Z., Wang, Q. L., Jin, X. & Guo, X. D. Fabrication of coated polymer microneedles for transdermal drug delivery. *Journal of Controlled Release* **265**, 14-21, doi:10.1016/j.jconrel.2017.03.383 (2017).

42 Loizidou, E. Z. *et al.* Structural characterisation and transdermal delivery studies on sugar microneedles: Experimental and finite element modelling analyses. *European Journal of Pharmaceutics and Biopharmaceutics* **89**, 224-231, doi:10.1016/j.ejpb.2014.11.023 (2015).

43 Park, J. H., Allen, M. G. & Prausnitz, M. R. Polymer microneedles for controlled-release drug delivery. *Pharmaceutical Research* **23**, 1008-1019, doi:10.1007/s11095-006-0028-9 (2006).

44 Liang, D. *et al.* In vitro non-viral gene delivery with nanofibrous scaffolds. *Nucleic Acids Research* **33**, e170-e170, doi:10.1093/nar/gni171 (2005).

45 Yang, Y. *et al.* Core-sheath structured fibers with pDNA polyplex loadings for the optimal release profile and transfection efficiency as potential tissue engineering scaffolds. *Acta Biomater* **7**, 2533-2543, doi:10.1016/j.actbio.2011.02.031 (2011).

46 Nie, H. & Wang, C.-H. Fabrication and characterization of PLGA/HAp composite scaffolds for delivery of BMP-2 plasmid DNA. *Journal of Controlled Release* **120**, 111-121, doi:https://doi.org/10.1016/j.jconrel.2007.03.018 (2007).

47 Qiu, Y. *et al.* DNA-based vaccination against hepatitis B virus using dissolving microneedle arrays adjuvanted by cationic liposomes and CpG ODN. *Drug Deliv* **23**, 2391-2398, doi:10.3109/10717544.2014.992497 (2016).

48 Cole, G. *et al.* Dissolving microneedles for DNA vaccination: Improving functionality via polymer characterization and RALA complexation. *Hum Vaccin Immunother* **13**, 50-62, doi:10.1080/21645515.2016.1248008 (2017).

49 McCaffrey, J. *et al.* Transcending epithelial and intracellular biological barriers; a prototype DNA delivery device. *Journal of Controlled Release* **226**, 238-247, doi:https://doi.org/10.1016/j.jconrel.2016.02.023 (2016).

Chapter 6. ORAL MUCOSAL VACCINATION USING INTEGRATED FIBER MICRONEEDLES

6.1 ABSTRACT

Current understanding of oral mucosal immunity is limited by a lack of multifunctional delivery systems capable of overcoming the physical and immunological barriers of the oral mucosa. Microneedles can be designed with different geometries and vaccine release kinetics and tuning of these design attributes has led to optimized immune responses in dermal tissue. Solid coated microneedles have been used to overcome physical barriers of the oral mucosa for efficient vaccine delivery. However, these previous studies were limited to a single microneedle geometry with bolus vaccine release. Here, we characterize the humoral and cellular immune response to integrated fiber microneedle vaccines, which enable tunable geometry and release kinetics without compromising mechanical strength. These studies establish integrated fiber microneedles as a multifunctional delivery system for oral mucosal vaccination and motivate future work using the device as a tool to better understand oral mucosal immunity.

6.2 INTRODUCTION

The oral mucosa is promising site for vaccination, with a demonstrated ability to elicit robust cellular and humoral immune responses locally in the oral mucosa, at distal mucosal sites, and systemically.[1-3] However, the underlying mechanisms governing these responses are not well understood because of the diverse mucosal structures and dendritic cell subsets in different regions of the oral cavity. The oral mucosa contains a stratified squamous epithelial structure,

with permeability that varies with epithelial thickness (6-8 cell layers in the sublingual mucosa, 8-12 cell layers in the buccal mucosa).[4] This leads to varying vaccine delivery efficiency and depth which confounds studies comparing the immunogenicity of these two tissues.[5] Dendritic cell subsets also vary throughout the oral mucosa. In both the sublingual and buccal mucosa, Langerhans cells (LCs) are present in the epithelium and immunogenic interstitial DCs (iDCs) are present deeper in the lamina propria. However, the buccal mucosa contains LCs and iDCs at a higher frequency than the sublingual mucosa,[6-8] and the sublingual lamina propria contains a large population of macrophage-like antigen presenting cells which likely mediate tolerance in mice.[7] The buccal mucosa of mice also contains a population of langerin+ iDCs that are thought to activate CD8+ T cells through cross-presentation.[9] The antigen presenting cell population in the buccal mucosa is therefore an attractive target for vaccination, but buccal vaccination studies have been limited by the poor permeability of the buccal mucosa.[10,11]

Recently microneedles have gained interest as an alternative delivery system for the oral mucosa[5,12-16] because of their demonstrated ability to painlessly overcome physical delivery barriers in dermal tissue.[17,18] Microneedles have been delivered into the oral mucosa at an average delivery depth of 50% of the needle height,[5,13] which is similar to delivery depths reported in dermal tissue.[19,20] Microneedles have been used to increase the delivery efficiency of small molecule dyes into the oral mucosa by 10-fold compared to topical administration.[5,12,21] Previous studies of microneedle-mediated oral mucosal vaccine delivery have demonstrated feasibility, but have been limited primarily to coated solid microneedles with a single geometry and bolus release kinetics.[5,13-16]

Dermal microneedle vaccine studies are prevalent, and there is a demonstrated effect of microneedle geometry, vaccine release kinetics, and microneedle delivery site on cellular and

humoral immunity. Several experimental studies and a computational models have shown that antigen presenting cell activation and humoral immune responses can be optimized by varying microneedle geometry parameters such as delivery area, density, and length.[22-25] Microneedles formulated for sustained antigen release in dermal tissue have resulted in prolonged local inflammation for up to 11 days following delivery, leading to a 3-fold increase in antigen-specific CD8+ T cell responses and a 1300-fold increase in serum IgG titers compared to bolus release microneedles.[26,27] Delivery site also has a significant effect on dermal microneedle vaccination, with delivery in the ear pinna resulting in significantly higher antibody titers compared to the ventral abdomen.[22] While each of these factors contributes to the immunogenicity of dermal microneedle vaccines, these effects have not been evaluated in the oral mucosa.

Here, we characterize the humoral and cellular immune responses to integrated fiber microneedles with varying geometry and material configuration when delivered in the murine buccal or sublingual mucosa. Shorter integrated fiber microneedle vaccines with primarily burst release delivered to the sublingual mucosa elicit significantly higher serum IgG antibody concentrations compared to topical vaccination with a swab. Additionally, this same microneedle vaccine design delivered to the buccal or sublingual mucosa results in splenocytes with antigen-specific interferon-γ secretion. Delivery of longer integrated fiber microneedles in the buccal mucosa resulted in a more Th-1 biased immune response. Finally, integrated fiber microneedles with sustained antigen and adjuvant release result in a delayed peak serum IgG response and high levels of non-specific interferon-γ secretion in the draining lymph nodes. These foundational studies establish the basic capabilities of integrated fiber microneedle vaccines and motivate their further development as a tool to understand and optimize oral mucosal vaccines.

6.3 RESULTS AND DISCUSSION

6.3.1 *Fabrication of integrated fiber microneedles with varying dimensions and material configurations*

To demonstrate the tunability of the integrated fiber microneedle system, three different designs were prepared (Figure 6.1a). Two designs, integrated fiber microneedles (iFMD) and reverse integrated fiber microneedles (riFMD), consisted of pyramidal shaped microneedles with base width 100 μm and height 300 μm arranged in an array of 77 needles. Based on previous studies of microneedle insertion, microneedles with these dimensions are expected to penetrate 100-200 μm into tissue, which is approximately the depth of the lamina propria.[13] These designs varied in their material configuration, with iFMD consisting of polyester fibers surrounded by a water soluble backfill matrix, and riFMD consisting of water soluble fibers surrounded by a polyester backfill matrix. These different material configurations provide two different approaches to control the release of agents from the integrated fiber microneedles. A third microneedle design, long integrated fiber microneedles (liFMD) consisted of conical shaped microneedles with base width 300 μm and height 800 μm arranged in an array of 25 needles. These longer microneedles were designed to penetrate deeper into the lamina propria and access different populations of antigen presenting cells.[8,28]

Two-layer collectors were fabricated as previously described[29] using a 5 wt% carbon black-PDMS conductive layer and an approximately 270 µm thick insulative layer or a 7.5 wt% carbon black-PDMS conductive layer and an approximately 620 µm thick insulative layer for the iFMD and liFMD, respectively (Figure 6.1a, step 1). Polyester (iFMD, liFMD) or water soluble (riFMD) fibers were then electrospun onto the collectors (Figure 6.1a, step 2). To improve the mechanical stiffness of the fiber scaffolds and to create a backing layer, the collectors were then filled with an aqueous polymer solution (iFMD, liFMD) or a solution of polyester in acetone (riFMD) (Figure 6.1a, step 3). To eliminate the need to remove the polyester backing from the riFMDs after delivery, the polyester solution was wiped from the collector surface after filling (Figure 6.1a, step 3i), and an aqueous polymer solution was added to create a dissolving backing

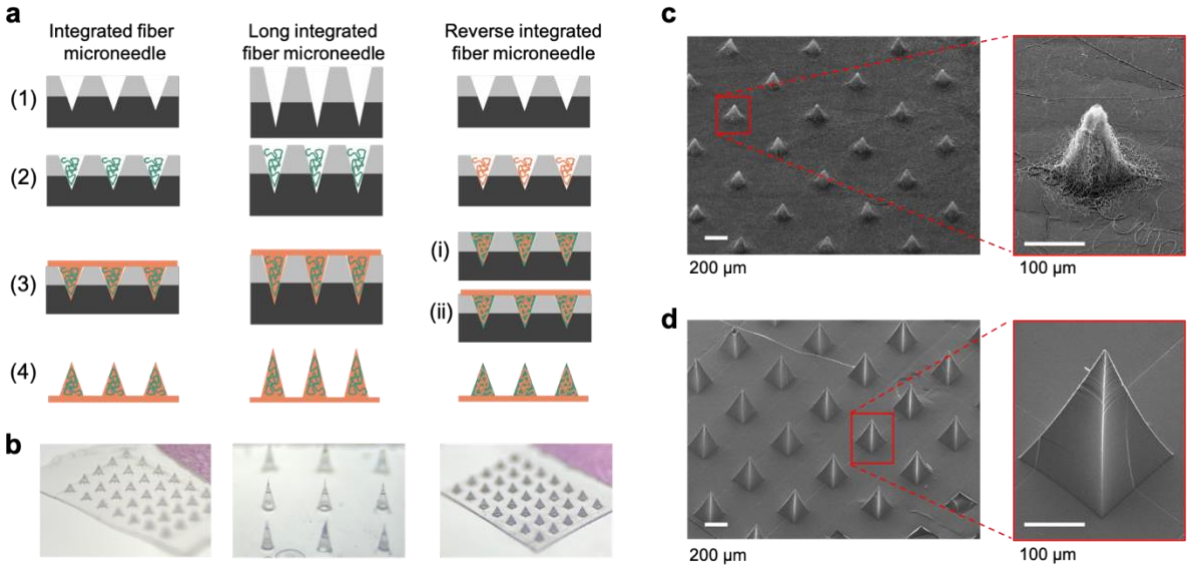

Figure 6.1. Fabrication of integrated fiber microneedles with varying dimensions and material configurations

a) Schematics of the fabrication approaches for integrated fiber microneedles, long integrated fiber microneedles, and reverse integrated fiber microneedles. Each variation follows a general approach of electrospinning onto two-layer negative microneedle molds with a conductive base layer and insulative surface layer, followed by filling with a polymer solution to provide mechanical stiffness and a backing layer. Integrated fiber microneedles and long integrated fiber microneedles consist of biodegradable polyester fibers (green) and a water soluble backfill (orange), while reverse integrated fiber microneedles consist of water soluble fibers (orange), biodegradable polyester backfill (green), and a water soluble backing layer (orange). b) Stereoscope images of each microneedle design suggest uniform microneedle arrays. The unique microneedle mold configuration used here leads to fiber conformation to the microneedle mold, demonstrated by (c) SEM images of fibers after removal from the mold. d) After filling with the matrix material, integrated fiber microneedles are smooth with sharp tips.

layer (Figure 6.1a, step 3ii). Each completed design appeared to replicate the collector well and produce uniform microneedle arrays (Figure 6.1b). SEM imaging confirmed that electrospun fibers were able to conform well to the iFMD collectors (Figure 6.1c), and that the completed microneedles were smooth with sharp tips approximately 5 μm in diameter (Figure 6.1d).

6.3.2 *Mechanical and release characterization of distinct microneedle designs*

A key function of each microneedle design is its ability to penetrate tissue. Previous work from our group and others suggests that compression data can be used to predict the tissue penetration capabilities of microneedles.[18,29,30] Each microneedle design (iFMD, liFMD, riFMD) was compressed using an Instron Universal Testing System following the same methods used previously.[29] Microneedles with the same geometry (iFMD and riFMD) exhibited a steady change in load as the needles were compressed, indicative of needle tip compression (Figure 6.2a).[31] The riFMDs were slightly stiffer than the iFMDs, indicated by a higher slope of the compression curve. This is consistent with previous studies, which have demonstrated that microneedle mechanical properties depend on the properties of the needle fill material.[17] Meanwhile, liFMDs had a distinct shoulder at approximately 0.15 mm extension, likely indicating needle bending.[31] The mean failure force for each design, defined as the load per needle at 0.1 mm extension, surpassed the predicted force to penetrate tissue (0.02 N/needle) by 5 to 6-fold, with no significant differences between the microneedle designs (Figure 6.2b).

We also evaluated the effect of integrated fiber microneedle material configuration on release of a model protein, bovine serum albumin (BSA). Based on previous work from our

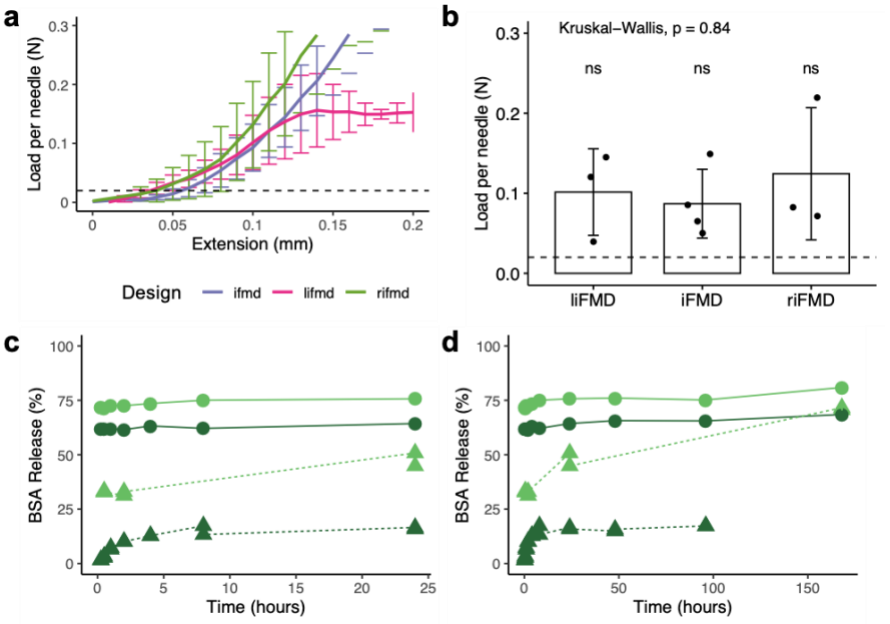

Figure 6.2. Mechanical strength is maintained when tuning integrated fiber microneedle geometry or material configuration

a) Compression of integrated fiber microneedles, long integrated fiber microneedles, and reverse integrated fiber microneedles under an axial load. Curves represent the mean of at least three microneedle array replicates, and error bars represent standard deviations. b) Mean and standard deviation of the failure force of each microneedle design, defined as the load per needle at 0.1 mm extension. Groups were compared using Kruskal-Wallis test, which determined no significant difference (p = 0.84). Horizontal dashed line in a) and b) represents the predicted load per needle required for tissue penetration (0.02 N). c) Early and d) late release of bovine serum albumin (BSA) mediated by two different material configurations (● = polyester fiber, ▲= polyvinyl alcohol fiber coated with polyester) and two different polyesters (dark green = PLGA, light green = PLLA).

group, we expected that protein loaded into polyester fibers would result in an initial burst release of surface associated protein, followed by slow sustained release. We observed that selection of polyester fiber material primarily determined the percent burst release, with PLLA resulting in 70% burst and PLGA resulting in 60% burst (Figure 6.2c,d). After the burst, protein released from PLLA or PLGA fibers at rates of approximately 0.2% or 0.25% per day, respectively, over two weeks. We expected that we could reduce this burst release by "reversing" the material configuration. In the reverse integrated fiber microneedles, protein loaded fibers were fabricated using water soluble polymers (polyvinyl alcohol) and microneedle matrix was fabricated using a polyester as a rate limiting layer. Previous studies have demonstrated the function of polyester coatings to reduce burst release of proteins from microneedles.[32] When we

evaluated the release of BSA from these reverse integrated fiber microneedles, we saw an approximately 3-fold reduction in the burst release for PLLA and essentially no burst release for a PLGA matrix (Figure 6.2c,d). With this material configuration, we observed a more dramatic difference in the sustained release rates, with a PLLA matrix resulting in 5.4% release per day and a PLGA matrix resulting in 2.1% release per day. Without the large burst release, more of the protein is available for controlled release mediated by degradation of the polyester, dissolution of the PVA fiber, and diffusion of the protein out of the needles. Detailed analysis of the contribution of each of these release mechanisms is beyond the scope of this paper, but this would be interesting to explore in future work to better understand the capabilities of this integrated fiber microneedle material configuration. Together, these data suggest that our integrated fiber microneedle system can be tuned with respect to needle geometry and material configuration to control the release of agents while maintaining mechanical strength.

6.3.3 *Integrated fiber microneedles are immunogenic in the buccal mucosa and in dermal tissue*

We designed an initial pilot vaccination study using ovalbumin as a model antigen to determine if the iFMDs could induce a systemic humoral immune response when delivered either dermally or buccally in mice. CpG-ODN and GMCSF were selected as adjuvants based on published work demonstrating their ability to recruit and activate dendritic cells.[33,34] The PLGA electrospun fibers contained 20 µg of OVA, while the remaining 180 µg of OVA and both adjuvants were formulated into the microneedle PVP backfill material (Figure 6.3a).

OVA specific serum IgG responses elicited by iFMD delivery in the buccal mucosa surpassed those elicited by delivery in dermal tissue both at the peak of the response and at the endpoint of the study (Figure 6.3b). We observed a 19-fold increase in OVA specific serum IgG for the strongest responder in the buccal microneedle group from before vaccination to day 42, which continued to increase until the endpoint of the study (Figure 6.3c). The OVA specific serum IgG in the dermal iFMD group was increased only up to 4-fold from before vaccination to day 28 (Figure 6.3c). At the study endpoint, splenocytes and lymphocytes from vaccinated mice and naïve mice were re-stimulated *ex vivo* with OVA. Splenocytes from both mice in the buccal iFMD group exhibited antigen specific interferon-γ secretion, compared to only one mouse in the

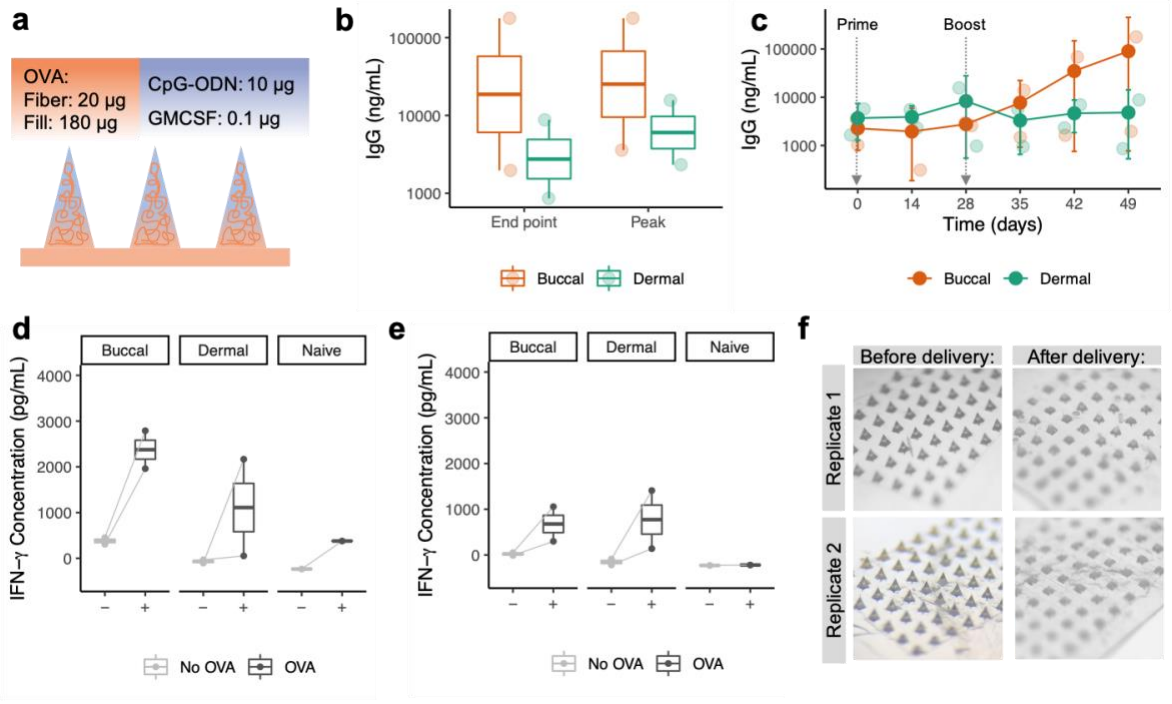

Figure 6.3. Integrated fiber microneedles are immunogenic in the buccal mucosa and in dermal tissue

(a) Schematic of antigen and adjuvant loading in integrated fiber microneedles. (b) OVA-specific serum IgG concentration at study endpoint and at the peak for each mouse after iFMD delivery in the buccal mucosa or dermal tissue on day 0 and day 28. (c) Kinetics of OVA-specific serum IgG concentration for the duration of the study. Shown are the mean ± s.d. of n=2 biological replicates. Individual replicates are plotted as transparent data points. At the study endpoint, splenocytes (d) and lymphocytes from the submandibular lymph nodes (e) were re-stimulated with OVA (1 mg/mL) ex vivo for 72 hours in the presence of ConA (10 µg/mL). Cell culture supernatants were assayed for IFN-g using ELISA as a measure of OVA-specific T cell function. (f) Stereoscope images of iFMD before and after delivery to the dermal tissue.

dermal iFMD group (Figure 6.3d). This trend was observed in the re-stimulation of lymphocytes collected from the superficial cervical and submandibular lymph nodes of mice in both groups (Figure 6.3e).

It was surprising that the dermal microneedle group exhibited such a weak response based on previous literature reporting robust immune responses from the dermal route.[22-27] To better understand the delivery efficiency via the dermal route, we measured the needle height reduction after dermal iFMD delivery. Needle height was reduced by 50% to 82% for the two replicates (Figure 6.3f), which encompasses approximately the maximum and minimum expected microneedle delivery depth based on previous studies.[19,20] Based on these measurements, we concluded that the low response in the dermal microneedle group was not due to insufficient needle penetration. It is possible that the stronger humoral and cellular immunity observed in the buccal microneedle group was due to more rapid or more complete needle dissolution in the moist buccal mucosa, resulting in an effective higher dose. Overall, this pilot study suggested that integrated fiber microneedles are immunogenic in a mouse model, which motivated our further exploration of this system in the oral mucosa.

6.3.4 *Decoupling contribution of the fibers and backfill to the iFMD immune response*

Given the robust immune responses elicited by buccal iFMD vaccination in our pilot study, we sought to characterize the response to the antigen dose delivered from either the fiber or backfill component of the iFMD. Previous studies have established that delivery of a large bolus vaccine dose combined with a small, sustained vaccine dose can elicit significantly more robust immunity compared to either bolus or sustained delivery alone.[26,27] To test this with the iFMD system, we fabricated microneedles containing either 20 µg of OVA in the fibers (OVA Fiber (20)) or 180 µg of OVA in the backfill matrix (OVA Backfill (180)). The microneedle

materials design was kept constant (PLGA fibers with PVA and PVP backfill), and both microneedle formulations contained 10 µg CpG-ODN and 100 ng GMCSF as adjuvants in the backfill matrix (Figure 6.4a).

Mice were immunized with one of the two different microneedle designs in either the buccal or sublingual mucosa on day 0 and day 14. At the peak and study endpoint for each group, OVA-specific serum IgG concentrations were reduced more than 10-fold compared to the pilot study of buccal iFMD vaccination (Figure 6.4b). From the IgG concentration kinetics, it was clear that the high response observed for one mouse in the buccal OVA Backfill (180) group

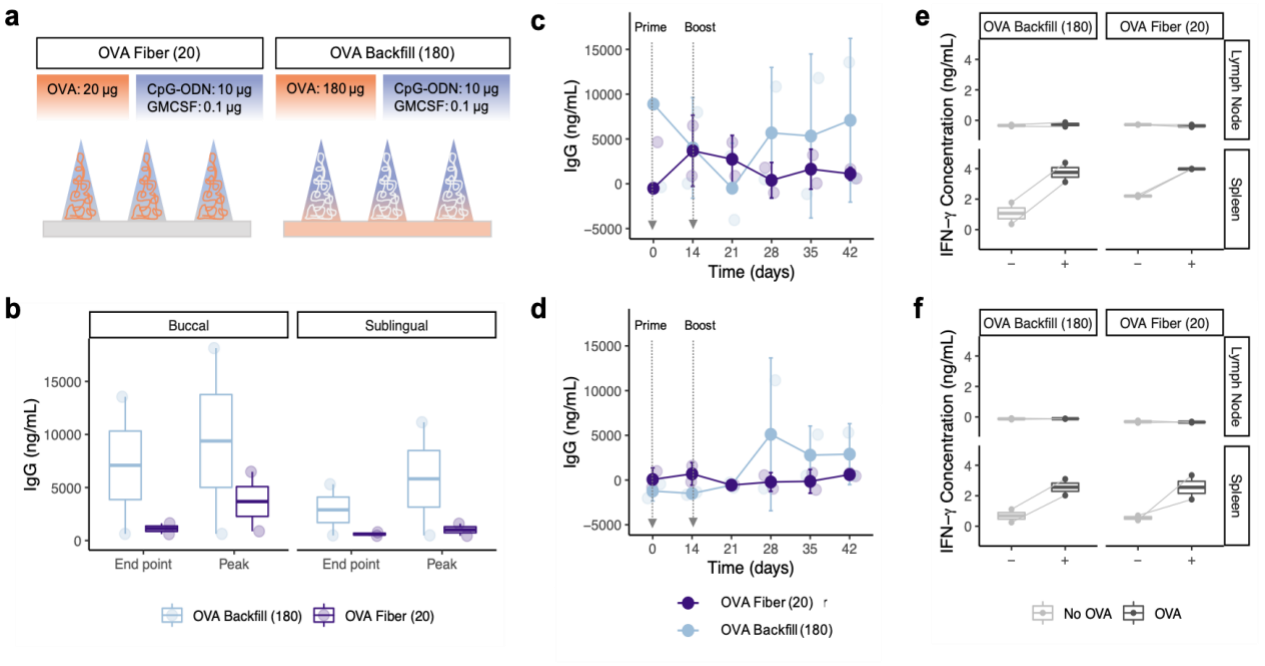

Figure 6.4. Antigen delivery by either individual component of integrated fiber microneedles is insufficient to elicit humoral or cellular immunity

(a) Schematic of antigen and adjuvant loading in integrated fiber microneedles. In this study, OVA was only incorporated into the polyester fibers of the iFMD (OVA Fiber (20)), or the backfill matrix of the iFMD (OVA Backfill (180)). (b) OVA-specific serum IgG concentration at study endpoint and at the peak for each mouse after iFMD delivery in the buccal or sublingual mucosa on day 0 and day 14. Kinetics of OVA-specific serum IgG concentration for the duration of the study following delivery in the buccal (c) or sublingual mucosa (d). Shown are the mean ± s.d. of n=2 biological replicates. Individual replicates are plotted as transparent data points. At the study endpoint, splenocytes and lymphocytes from the draining lymph nodes of mice vaccinated in the buccal (e) or sublingual (f) mucosa were re-stimulated with OVA (1 mg/mL) ex vivo for 72 hours in the presence of ConA (10 µg/mL). Cell culture supernatants were assayed for IFN-g using ELISA as a measure of OVA-specific T cell function.

was due to a high background signal before vaccination (Figure 6.4c). The strongest response was observed for the sublingual OVA Backfill (180) group, but the IgG concentration began to decline 3 weeks after the boost (Figure 6.4d), whereas in the pilot iFMD study, the IgG concentration was continuing to increase at this time point. Overall, both iFMD designs evaluated in this study elicited weak OVA-specific serum IgG responses when delivered to the buccal or sublingual mucosa.

Splenocytes from mice immunized with OVA Fiber (20) microneedles and OVA Backfill (180) microneedles in the buccal mucosa secreted approximately 2-fold and 4-fold more IFN-γ, respectively, when re-stimulated with OVA compared to culture without OVA (Figure 6.4e). A similar trend was observed from mice immunized in the sublingual mucosa (Figure 6.4f). Though some antigen-specific IFN-γ secretion was measured, it was less than that observed from buccal iFMD vaccination in the pilot study (5-fold increase in IFN-γ with OVA re-stimulation). While the re-stimulation data potentially suggests the difference between OVA Fiber (20), OVA Backfill (180), and the iFMD is a simple dose dependence, the OVA-specific serum IgG concentration following iFMD vaccination (35,000 ng/mL) is greater than the sum of the OVA Fiber (20) and OVA Backfill (180) components individually (8,200 or 3,500 ng/mL for buccal or sublingual, respectively). Together, these data suggest that robust immune responses with the iFMD system require antigen to be delivered in the fiber component and the backfill component.

6.3.5 *Controlled release riFMD design results in delayed peak IgG response and non-specific T cell activation*

Having established the basic immunogenicity of the baseline iFMD formulation, we next sought to characterize the humoral and cellular response to the riFMD formulation. This design

incorporated the entire dose of antigen and adjuvant in PVA fibers, then the microneedle mold was filled with a solution of PLGA to form the needle structure and to act as a rate-limiting layer. When evaluated *in vitro,* this design exhibited reduced burst release and a faster sustained release rate compared to the baseline iFMD (Figure 6.2c,d).

Antibody concentrations following buccal riFMD vaccination increased steadily until the study endpoint, while sublingual riFMD vaccination resulted in overall higher antibody concentrations that had a distinct peak (Figure 6.5a,b). This peak occurred late in the study, 7 weeks after the boost dose, and had a lower magnitude than the iFMD from the pilot study

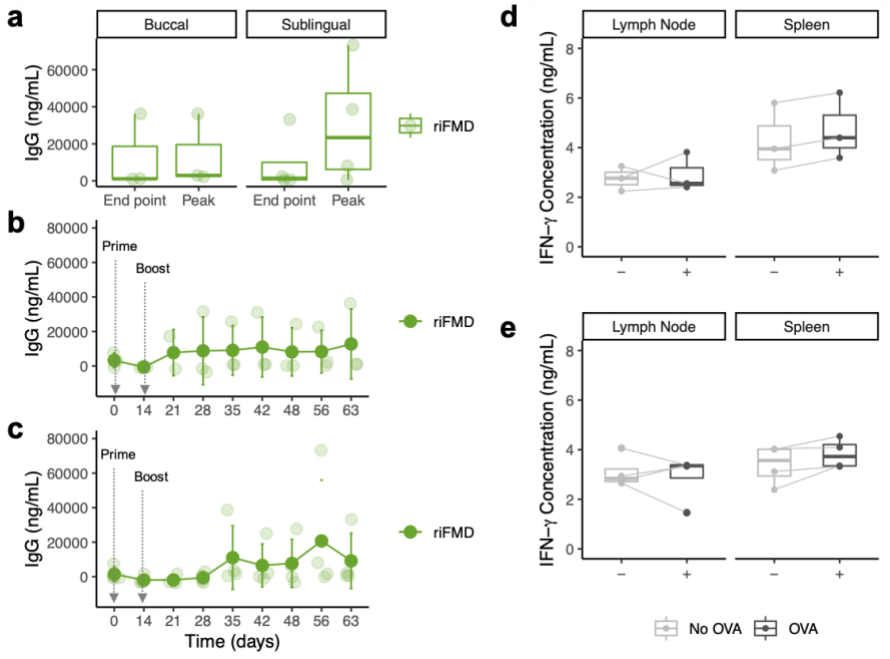

Figure 6.5. Controlled release riFMD design results in delayed peak IgG response and non-specific IFN-γ secretion

(a) OVA-specific serum IgG concentration at study endpoint and at the peak for each mouse after riFMD delivery in the buccal or sublingual mucosa on day 0 and day 14. OVA-specific serum IgG concentration kinetics for 9 weeks following initial vaccination with riFMD in the (b) buccal mucosa (n=3) or the (c) sublingual mucosa (n=4). Data are plotted as the mean ± s.d. of biological replicates. Individual replicates are plotted as transparent data points. At the study endpoint, splenocytes and lymphocytes from the superficial cervical and submandibular lymph nodes were cultured ex vivo for 72 hours in the presence of ConA (10 µg/mL) with or without OVA (1 mg/mL). Cell culture supernatants were assayed for IFN-g using ELISA as a measure of antigen specific T cell function. Re-stimulation analysis was performed for mice vaccinated with riFMD in the buccal (d) or sublingual (e) mucosa.

(20,700 ng/mL compared to 35,000 ng/mL for the buccal iFMD) (Figure 6.5c). This was anticipated based on the slower *in vitro* protein release kinetics from riFMD. Although the humoral response to this particular riFMD design was weak, it is likely based on previous work that this response could be optimized with further tuning of the materials selection or configuration of the riFMD.[27]

IFN-γ secretion from lymphocytes and splenocytes appeared to be independent of the presence of OVA (Figure 6.5d,e). However, IFN-γ secretion overall for both delivery routes was higher than iFMD vaccination from the pilot study, particularly in the lymph nodes (4-fold increase). It is possible that this was caused by the sustained release of antigen and adjuvant with this material configuration, which has led to prolonged local inflammation in previous studies.[26]

6.3.6 *Integrated fiber microneedle length affects serum antibody kinetics and isotype balance when administered to the buccal mucosa*

Several different microneedle designs have been evaluated for oral mucosal vaccination, but the effect of microneedle design on immune response has not been evaluated. Given the importance of microneedle geometry and vaccine release kinetics in dermal microneedle vaccination,[25-27] we were interested in characterizing the effect of these factors on serum antibody responses following oral mucosal vaccine administration.

Mice were immunized in the buccal mucosa with iFMDs (n=3) or liFMDs (n=2) containing 180 µg OVA and adjuvants (10 µg CpG-ODN, 0.1 µg GMCSF) in the backfill matrix and 20 µg OVA in PLGA fibers. As a control group, mice were immunized with 200 µg OVA and adjuvants in a saline suspension administered topically to the buccal mucosa using a cotton tipped swab. All mice were immunized on day 0 and day 14. Vaccination with iFMD resulted in robust OVA-specific IgG (endpoint mean 86,000 ng/mL), while vaccination with the topical swab application resulted in no measurable response (Figure 6.6a). Vaccine delivery using

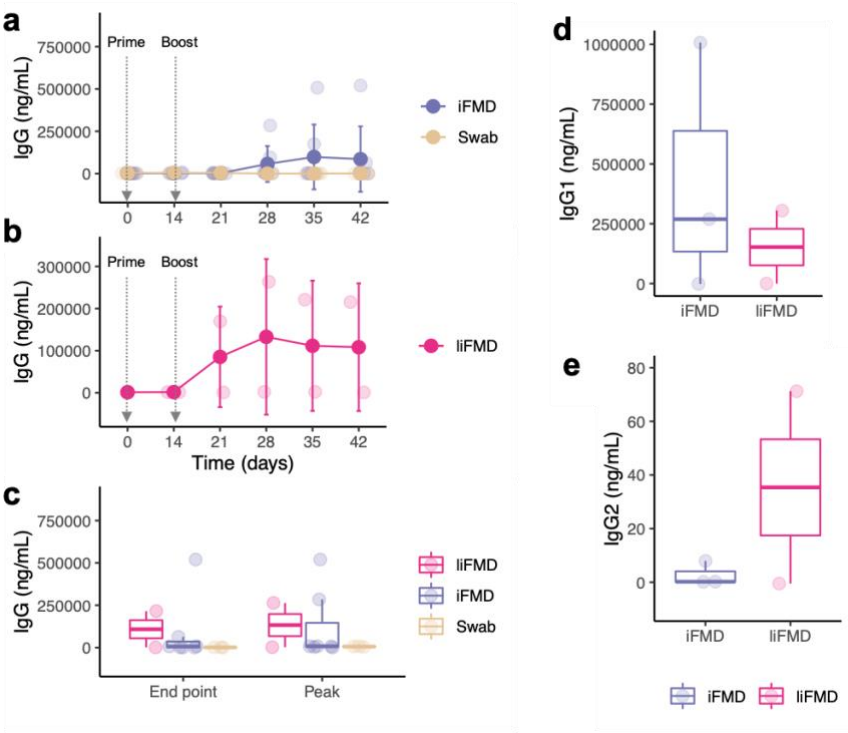

Figure 6.6. Integrated fiber microneedle design affects serum antibody kinetics and isotype balance when administered to the buccal mucosa

C57Bl/6J mice were vaccinated on day 0 and day 14 with 200 µg OVA, 10 µg CpG-ODN, and 0.1 µg GMCSF delivered by iFMD, liFMD, or a cotton tipped swab. iFMD and liFMD contained 20 µg OVA in PLGA fibers and 180 µg OVA in the PVP backfill matrix. OVA-specific serum IgG concentration kinetics for 6 weeks following initial vaccination with a) iFMD (n=7), swab (n=4), or b) liFMD (n=2). c) Serum IgG concentration at the study endpoint and peak following vaccination with iFMD, liFMD, or a cotton tipped swab. d) The serum sample containing the peak IgG concentration for mice in the iFMD (n=3) and liFMD (n=2) groups were assayed for IgG1 and e) IgG2 by ELISA. Data are plotted as the mean ± s.d. of biological replicates. Individual replicates are plotted as transparent data points.

liFMD demonstrated potential for robust IgG responses in the buccal mucosa, with a mean IgG concentration of 108,000 ng/mL at the study endpoint (Figure 6.6b). This response developed faster than the iFMD, with measurable IgG concentrations occurring just 1 week after the boost. There was also less of a difference between the peak and endpoint IgG concentrations for liFMD compared to iFMD, suggesting a more sustained IgG response (Figure 6.6c).

Based on the strong peak IgG responses measured for integrated fiber microneedles with different geometries, we were interested in determining the specific concentrations of IgG1 and IgG2a for these samples. The serum sample containing the peak IgG concentration for mice in the iFMD (n=3) and liFMD (n=2) groups were assayed for IgG1 and IgG2a by ELISA. We observed a distinct decrease in IgG1 concentration and increase in IgG2a concentration for vaccine administration with liFMD compared to iFMD (Figure 6.6d,e). This data suggests that in the buccal mucosa, an increase in microneedle length creates a more balanced Th1/Th2 immune response. This could be caused by liFMD vaccine delivery deeper into the buccal lamina propria, which contains interstitial dendritic cells that are required for IgG2a/c isotype responses[35] and langerin+ interstitial dendritic cells with potential for cross-presentation.[36] Similar trends have been observed in previous studies where vaccination in the surface of the oral mucosa resulted in predominately IgG1 antibodies, while vaccination using methods delivering vaccine deeper in the mucosa, like jet injection or hypodermic needle injection, resulted in a higher ratio of IgG2a antibodies.[3,37] No previous study has evaluated the effect of microneedle length on antibody isotype response after delivery in the oral mucosa. This finding motivates continued exploration of microneedle geometries to optimize immune responses to oral mucosal vaccination.

6.3.7 *Integrated fiber microneedle vaccines elicit robust serum antibody responses upon delivery to the sublingual mucosa*

Only one previous study of oral mucosal vaccination compared the immune response elicited by microneedle vaccine application to different locations in the oral mucosa.[5] However, this study was performed in rabbits and resulted in overall weak immune responses. Since we observed the potential for robust humoral immune responses to various iFMD vaccine designs in the buccal mucosa, we were interested in further evaluating the responses to these iFMDs in the sublingual mucosa using the same vaccine loading schemes and study timelines.

Serum antibody concentrations in the iFMD sublingual group were significantly ($p < 0.05$) higher than those measured in mice immunized by swab application of a vaccine suspension to the sublingual mucosa on day 28 and day 35 of the study (Figure 6.7a). In this group, we observed the potential for rapid development of antigen-specific antibodies, with the strongest responding mouse nearly reaching its peak value just one week after the boost vaccination. When administered sublingually, liFMDs elicited weak antibody responses, reaching a peak value of approximately 10,000 ng/mL three weeks after the boost dose (Figure 6.7b). Both iFMD and liFMD elicited greater peak antibody responses compared to the topical swab control (Figure 6.7c). Sublingual iFMD vaccination resulted in primarily IgG1 antibodies, suggesting a Th-2 biased immune response (Figure 6.7d,e).

Together, these results suggest that sublingual iFMD vaccination leads to a significantly increased humoral immune responses compared to topical sublingual vaccination using a swab. This is consistent with previous work demonstrating that microneedle disruption of the buccal mucosa increases vaccine delivery efficiency and delivery rate compared to delivery without microneedles.[16] Additionally, our results suggest the immune response generated from microneedle-mediated oral mucosal vaccination is dependent on the delivery site, with iFMD inducing higher antibody concentrations when delivered to the sublingual mucosa (endpoint mean 146,000 ng/mL) compared to the buccal mucosa (endpoint mean 86,000 ng/mL). This is in

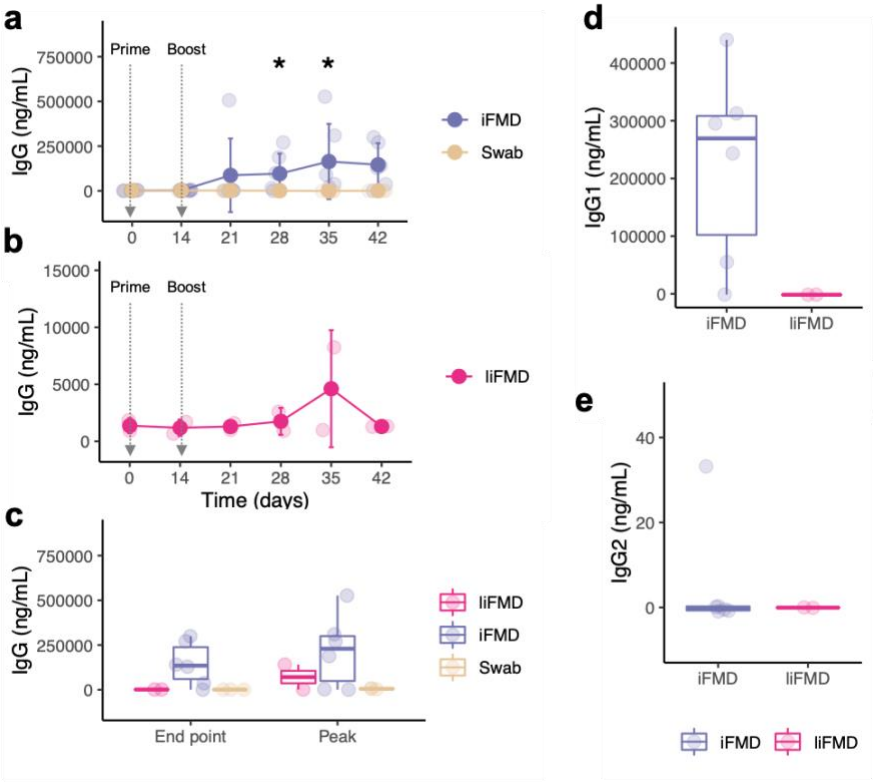

Figure 6.7. Integrated fiber microneedle vaccines elicit robust serum antibody responses upon delivery to the sublingual mucosa

*C57Bl/6J mice were vaccinated on day 0 and day 14 with 200 µg OVA, 10 µg CpG-ODN, and 0.1 µg GMCSF delivered by iFMD, liFMD, or a cotton tipped swab. iFMD and liFMD contained 20 µg OVA in PLGA fibers and 180 µg OVA in the PVP backfill matrix. a) OVA-specific serum IgG concentration kinetics for 6 weeks following initial vaccination with iFMD (n=6, *p<0.05), swab (n=4), or b) liFMD (n=2). c) Serum IgG concentration at the study endpoint and peak following vaccination with iFMD, liFMD, or a cotton tipped swab. d) The serum sample containing the peak IgG concentration for mice in the iFMD (n=6) and liFMD (n=2) groups were assayed for IgG1 and e) IgG2. Data are plotted as the mean ± s.d. of biological replicates. Individual replicates are plotted as transparent data points.*

contrast to previous work in rabbits,[5] but could be explained by the distinct structures and antigen presenting cell populations in the murine buccal and sublingual mucosa. The sublingual epithelium is approximately half the thickness of the buccal epithelium,[4] meaning iFMDs likely deliver vaccine to more immunogenic iDCs in the lamina propria of the sublingual mucosa compared to LCs in the epithelium of the buccal mucosa. It was initially surprising that the immune response to liFMD vaccination was much weaker than iFMD vaccination in the sublingual mucosa and liFMD vaccination in the buccal mucosa. It is possible that in the sublingual mucosa, the liFMD geometry results in less optimal *in vivo* release kinetics compared to the iFMD geometry, resulting in a weaker response. It is possible that this change in release kinetics was also present in the buccal mucosa, but robust responses were still observed from the liFMD because of the higher frequency of iDCs in the lamina propria compared to the sublingual mucosa.

6.3.8 *Integrated fiber microneedle vaccines elicit antigen specific T cell responses in the spleen*

To evaluate cellular immune responses to iFMD vaccination in the buccal and sublingual mucosa, mice were sacrificed at the study endpoint (56 days), and cells from the spleens and draining lymph nodes were re-stimulated *ex vivo* with OVA. Buccal and sublingual iFMD vaccination resulted in significant ($p<0.05$) OVA-specific IFN-γ secretion from splenocytes (Figure 6.8a,c). A similar increase in IFN-γ secretion occurred following buccal and sublingual liFMD vaccination, but the size of each group was too small to reach statistical significance. OVA-specific IFN-γ secretion from lymphocytes was the greatest for iFMD vaccination in the buccal or sublingual mucosa (Figure 6.8b,d). Buccal liFMD vaccination appeared to result in a higher cellular response than sublingual liFMD vaccination, consistent with the humoral immunity results. Together, these data further support the immunogenicity of iFMD in both the

buccal and sublingual mucosa. The increased OVA-specific IFN-γ secretion compared to topical delivery using a swab strengthens the growing body of work demonstrating the ability of microneedles to improve vaccination in the oral mucosa.

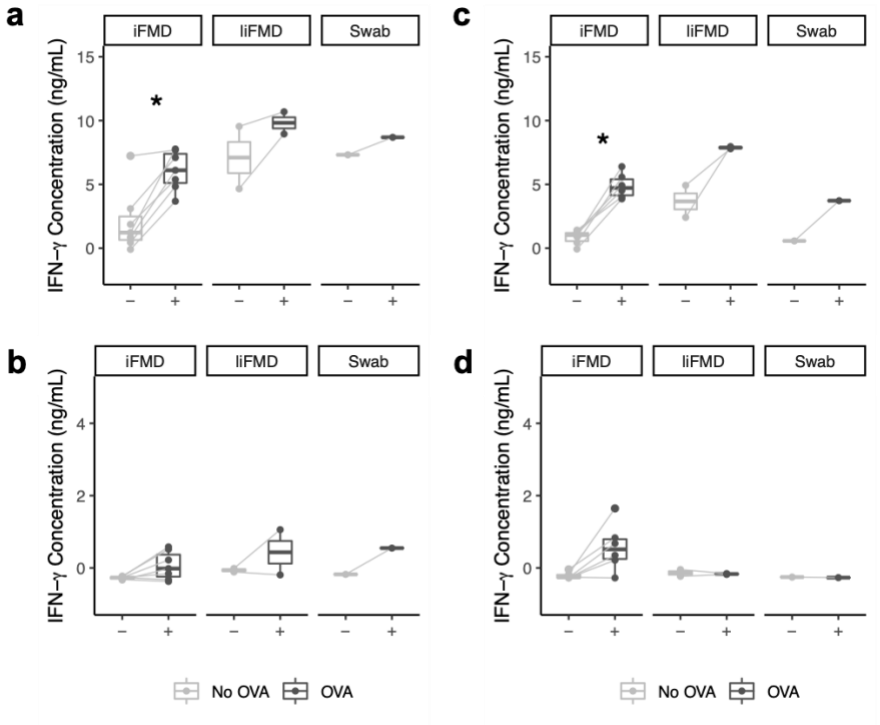

Figure 6.8. Integrated fiber microneedle vaccines elicit antigen specific T cell responses in the spleen

*At the study endpoint, splenocytes (a, c) and lymphocytes from the submandibular lymph nodes (b, d) were re-stimulated with OVA (1 mg/mL) ex vivo for 72 hours in the presence of ConA (10 µg/mL). Cell culture supernatants were assayed for IFN-γ using ELISA as a measure of antigen specific T cell function. IFN-γ concentration from cells cultured without OVA were compared to those cultured with OVA using a Wilcoxon signed rank test to determine statistical significance (*p<0.05). Re-stimulation analysis was performed for mice vaccinated with each microneedle design or topical swab control in the buccal (a, b) or sublingual (c, d) mucosa.*

6.4 CONCLUSIONS

This is the first study evaluating the immunogenicity of a novel and highly tunable integrated fiber microneedle design. We demonstrated that integrated fiber microneedle geometry and material configuration can be tuned without changes to the general fabrication process and with no significant effect on mechanical failure force. This enables evaluation of the effect of features like microneedle length and vaccine release on immunogenicity. We also evaluate for the first time the effect of microneedle length and vaccine release kinetics on humoral and cellular immunity elicited from oral mucosal delivery. Delayed vaccine release kinetics resulted in a delayed peak antibody response and elevated non-specific cytokine secretion from splenocytes and lymphocytes. We found that microneedle length influenced humoral immunogenicity in a site dependent manner, with an increase in length leading to a greater Th1 bias when administered to the buccal mucosa, but a weaker overall humoral response when administered to the sublingual mucosa. Long microneedles may have resulted in less optimal vaccine delivery kinetics in the sublingual mucosa compared to the iFMD. This effect may also have occurred in the buccal mucosa, but in this tissue, it is likely that the longer microneedles accessed the iDCs present in the lamina propria. Meanwhile, cellular immunity did not appear to be site dependent, with integrated fiber microneedles eliciting significant antigen-specific responses in splenocytes after buccal or sublingual delivery. No previous study has made this direct comparison, so this result warrants further investigation of other cytokines secreted by these cells and a deeper analysis of the cellular phenotype. Together, these results motivate continued exploration of microneedle designs that can control vaccine delivery depth and release kinetics in the oral mucosa to further optimize oral mucosal vaccines and to develop a better understanding of the complex oral mucosal immune system.

6.5 Materials and Methods

6.5.1 *Preparation of two-layer microneedle mold collectors*

Master molds with four arrays of 77 pyramidal features with 100 μm base width and height and 300 μm height were designed in Autodesk Inventor and 3D printed using IP-S resin on an indium tin oxide coated glass substrate using the Nanoscribe Photonic Professional GT2 using a 25X objective lens in shell mode. After developing the resist according to the manufacturer's instructions, completed master molds were placed within an outer mold 3D printed in poly(lactic acid) with a FlashForge Finder at the University of Washington CoMotion Makerspace. The completed master was then coated with silane (trichloro(1H,1H,2H,2H-perfluorooctyl)silane, Sigma Aldrich) to prevent adhesion of cast molds. The desired volume of PDMS (mixed at 1:10 ratio curing agent: pre-polymer, Sylgard 184, Dow Corning) was added to the master mold and cured at room temperature for 24 hours. A conductive carbon black PDMS composite (C-PDMS) was prepared by incorporating 5wt% carbon black (Vulcan XC 72R, particle size 50 nm, Fuel Cell Store) into the PDMS pre-polymer and curing agent by manual mixing with a spatula, and then 3 milliliters of the completed C-PDMS mixture was added to the master mold. The entire mold was then placed on a rotating platform shaker at the highest setting for 15 hours. The C-PDMS was then cured in an oven at 37°C for 24 hours, and the completed collector was removed from the master mold.

6.5.2 *Preparation of protein loaded electrospun fibers*

Polyester fibers were prepared using a 10% (w/v) solution of PLGA (50:50 ester terminated 0.55-0.75 dL/g inherent viscosity B6010-2P, Lactel) in HFIP or a 15% (w/v) solution of PLLA (Ester terminated 1.06 dL/g inherent viscosity) in HFIP. Immediately prior to

electrospinning, 0.2% Tween 20 was added to the organic polymer solution and vortexed for 5 seconds. In a separate tube, ovalbumin (>95% purity, Invivogen) was dissolved at 40 mg/mL in a 5 % (w/v) solution of PVA (P1180, USP grade, Spectrum Chemical). The emulsion aqueous phase was added dropwise to the organic phase while vortexing. Volumes of each phase were selected to achieve a 40% v/v aqueous phase emulsion. The completed emulsion was electrospun onto a two-layer microneedle mold collector using a 2 µL/min flow rate, needle tip to collector distance of 10 cm, and 20 kV voltage. After electrospinning, fibers were sterilized by exposure to ultraviolet light for one hour in a biosafety cabinet.

6.5.3 *Preparation of integrated fiber microneedles*

Integrated fiber microneedles were prepared using sterile solutions of 30% w/v polyvinylpyrrolidone (10 kDa, Sigma Aldrich) and 10% w/v polyvinyl alcohol (P1180, USP grade, Spectrum Chemical) in water. GMSCF (Peprotech) and CpG-ODN (Invivogen) were incorporated into the PVP (iFMD) or PVA (liFMD) solutions to achieve a final dose per microneedle array of 10 µg CpG-ODN and 0.1 µg GMCSF. With the exception of the OVA fiber (20) integrated fiber microneedles, the PVP or PVA solution also contained OVA to achieve a final dose per microneedle array of 180 µg. This solution was added to the surface of the microneedle mold containing fibers. Reverse integrated fiber microneedles were prepared by adding a 10% w/v solution of PLGA in acetone or a 15% w/v solution of PLLA in HFIP to the surface of the microneedle mold containing fibers. For both material configurations, the mold was then placed in a vacuum chamber under house vacuum for 1 minute (iFMD, liFMD) or two minutes (riFMD). This vacuum procedure was repeated twice for iFMD, then 10% w/v PVA in water was added to the mold surface followed by an additional minute of vacuum. For liFMD, the vacuum procedure was repeated twice followed by addition of 5% w/v PVA in water, then

two additions of 10% w/v PVA in water, with 1 minute vacuum cycles between each addition. For riFMD, the polyester solution addition and 2 minute vacuum cycle was repeated four times with excess polyester removed from the surface of the microneedle mold between each cycle using a Kimwipe dipped in acetone. Finally, for each microneedle design, an additional volume of PVA solution was added to ensure the microneedle patch had a backing robust enough to handle. iFMD and liFMD were dried overnight, and riFMD were dried for three days prior to removal from the mold.

6.5.4 *Protein release*

Protein release kinetics were evaluated at 37ºC in a rotating incubator (200 rpm) with PBS (pH 7.4) as the release media. At each time point, a 500 µL aliquot of the release media was removed to a clean tube and replaced with fresh PBS. Protein content from all release time points was measured using the Micro BCA Protein Assay Kit (Thermo Scientific) according to the manufacturer's instructions for the microplate procedure. Percent release was calculated using the theoretical protein loading.

6.5.5 *Compression under axial load*

Compression testing of microneedle arrays was performed on an Instron Universal Testing System (Model 5943). iFMD were tested in arrays of 77 needles, liFMD were tested in arrays of either 10 or 15 needles, and riFMD were tested in arrays of 38 needles. For all microneedle designs, arrays were inspected before testing and the needle number was adjusted to account for any needles that were broken or damaged during storage. The microneedle array was mounted to a microscope slide with double-sided tape, and the slide was then secured to the fixed base plate with double-sided tape. A flat stainless-steel disc adapter was attached to the

load cell. The load cell moved toward the fixed base plate at a rate of 20 μm/s. The instrument began collecting data when the measured load exceeded 0.08 N. The experiment ended either when the load reached 25 N or when the length of the experiment reached 45 seconds.

6.5.6 *Vaccine administration*

Animal studies were performed according to a protocol approved by the University of Washington Institutional Animal Care and Use Committee. Female C57BL/6J mice (6 weeks old) were purchased from The Jackson Laboratory (Bar Harbor, ME). Prior to vaccination, mice were weighed, then anesthetized using isoflurane, and a blood sample was collected via the submental route. Mice receiving vaccine via the oral route were then anesthetized by administration of 32.5 mg/kg ketamine and 2.2 mg/kg xylazine via intraperitoneal injection. For oral topical delivery, mice were laid horizontally on their side, and the mouth was gently opened using forceps. Vaccine was slowly administered (7 μL total volume) using a 20 μL pipet. Mice were kept horizontal for 5 minutes following delivery. For oral microneedle delivery, mice were restrained using a custom-built restraint, similar to an intubation restraint, that held mice from the upper incisors. The microneedle patches were diced into two pieces prior to delivery. To achieve the desired dose with the reverse integrated fiber microneedles, a total of three microneedle patches were delivered. The mouth was gently opened using forceps and the microneedle patches were applied to the buccal or sublingual mucosa with gentle pressure applied with forceps for 1 minute. The microneedle patch remained in the tissue for 5 additional minutes to allow for dissolution of the patch backing. For dermal microneedle delivery, mice were anesthetized using only isoflurane. Microneedle patches were applied to the ventral ear skin using fingertips. Pressure was applied for 1 minute, then patches remained in skin for 5

additional minutes to allow for needle dissolution. The patch backing was then removed, and the mouse was allowed to recover from anesthesia.

6.5.7 *Serum collection*

Blood was collected at predetermined time points via the submental route. Blood was incubated at 4ºC for 24 hours after collection. Blood samples were then centrifuged at 5000 x g for 10 minutes, and the supernatant was carefully removed and transferred to a clean centrifuge tube. The samples were then centrifuged again at 5000 x g for 10 minutes, and the supernatant was removed to a clean 0.6 mL microcentrifuge tube. Samples were stored at -20ºC and were assayed within 6 months of collection.

6.5.8 *Serum antibody ELISA*

ELISA plates (Corning™ Clear Polystyrene 96-Well Microplates for ELISA) were coated with 5 µg/mL OVA (>95% purity, Invitrogen) in 10 mM sodium bicarbonate at 4ºC overnight. Plates were washed with PBS containing 0.05% v/v Tween-20 (PBS-T), then blocked with 2% w/v BSA (Sigma, Bovine Serum Albumin - cold ethanol fraction, pH 5.2, ≥96%) in PBS-T for two hours at room temperature. After blocking, plates were washed again with PBS-T. Serial dilutions of antibody standards (BioLegend, Biotin anti-mouse IgG1 antibody or Biotin anti-mouse IgG2a antibody) starting at 100 ng/mL (IgG1) or 10 ng/mL (IgG2a) were added to wells coated with OVA (2 technical replicates) and wells without OVA (1 replicate) to account for non-specific binding. Samples were incubated for two hours at 37ºC. Plates were then washed with PBS-T and detection antibody (Goat anti-mouse IgG (H+L) HRP conjugate, Invitrogen; biotin anti-mouse IgG1, biotin anti-mouse IgG2a, BioLegend) was added to the plate and incubated at 37ºC for two hours. IgG and IgG1 detection antibody were added at a 5000x

dilution, IgG2a detection antibody was added at a 3000x dilution. IgG1 and IgG2a plates were washed again with PBS-T, then streptavidin-HRP (BioLegend) was added to the wells at a 3000x dilution. Plates were washed again with PBS-T, and then TMB substrate (BioLegend) was added and incubated for 1 hour at room temperature. After addition of 1M HCl stop solution, absorbance was measured at 450 nm with wavelength correction at 620 nm using a plate reader (Tecan Infinite 200 Pro). Antibody concentrations were quantified using a standard curve fit after subtracting the non-specific signal from wells without OVA coating.

6.5.9 *Ex vivo re-stimulation*

Spleens, submandibular lymph nodes, and superficial cervical lymph nodes were collected from sacrificed mice and digested by incubation with collagenase-D (Roche) at 37 ºC for 30 minutes. Cells were collected from the digested tissues by gently pressing through a 70 µm cell strainer into a 50 mL conical tube using the plunger of a 1 mL syringe. The plunger and the strainer were then rinsed with 10 mL of sterile PBS into the 50 mL conical tube. Cell suspensions were then centrifuged 1500 rpm for 5 minutes at 4 ºC. After this initial collection, cells collected from spleens were re-suspended in 5 mL of red blood cell lysis buffer (155 mM NH_4Cl, 10 mM $KHCO_3$, 0.1 mM EDTA in double distilled water) for 2 minutes followed by addition of 15 mL sterile PBS. Cells collected from lymph nodes were re-suspended in PBS, then all cells were passed through a 70 µm cell strainer into a fresh 50 mL conical tube. Cell suspensions were then centrifuged at 1500 rpm for 5 minutes at 4 ºC. All cells were strained and centrifuged again following the same procedure. After the final centrifugation step, cells collected from spleens were re-suspended in 10 mL PBS and cells collected from lymph nodes were re-suspended in 5 mL PBS for cell counting. After counting, cells were collected by centrifugation at 1500 rpm for 5 minutes at 4 ºC, then re-suspended in supplemented media

(429.5 mL RPMI 1640, 2 mM L-glutamine, 5 mL HEPES, 5 mL NE Amino Acids, 5 mL sodium pyruvate, 0.5 mL 2-mercaptoethanol, 5 mL penicillin – 100 U/mL and streptomycin – 100 µg/mL, and 50 mL heat inactivated fetal bovine serum) containing 10 µg/mL concanavalin-A (Sigma) and either with 1 mg/mL OVA or without OVA. Cells were plated at a concentration of 1 million cells/mL in 96 well U-bottom plates. Supernatants were collected after 72 hours of culture and assayed for interferon-γ using an interferon-γ ELISA kit (Peprotech) following the manufacturer's instructions.

6.5.10 *Statistical methods*

All statistical analysis was performed using R, specifically the ggpubr package. Comparisons of the means of more than two groups were performed using the Kruskal-Wallis test. Means of paired samples were compared using the Wilcoxon signed rank test, while means of unpaired samples were compared using the unpaired two-samples Wilcoxon test.

6.6 ACKNOWLEDGEMENTS

SEM imaging was conducted at the Washington Nanofabrication Facility, a National Nanotechnology Coordinated Infrastructure (NNCI) site at the University of Washington, which is supported in part by funds from the Molecular Engineering & Sciences Institute, the Clean Energy Institute, the Washington Research Foundation, the M. J. Murdock Charitable Trust, the National Science Foundation and the National Institutes of Health. This work was supported by NIH/NIHCD grant DP2HD075703 to KAW. RC would like to acknowledge additional support from the NSF Graduate Research Fellowship (DGE-1256082) and the University of Washington STD & AIDS Research Training Fellowship Program (NIH 2T32AI007140-41).

6.7 REFERENCES

1 Cho, H. J. *et al.* Enhanced humoral and cellular immune responses after sublingual immunization against human papillomavirus 16 L1 protein with adjuvants. *Vaccine* **28**, 2598-2606, doi:10.1016/j.vaccine.2010.01.013 (2010).

2 Gallorini, S. *et al.* Sublingual immunization with a subunit influenza vaccine elicits comparable systemic immune response as intramuscular immunization, but also induces local IgA and TH17 responses. *Vaccine* **32**, 2382-2388, doi:10.1016/j.vaccine.2013.12.043 (2014).

3 Lundholm, P., Asakura, Y., Hinkula, J., Lucht, E. & Wahren, B. Induction of mucosal IgA by a novel jet delivery technique for HIV-1 DNA. *Vaccine* **17**, 2036-2042 (1999).

4 Thirion-Delalande, C. *et al.* Comparative analysis of the oral mucosae from rodents and non-rodents: Application to the nonclinical evaluation of sublingual immunotherapy products. *PLOS ONE* **12**, e0183398, doi:10.1371/journal.pone.0183398 (2017).

5 Ma, Y. *et al.* Vaccine delivery to the oral cavity using coated microneedles induces systemic and mucosal immunity. *Pharm Res* **31**, 2393-2403, doi:10.1007/s11095-014-1335-1 (2014).

6 Mascarell, L. *et al.* Oral dendritic cells mediate antigen-specific tolerance by stimulating TH1 and regulatory CD4+ T cells. *J Allergy Clin Immunol* **122**, 603-609.e605, doi:10.1016/j.jaci.2008.06.034 (2008).

7 Song, J.-H. *et al.* CCR7-CCL19/CCL21-Regulated Dendritic Cells Are Responsible for Effectiveness of Sublingual Vaccination. *The Journal of Immunology* **182**, 6851, doi:10.4049/jimmunol.0803568 (2009).

8 Hovav, A. H. Dendritic cells of the oral mucosa. *Mucosal Immunol* **7**, 27-37, doi:10.1038/mi.2013.42 (2014).

9 Le Borgne, M. *et al.* Dendritic cells rapidly recruited into epithelial tissues via CCR6/CCL20 are responsible for CD8+ T cell crosspriming in vivo. *Immunity* **24**, 191-201, doi:10.1016/j.immuni.2006.01.005 (2006).

10 Kraan, H. *et al.* Buccal and sublingual vaccine delivery. *Journal of Controlled Release* **190**, 580-592, doi:http://dx.doi.org/10.1016/j.jconrel.2014.05.060 (2014).

11 Harris, D. & Robinson, J. R. Drug delivery via the mucous membranes of the oral cavity. *Journal of pharmaceutical sciences* **81**, 1-10 (1992).

12 Ma, Y., Boese, S. E., Luo, Z., Nitin, N. & Gill, H. S. Drug coated microneedles for minimally-invasive treatment of oral carcinomas: development and in vitro evaluation. *Biomed Microdevices* **17**, 44, doi:10.1007/s10544-015-9944-y (2015).

13 McNeilly, C. L. *et al.* Microprojection arrays to immunise at mucosal surfaces. *J Control Release* **196**, 252-260, doi:10.1016/j.jconrel.2014.09.028 (2014).

14 Wang, X. T., Wang, N., Li, N., Zhen, Y. Y. & Wang, T. Multifunctional particle-constituted microneedle arrays as cutaneous or mucosal vaccine adjuvant-delivery systems. *Human Vaccines & Immunotherapeutics* **12**, 2075-2089, doi:10.1080/21645515.2016.1158368 (2016).

15 Zhen, Y. *et al.* Multifunctional liposomes constituting microneedles induced robust systemic and mucosal immunoresponses against the loaded antigens via oral mucosal vaccination. *Vaccine* **33**, 4330-4340, doi:10.1016/j.vaccine.2015.03.081 (2015).

16 Oh, Y. J. *et al.* Ovalbumin and cholera toxin delivery to buccal mucus for immunization using microneedles and comparison of immunological response to transmucosal delivery. *Drug Deliv Transl Res*, doi:10.1007/s13346-021-00964-z (2021).

17 Park, J.-H., Allen, M. G. & Prausnitz, M. R. Biodegradable polymer microneedles: Fabrication, mechanics and transdermal drug delivery. *Journal of Controlled Release* **104**, 51-66, doi:http://dx.doi.org/10.1016/j.jconrel.2005.02.002 (2005).

18 Davis, S. P., Landis, B. J., Adams, Z. H., Allen, M. G. & Prausnitz, M. R. Insertion of microneedles into skin: measurement and prediction of insertion force and needle fracture force. *Journal of Biomechanics* **37**, 1155-1163, doi:10.1016/j.jbiomech.2003.12.010 (2004).

19 DeMuth, P. C., Garcia-Beltran, W. F., Ai-Ling, M. L., Hammond, P. T. & Irvine, D. J. Composite Dissolving Microneedles for Coordinated Control of Antigen and Adjuvant Delivery Kinetics in Transcutaneous Vaccination. *Advanced Functional Materials* **23**, 161-172, doi:10.1002/adfm.201201512 (2013).

20 Chen, M. C., Huang, S. F., Lai, K. Y. & Ling, M. H. Fully embeddable chitosan microneedles as a sustained release depot for intradermal vaccination. *Biomaterials* **34**, 3077-3086, doi:10.1016/j.biomaterials.2012.12.041 (2013).

21 Serpe, L. *et al.* Influence of salivary washout on drug delivery to the oral cavity using coated microneedles: An in vitro evaluation. *Eur J Pharm Sci* **93**, 215-223, doi:10.1016/j.ejps.2016.08.023 (2016).

22 van der Maaden, K. *et al.* Parameter optimization toward optimal microneedle-based dermal vaccination. *Eur J Pharm Sci* **64**, 18-25, doi:10.1016/j.ejps.2014.08.004 (2014).

23 Widera, G. *et al.* Effect of delivery parameters on immunization to ovalbumin following intracutaneous administration by a coated microneedle array patch system. *Vaccine* **24**, 1653-1664, doi:10.1016/j.vaccine.2005.09.049 (2006).

24 Römgens, A. M., Bader, D. L., Bouwstra, J. A. & Oomens, C. W. J. Predicting the optimal geometry of microneedles and their array for dermal vaccination using a computational model. *Computer Methods in Biomechanics and Biomedical Engineering* **19**, 1599-1609, doi:10.1080/10255842.2016.1173684 (2016).

25 van der Maaden, K., Sekerdag, E., Jiskoot, W. & Bouwstra, J. Impact-insertion applicator improves reliability of skin penetration by solid microneedle arrays. *AAPS J* **16**, 681-684, doi:10.1208/s12248-014-9606-7 (2014).

26 DeMuth, P. C., Min, Y., Irvine, D. J. & Hammond, P. T. Implantable Silk Composite Microneedles for Programmable Vaccine Release Kinetics and Enhanced Immunogenicity in Transcutaneous Immunization. *Advanced Healthcare Materials* **3**, 47-58, doi:10.1002/adhm.201300139 (2014).

27 Boopathy, A. V. *et al.* Enhancing humoral immunity via sustained-release implantable microneedle patch vaccination. *Proceedings of the National Academy of Sciences* **116**, 16473-16478, doi:10.1073/pnas.1902179116 (2019).

28 Aramaki, O., Chalermsarp, N., Otsuki, M., Tagami, J. & Azuma, M. Differential expression of co-signal molecules and migratory properties in four distinct subsets of migratory dendritic cells from the oral mucosa. *Biochem Biophys Res Commun* **413**, 407-413, doi:10.1016/j.bbrc.2011.08.099 (2011).

29 Creighton, R. L., Phan, J. & Woodrow, K. A. In situ 3D-patterning of electrospun fibers using two-layer composite materials. *Scientific Reports* **10**, doi:10.1038/s41598-020-64846-z (2020).

30 Park, J. H., Yoon, Y. K., Choi, S. O., Prausnitz, M. R. & Allen, M. G. Tapered conical polymer microneedles fabricated using an integrated lens technique for transdermal drug delivery. *IEEE Trans Biomed Eng* **54**, 903-913, doi:10.1109/TBME.2006.889173 (2007).

31 Gittard, S. D. *et al.* The Effects of Geometry on Skin Penetration and Failure of Polymer Microneedles. *Journal of adhesion science and technology* **27**, 227-243, doi:10.1080/01694243.2012.705101 (2013).

32 Park, S. C., Kim, M. J., Baek, S.-K., Park, J.-H. & Choi, S.-O. Spray-Formed Layered Polymer Microneedles for Controlled Biphasic Drug Delivery. *Polymers* **11**, doi:10.3390/polym11020369 (2019).

33 Ali, O. A., Huebsch, N., Cao, L., Dranoff, G. & Mooney, D. J. Infection-mimicking materials to program dendritic cells in situ. *Nature Materials* **8**, 151-158, doi:10.1038/nmat2357 (2009).

34 Kim, J. *et al.* Injectable, spontaneously assembling, inorganic scaffolds modulate immune cells in vivo and increase vaccine efficacy. *Nature Biotechnology* **33**, 64-U241, doi:10.1038/nbt.3071 (2015).

35 Nagao, K. *et al.* Murine epidermal Langerhans cells and langerin-expressing dermal dendritic cells are unrelated and exhibit distinct functions. *Proceedings of the National Academy of Sciences of the United States of America* **106**, 3312-3317, doi:10.1073/pnas.0807126106 (2009).

36 Nudel, I. *et al.* Dendritic cells in distinct oral mucosal tissues engage different mechanisms to prime CD8+ T cells. *J Immunol* **186**, 891-900, doi:10.4049/jimmunol.1002943 (2011).

37 Etchart, N. *et al.* Dendritic cells recruitment and in vivo priming of CD8+ CTL induced by a single topical or transepithelial immunization via the buccal mucosa with measles virus nucleoprotein. *J Immunol* **167**, 384-391 (2001).

Chapter 7. CONCLUSIONS

7.1 SUMMARY

The oral mucosa is an easily accessible site for mucosal vaccination, and oral mucosal vaccines have demonstrated an ability to induce systemic immunity and mucosal immunity at distant mucosal tissues such as the gastrointestinal tract and reproductive tract. However, further development of oral mucosal vaccines has been partly hindered by a lack of multifunctional delivery systems capable of incorporating diverse vaccine formulations at different doses and spatial and temporal control of vaccine delivery. In this work, we have focused on the development and preliminary evaluation of a dissolving microneedle device incorporating electrospun fibers to address this gap in the field of oral mucosal vaccination.

The design goal of our device was to combine the unique agent encapsulation, controlled release, and microarchitecture attributes of electrospun fibers with the mechanical attributes of dissolving microneedles. In the first specific aim of this work, we pursued an *in situ* approach to generate three-dimensional electrospun fiber structures. Using this strategy, we were able to integrate electrospun fibers into dissolving microneedles without altering their microarchitecture, and without depositing large amounts of fiber in the microneedle array backing. We demonstrated using finite element method simulations and experimentally that this *in situ* electrospun fiber patterning approach is feasible over a wide range of length scales and for different fiber materials. Therefore, this versatile method could be further explored for other applications of three-dimensional fiber structures such as tissue engineering or microfluidics.

A key question in the field of oral mucosal vaccines is the role of vaccine composition and dose on the resulting immune response. Therefore, an ideal device designed for oral mucosal vaccination should enable encapsulation of diverse active pharmaceutical agents at a range of

relevant doses. In our second aim, as a first step toward demonstrating the formulation capabilities of integrated fiber microneedles, we developed biologic fiber formulations with loadings relevant for the microneedle device, and we demonstrated *in situ* integration of fibers containing a model small molecule, protein, or nucleic acid. We also demonstrated two specific examples in which integrated fiber microneedles can overcome limitations of conventional matrix microneedles. Together, the work in this aim demonstrates how integrated fiber microneedles are a versatile delivery device that can contribute to the field of oral mucosal vaccination and the broader field of microneedle drug and vaccine delivery.

Previous studies of microneedle-mediated vaccination in the oral mucosa have been limited and overall have demonstrated weak systemic immune responses. In our third specific aim, we characterized the cellular and humoral immune response to three distinct integrated fiber microneedle designs with two different lengths and two different protein release rates. We found that integrated fiber microneedle vaccines elicit significant humoral immune responses when delivered to the sublingual mucosa and significant cellular immune responses when delivered to either the buccal or sublingual mucosa. Furthermore, we observed that microneedle length affects humoral immunity in a site-specific manner and slowing vaccine release rate delays the peak antibody concentration. The work in this aim establishes the function of the integrated fiber microneedle device as an oral mucosal delivery system and motivates future work using this device as a tool to better understand oral mucosal immunity.

7.2 LIST OF PUBLICATIONS AND PRESENTATIONS

7.2.1 *Publications*

1. **Creighton, R.**, Phan, J., Woodrow, K.A. In situ 3D patterning of electrospun fibers using two-layer composite materials. Scientific Reports (2020) 10, 7949. PMCID: PMC7224382
   - Chapter 3

2. ***Creighton, R.**, *Suydam, I., Ebner, M., Afunugo, W., Bever, A., Cao, S., Jiang, Y., Woodrow, K. Sustained Intracellular Raltegravir Depots Generated with Prodrugs Designed for Nanoparticle Delivery. ACS Biomater. Sci. Eng. (2019) 5, 8, 4013-4022. PMCID: PMC7591136
*Authors contributed equally

3. **Creighton, R.**, Woodrow, K.A. Microneedle-mediated vaccine delivery to the oral mucosa. Adv. Healthc. Mater. (2018) 8, 1801180. PMCID: PMC6476557
   - Chapter 2

7.2.2 *Patent*

(pending) **Creighton, R.L.**; Woodrow, K.A. Integrated fiber microneedle device for drug and vaccine delivery. U.S. Application No. 16/546,098

7.2.3 *Presentations at national conferences*

Creighton, R., Phan, J., Woodrow, K.A. "*In situ* integration of electrospun fibers with microneedles" Oral Presentation and Poster Presentation at the Society for Biomaterials Annual Meeting and Exposition, Seattle, WA, April 3, 2019.

Creighton, R., Ebner, M., Afunugo, W., Bever, A., Cao, S., Jiang, Y., Woodrow, K., Suydam, I. "A prodrug strategy to improve drug loading and determine intracellular release from nanoparticle systems" Oral Presentation at the Biomedical Engineering Society Annual Meeting, Phoenix, AZ, October 14, 2017

VITA

Rachel Creighton earned her B.S. in Materials Engineering from Iowa State University in 2015, where she minored in Bioengineering. Rachel was also a graduate of the University Honors Program. Rachel was involved in research throughout her undergraduate education, first in Dr. Kaitlin Bratlie's laboratory at Iowa State, and later in Dr. Karl Berggren's laboratory at the Massachusetts Institute of Technology. Through these formative experiences, Rachel established her diverse research interests in biomaterials and microfabrication. She began her doctoral work at the University of Washington in 2015 in the department of Bioengineering with Dr. Kim Woodrow. Here, she used her previous experience with biomaterials, microfabrication, and electronic materials to develop, formulate, and evaluate integrated fiber microneedle vaccines. In her free time, Rachel enjoys gardening, sewing, golfing, hiking, and backpacking.